CHARACTERISATION AND MODELLING OF A UNIFORMLY GRADED, WELL-ROUNDED COARSE SAND

By

PASCALE C. ROUSE

Civil Engineering, University of Chile, 2003
B.Sc., University of Chile, 2001

A THESIS SUBMITTED IN PARTIAL FULFILMENT OF
THE REQUIREMENTS FOR THE DEGREE OF
MASTER OF APPLIED SCIENCE

in

THE FACULTY OF GRADUATE STUDIES
(CIVIL ENGINEERING)

THE UNIVERSITY OF BRITISH COLUMBIA
September 2005

ABSTRACT

Strength parameters and intrinsic properties of sand are very important for engineering design. It is well known that such properties depend on factors including grain size distribution, fines content, mineralogy and grain shape. Recently, several authors have sought to establish a relation between the constant volume friction angle, as well as the maximum and minimum void ratios, and the roundness of the sand grains. Little information exists on well-rounded sands. A series of triaxial tests were performed on a uniformly graded, well-rounded coarse sand (R=0.81). Interpretation of the results confirms the available relations, and provides a link between the data on commonly found sands (0.2<R<0.7) and glass beads (R≅1.0). Additionally a comparison of drained and undrained triaxial test data indicates $\phi_{MC} \cong \phi_{PT} \neq \phi_{CV}$, $\phi_{CV} \cong \phi_{MO}$, $\phi_{MO} \cong \phi_{PT} + 3°$ and ϕ_{CV} is very similar to ϕ_{rep}.

The behaviour of the well-rounded sand is modelled using the critical state soil mechanics constitutive model, NorSand. The results show that the parameters needed for the model fall within the expected range of values, and that NorSand captures both the drained and undrained response of the sand in triaxial testing. However, the volumetric coupling coefficient N, shows an unusual value indicative of unusual dilation of this sand. To account for this, a modification of the flow rule is proposed.

In addition, the NorSand constitutive model is implemented in the commercially available software FLAC. For this, the standard method used within FLAC, F=0, will not work. But by solving $\dot{F} = 0$ it is possible to introduce any critical state soil mechanics (CSSM) constitutive model. This approach is described in detail for two selected CSSM models, Original Cam Clay and NorSand.

TABLE OF CONTENTS

	Page
Abstract	ii
List of tables	vi
List of figures	vii
List of symbols	x
Acknowledgments	xiii
CHAPTER I: INTRODUCTION	1
1.1. Purpose of the study	2
1.2. Organization of the thesis	3
CHAPTER II: LITERATURE REVIEW	4
2.1. Behaviour of sands	4
2.1.1. General stress-strain behaviour of soils	4
2.1.2. Triaxial testing	5
2.1.3. Triaxial behaviour of sands	10
2.2. Definition of friction angles for sands	12
2.2.1. Angle of repose (ϕ_{rep})	12
2.2.2. Critical state or steady state friction angle (ϕ_{CV})	13
2.2.3. Peak friction angle (ϕ_p)	13
2.2.4. Maximum contraction friction angle (ϕ_{MC})	15
2.2.5. Phase transformation friction angle (ϕ_{PT})	16
2.2.6. Maximum obliquity friction angle (ϕ_{MO})	16
2.3. Definition of roundness and sphericity	17
2.3.1. Sphericity	17
2.3.2. Roundness	19
2.4. Critical State Soil Mechanics	22
2.4.1. General plasticity concepts	22
- *Elasticity:*	22
- *Yield surface, F:*	22
- *Normality:*	22

- *Plastic potential surface, Q:* 23
- *Hardening rule:* 24
- *Dilatancy:* 24
2.4.2. The critical state 27
2.4.3. Original Cam Clay formulation 30
2.4.4. Modified Cam Clay formulation 34
2.4.6. Stress – dilatancy 39
2.5. Critical state model for sands 43
2.6. Critical state models for sands and NorSand 47
2.6.1. The state parameter and overconsolidation 47
2.6.2. NorSand formulation 48
2.6.3. Determination of NorSand parameters 55

CHAPTER III: MATERIAL PROPERTIES 58

3.1. Description of the soil 58
3.3.1. Extreme void ratios 60
3.3.2. Angle of repose 63
3.3.3. Roundness and sphericity 63
3.2. Triaxial testing program 67
3.2.1. Description of the triaxial equipment 67
3.2.2. Data acquisition system 67
3.2.3. Calibration of the system and measurement resolutions 67
3.2.4. Preparation and testing of the specimen 69
3.3. Triaxial test results 70
3.3.1. Test description 71
3.3.2. Void ratio determination 71
3.3.3. Triaxial test results 73
3.3.4. Shear modulus 77

CHAPTER IV: ANALYSIS OF RESULTS 78

4.1. Friction angles results from triaxial test program 78
4.1.1. Constant volume friction angle (ϕ_{cv}) 78
4.1.2. Peak friction angle (ϕ_p) 81

4.1.3. Maximum contraction friction angle (ϕ_{MC}) 82

4.1.4. Phase transformation friction angle (ϕ_{PT}) 83

4.2. Comparison of Badger sand properties with literature 86

4.3. Analysis of NorSand results 89

4.3.1. Comparison between triaxial data and NorSand model for Badger sand 90

4.3.2. Determination of NorSand parameters 98

- *Critical state parameters* 98

- *Plastic parameters* 98

CHAPTER V: SUMMARY AND CONCLUSIONS 104

REFERENCES 109

APPENDIX A 117

APPENDIX B 147

LIST OF TABLES

page

Table 2.1: Effect of angularity and grading on peak friction angle 13
Table 2.2: Categories of roundness 20
Table 2.3: Stress-dilatancy relations 41
Table 2.4: Relations of M_i after different authors 42
Table 2.5a: Constitutive models for sands 45
Table 2.5b: Constitutive models for sands 46
Table 2.6: Summary of equations for NorSand 54
Table 2.7: Properties needed to describe the NorSand constitutive model and their typical range for sand 55
Table 2.8: Summary of CSSM constitutive models 57
Table 3.1: Properties of the grain size distribution curve 58
Table 3.2: e_{max} calculations for Badger sand 60
Table 3.3: e_{min} calculations for Badger sand 61
Table 3.4: Relation between t for a 95% confidence and size "n" of a sample 65
Table 3.5: Sphericity of Badger sand 65
Table 3.6: Roundness of Badger sand 66
Table 3.7: Codes and characteristics of tests 71
Table 4.1: Relative dilatancy index for Badger sand 81
Table 4.2: Rate of dilatancy for Badger sand 82
Table 4.3: Maximum contraction friction angle for Badger sand 82
Table 4.4: Phase transformation friction angle for Badger sand 84
Table 4.5: Different friction angles for Badger sand 86
Table 4.6: Values of roundness and void ratio for various sands 87
Table 4.7: Friction angles for Ottawa sand and Fraser River sand 88
Table 4.8: Parameters summary of NorSand for Badger sand 103
Table 5.1: Summary of Badger sand parameters 106
Table A.1: System of units used by FLAC 121
Table A.2: Parameter summary for NorSand model 143

LIST OF FIGURES

page

Figure 2.1: Effective stresses on a soil element 6
Figure 2.2: Drained and undrained stress path for compression triaxial test 11
Figure 2.3: Drained and undrained stress-strain response for (a) loose sand specimens (b) dense sand specimens 11
Figure 2.4: Contributions to shear strength of granular soils 14
Figure 2.5: Maximum obliquity friction angle and phase transformation friction angle 17
Figure 2.6: Measurement of pebble diameters 20
Figure 2.7: Relations between roundness and minimum and maximum void ratios 21
Figure 2.8: Mohr-Coulomb yield surface with an associated flow rule 25
Figure 2.9: Zones on the q-p' diagram 25
Figure 2.10: Definition of normality 26
Figure 2.11: Difference between rate and absolute definitions of dilatancy 26
Figure 2.12: Shape of the CSL 33
Figure 2.13: CSL in the e-ln(p') space 33
Figure 2.14: Work done in a quadrilateral element 36
Figure 2.15: Original Cam Clay yield surface 36
Figure 2.16: Modified Cam Clay yield surface 38
Figure 2.17: Illustration of consistency condition 38
Figure 2.18: Four-step loop to solve plasticity models 39
Figure 2.19: Nova's stress-dilatancy rule 42
Figure 2.20: Comparison of stress-dilatancy relations 43
Figure 2.21: Difference between state parameter and overconsolidation, infinity of NCL 50
Figure 2.22: NorSand image condition on yield surface (ys) 53
Figure 2.25: Definition of χ: D^P versus ψ 53
Figure 3.1: Grain size distribution curve of Badger sand 59
Figure 3.2: Microscope photograph: well-rounded particles 59
Figure 3.3: e_{max} and e_{min} determinations 62
Figure 3.4: Correlations between minimum and maximum void ratio 62
Figure 3.5: Angle of repose of Badger sand 64
Figure 3.6: Sphericity and roundness after Santamarina and Cho (2004) 66
Figure 3.7: Triaxial apparatus 68
Figure 3.8: Schematic diagram of UBC triaxial apparatus 68
Figure 3.9: Sand sample before testing (dummy sample) 72
Figure 3.10: Shape of the specimen after testing (CDP100) 72

Figure 3.11: Triaxial (CD) test results: a) deviator stress and b) volumetric strain 74
Figure 3.12: Triaxial (CU) test results: a) deviator stress and b) excess pore pressure 75
Figure 3.13: Triaxial test results: void ratio 76
Figure 3.14: Triaxial test results: stress path 76
Figure 3.15: G_{max} in function of mean stress for Badger sand 77
Figure 4.1: D_{min} versus η_{max} for CDP50, CDP100 and CDP150 80
Figure 4.2: Stress dilatancy plot for CDP100 80
Figure 4.3: Relation between angle of repose and maximum contraction friction angle 83
Figure 4.4: Relation between roundness and extreme void ratios 88
Figure 4.5: Relation between roundness and constant volume friction angle 89
Figure 4.6: Comparison of deviator stress and volumetric strain between triaxial data and NorSand model for CDP50 91
Figure 4.7: Comparison of deviator stress and volumetric strain between triaxial data and NorSand model for CDP100 92
Figure 4.8: Comparison of deviator stress and volumetric strain between triaxial data and NorSand model for CDP150 93
Figure 4.9: Comparison between CDP100 and NorSand model for a greater hardening 94
Figure 4.10: Comparison of deviator stress pore water pressure between triaxial data and NorSand model for CUP100 95
Figure 4.11: Comparison of deviator stress pore water pressure between triaxial data and NorSand model for CUP150 96
Figure 4.12: Comparison of deviator stress pore water pressure between triaxial data and NorSand model for CUP100, for R =2 97
Figure 4.13: Critical State Line and void ratios 100
Figure 4.14: Dilation at peak strength, D_{min}, as a function of the state parameter 100
Figure 4.15: Stress-Dilatancy comparison between NorSand and CDP100 102
Figure 4.16: Zoom of stress-dilatancy for CDP100 102
Figure A.1: General flow chart 119
Figure A.2: Example of FLAC model 120
Figure A.3: FLAC zone divided in 4 triangles; triangular element with velocity vectors; nodal force vector 120
Figure A.4: Positive shear stress (or strain) convention and associated distortion 122
Figure A.5: Force acting on a mass 128
Figure A.6: Flow chart Model Modified Cam Clay fish function 135
Figure A.7: Original Cam Clay fish function flow chart 139
Figure A.8: Comparison of deviator stress and volumetric strain for Original Cam Clay, between VBA code and FLAC results 140

Figure A.9: NorSand fish function flow chart 144
Figure A.10: Comparison of deviator stress and volumetric strain for NorSand, between VBA Code and FLAC results for a loose state 145
Figure A.11: Comparison of deviator stress and volumetric strain for NorSand, between VBA Code and FLAC results for a dense state 146

LIST OF SYMBOLS

C_c: coefficient of curvature

C_u: coefficient of uniformity

χ: dilatancy rate parameter

D: dilatancy

D^{ABS}: absolute dilatancy ($D^{ABS} = \varepsilon_v / \varepsilon_q$)

$\dot{D}$: rate of dilatancy ($\dot{D} = \dot{\varepsilon}_v / \dot{\varepsilon}_q$)

D_{min}: peak dilatancy

DR: relative density

D_{85}: the 85% size

D_{60}: the 60% size

D_{50}: the 50% size

D_{30}: the 30% size

D_{15}: the 15% size

D_{10}: the 10% size

dV: change of volume

e: void ratio

e_c: critical void ratio

e_{max}: maximum void ratio

e_{min}: minimum void ratio

ε_1: strain in principal direction 1

ε_2: strain in principal direction 2

ε_3: strain in principal direction 3

ε_v: volumetric strain ($\varepsilon_v = \varepsilon_1 + \varepsilon_2 + \varepsilon_3$)

ε_q: shear strain ($\varepsilon_q = 2/3(\varepsilon_1 - \varepsilon_3)$)

η: effective stress ratio ($\eta = q/p'$)

E: Young's modulus

F: yield surface

G: elastic shear modulus

H: hardening parameter

I_e: void ratio difference

I_r: NorSand elastic property

I_R: *relative dilatancy index*

κ: *slope of the elastic line in the e-ln(p') space*

K: *Rowe's constant*

K: *bulk modulus*

λ: *slope of the critical state line in the e-ln(p') space*

λ_s: *plastic multiplicator*

Γ: *void ratio at p' = 1kPa*

M: *critical effective stress ratio*

M_i: *M at image condition*

N: *Nova's volumetric coupling parameter*

ν : *Poisson's ratio*

p' : *mean effective stress*

p_c': *mean effective stress at critical state*

p_{cn}': *mean consolidation pressure of the current yield surface*

p_i': *p' at image condition*

ψ: *state parameter*

ψ_i: *state parameter at image condition*

υ: *specific volume*

ϕ_{repose}: *angle of repose*

ϕ_{CV}: *constant volume friction angle*

ϕ_p: *peak friction angle*

ϕ_{MC}: *maximum contraction friction angle*

ϕ_{PT}: *phase transformation friction angle*

ϕ_{MO}: *maximum obliquity friction angle*

q : *deviator stress invariant*

Q: *plastic potential*

R: *roundness, overconsolidation ratio*

S: *sphericity*

σ_1': *effective stress in principal direction 1*

σ_2': *effective stress in principal direction 2*

σ_3': *effective stress in principal direction 3*

θ: *Lode angle*

u: *pore water pressure*

V: *volume*

V_0: *initial volume*

V_s: *volume of solids*

W: *work*

Notes:

- *The superscripts "e" and "p" refer to elastic and plastic, respectively*
- *The subscript "tc" refers to triaxial compression*
- *The symbol* $\dot{}$ *refers to "rate of" or "increment"*

ACKNOWLEDGMENTS

I would like to thank my supervisors, Dr. Dawn Shuttle and Dr. Jonathan Fannin, for their time and guidance during this study. Without their support and advice this study would not have been possible.

I would also like to thank Dr. Mike Jefferies for his personal communication and very useful comments, and Dr. John Howie for reviewing this manuscript and providing helpful input.

Thanks to my colleagues in the Graduate Soil Mechanics Laboratory at UBC for their useful discussions and help.

Finally, I would like to thank Pablo for his support and love during this process and his understanding when working until late and on weekends.

CHAPTER I: INTRODUCTION

The engineering study of soils requires a knowledge of the stress-strain behaviour of the material and its intrinsic properties, such as maximum and minimum void ratios and strength parameters. The constant volume friction angle is of particular interest, given the importance of this parameter to engineering analyses. In the case of coarse-grained soils, factors including grain size distribution, fines content, mineralogy and grain shape all influence the intrinsic properties such as void ratio and friction angle. Recent efforts have sought to correlate the influence of the grain shape, quantified by an index value of roundness (R), on these intrinsic properties of sands. Several authors have found that the minimum and maximum void ratios, as well as the constant volume friction angle, decrease as the roundness of the particles increases. Most of the studies make reference to sub-angular to rounded sands ($0.1<R<0.7$), and to perfectly spherical glass beads ($R\approx1$). It transpires that few data are published for the intervening grain shape given by well-rounded sands.

In addition, numerical modelling is more commonly used in engineering design, as well as for behaviour prediction of soils and structures. Different constitutive models of varying complexity have been developed in order to capture soil behaviour. These models have been implemented in simple codes such as Visual Basic for Applications (VBA) or in more complex commercially available software.

This study addresses the influence of grain shape on the behaviour of sands: more specifically, it examines the influence of roundness on properties such as minimum and maximum void ratio, and the angle of shearing resistance. Additionally, the NorSand constitutive model is evaluated for its ability to capture the behaviour of a well-rounded sand.

Given the focus of the research, a laboratory testing program was undertaken on a uniformly graded, well-rounded coarse sand, referred to as "Badger sand", in order to determine its properties. The roundness of Badger sand was quantified, and its strength properties established from analysis of the response to drained and undrained loading in triaxial compression. The findings were related to, and then compared with, available data for sands in the literature.

The comparison makes reference to the state of the art on the quantification of various friction angles used to characterize the response to shearing, including the constant volume friction angle, phase transformation friction angle and maximum contraction friction angle, among others.

The NorSand constitutive model was used to predict the behaviour of Badger sand. NorSand has been able to capture the behaviour of sands such as, Erksak sand (Jefferies and Shuttle, 2005), Brasted sand (Jefferies and Shuttle, 2002) and Ticino sand (Shuttle and Jefferies, 1998) which are more angular sands than Badger sand. An objective of this study is to verify that NorSand is also able to capture the behaviour of well-rounded sands, such as Badger sand.

1.1. Purpose of the study

The main objectives of this study are:

- Measure physical properties of Badger sand grains, such as roundness, and the grain assembly, such as minimum and maximum void ratio.
- Determine strength parameters of Badger sand, including the angle of repose, failure envelope friction angle, phase transformation friction angle, maximum contraction friction angle and constant volume friction angle.
- Correlate the roundness of Badger sand with its extreme void ratios, and constant volume friction angle, and contrast those findings with relations for sands in the literature.
- Compare the relative magnitude of the different friction angles obtained for Badger sand, and examine the implications for characterization of well-rounded sands.
- Determine the elastic, plastic and critical state properties of Badger sand for modelling purposes.
- Capture the behaviour of Badger sand with the NorSand constitutive model within FLAC.

To meet these objectives, a triaxial testing program was undertaken and the results obtained used to establish parameters for the sand that were verified through comparison with findings reported in the literature. Finally, parameters needed for the NorSand constitutive model are obtained.

1.2. Organization of the thesis

In Chapter II a literature review is presented explaining the drained and undrained behaviour of sands, defining the different friction angles mobilized during laboratory testing and introducing two concepts for characterization of the grain shape, namely, roundness and sphericity. In addition, the concept of critical state soil mechanics (CSSM) is defined and a description provided for three constitutive models (Original Cam Clay, Modified Cam Clay and NorSand) that are based on the CSSM.

Chapter III describes the sand used for this research and the program of laboratory testing undertaken in the graduate geotechnical laboratory at UBC. Results obtained from the laboratory testing program are also presented.

A discussion and analysis of results is presented in Chapter IV. First is a discussion of the parameters obtained from tests on the well-rounded badger sand described in Chapter III, followed by a comparison of those results with values for other sands found in the literature. Finally the NorSand model is used to fit the tests, and the parameters needed for modelling purposes are obtained and discussed.

A summary of these findings and the companion conclusions is given in Chapter V.

In addition the implementation of NorSand within FLAC (Fast Lagrangian Analysis of Continua) is explained in Appendix A. First a brief description of the FLAC program is presented, followed by an explanation of the steps taken to code the NorSand model.

CHAPTER II: LITERATURE REVIEW

The shear strength of a sand depends on several factors, including the type of loading (triaxial compression, triaxial extension, plane strain), type of drainage (drained or undrained), initial state (loose or dense), and initial fabric. Recently, it has been shown that the so-called intrinsic characteristics of sands are also a function of the shape of the grain particles. In order to capture the behaviour of sands, several constitutive models have been proposed. In this chapter, first, a general description of sand behaviour is given, followed by a definition of the various friction-related angles mobilized during the shearing of a sand specimen, after which the concepts of roundness and sphericity are reviewed. Then a description is provided of different constitutive models, starting with Original Cam Clay, followed by Modified Cam Clay, which are the first Critical State Soil Mechanics constitutive models, and finally a description of NorSand, the first CSSM constitutive model able to capture the real behaviour of sands.

2.1. Behaviour of sands

2.1.1. General stress-strain behaviour of soils

The general stresses and strains on a soil element are shown in Figure 2.1. Stresses acting perpendicular to the planes in the 1,2,3-direction are σ_{11}' , σ_{22}' and σ_{33}', respectively. The stresses σ_{ij}' are determined using the suffix i to indicate the direction of the normal stress to that plane and the suffix j to indicate the actual direction of the stress. The stress matrix can be written as:

$$\sigma_{ij}' = \begin{bmatrix} \sigma_{11}' & \sigma_{12}' & \sigma_{13}' \\ \sigma_{21}' & \sigma_{22}' & \sigma_{23}' \\ \sigma_{31}' & \sigma_{32}' & \sigma_{33}' \end{bmatrix} \qquad 2.1$$

where σ_{ij}' is symmetrical and $\sigma_{12}' = \sigma_{21}'$, $\sigma_{13}' = \sigma_{31}'$ and $\sigma_{32}' = \sigma_{23}'$, hence six independent components are needed to describe the stresses on a soil element.

Similarly, the stress increment is written as:

$$\dot{\sigma}_{ij}' = \begin{bmatrix} \dot{\sigma}_{11}' & \dot{\sigma}_{12}' & \dot{\sigma}_{13}' \\ \dot{\sigma}_{21}' & \dot{\sigma}_{22}' & \dot{\sigma}_{23}' \\ \dot{\sigma}_{31}' & \dot{\sigma}_{32}' & \dot{\sigma}_{33}' \end{bmatrix} \qquad 2.2$$

where $\dot{\sigma}_{ij}'$ is symmetrical and is the difference in effective stress due to the load increment applied to the element.

When the load increment is applied, the displacement of the element is decomposed in three parts comprising, displacement, rotation and distortion, and the corresponding strain increment can be written as:

$$\dot{\varepsilon}_{ij}' = \begin{bmatrix} \dot{\varepsilon}_{11}' & \dot{\varepsilon}_{12}' & \dot{\varepsilon}_{13}' \\ \dot{\varepsilon}_{21}' & \dot{\varepsilon}_{22}' & \dot{\varepsilon}_{23}' \\ \dot{\varepsilon}_{31}' & \dot{\varepsilon}_{32}' & \dot{\varepsilon}_{33}' \end{bmatrix} \qquad 2.3$$

where $\dot{\varepsilon}_{ij}'$ is symmetrical.

It is possible to find the principal stresses and strains in three orthogonal planes, where no shear stress or strain occurs. The stress matrix can be written as:

$$\begin{bmatrix} \sigma_1' & 0 & 0 \\ 0 & \sigma_2' & 0 \\ 0 & 0 & \sigma_3' \end{bmatrix} \qquad 2.4$$

where 1, 2 and 3 are the principal stress directions. The matrix for the stress increment and strain increment can be written under the same form, but the principal directions are not necessarily the same as the principal stress directions.

2.1.2. Triaxial testing

Compression triaxial tests are widely used to characterize the strength of soils. A cylindrical specimen is typically subjected to an hydrostatic confining pressure $(\sigma_0' = \sigma_3')$ and then sheared by means of an axial load $(\sigma_0' + \Delta\sigma' = \sigma_1')$. Axial displacement is measured as the specimen deforms; volumetric strain is measured if the test is performed under drained conditions, or pore water pressure if the test is undrained.

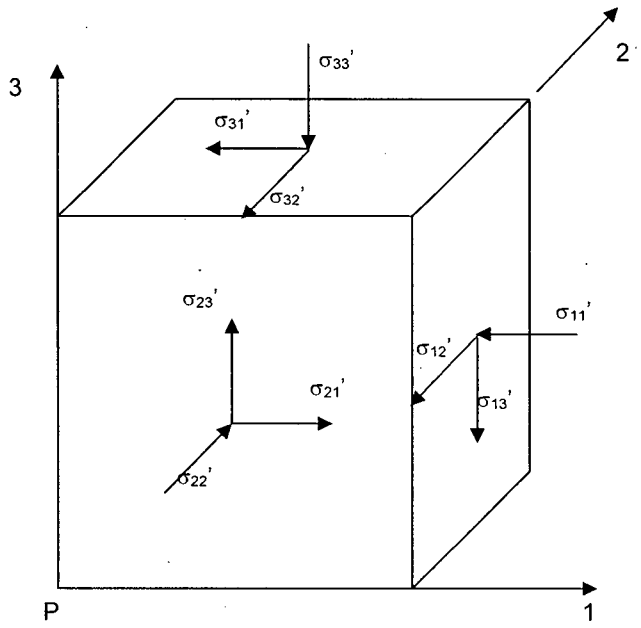

Figure 2.1: Effective stresses on a soil element

As the sample is loaded, it is possible to obtain a relation between stress and strain. The slope of the stress-strain curve gives the Young's modulus (or elastic modulus), given by:

$$E = \frac{\Delta\sigma'}{\varepsilon} \qquad 2.5$$

When the element in Figure 2.1 is subjected to an isotropic stress, the volumetric change, ε_v is:

$$\varepsilon_v = \frac{dV}{V_o} \qquad 2.6$$

where V_o is the initial volume of the element and dV is the change in volume.

The general strains in an elastic element having constant isotropic elastic stiffness are given by:

$$\varepsilon_1 = \frac{1}{E}\left(\Delta\sigma_1' - \nu\Delta\sigma_2' - \nu\Delta\sigma_3'\right)$$
$$\varepsilon_2 = \frac{1}{E}\left(-\nu\Delta\sigma_1' + \Delta\sigma_2' - \nu\Delta\sigma_3'\right) \qquad 2.7$$
$$\varepsilon_3 = \frac{1}{E}\left(-\nu\Delta\sigma_1' - \nu\Delta\sigma_2' + \Delta\sigma_3'\right)$$

where, ν is the Poisson's ratio.

The volumetric strain is the sum of the strains in the three principal directions, and is given by:

$$\varepsilon_v = \varepsilon_1 + \varepsilon_2 + \varepsilon_3 \qquad 2.8$$

From the principal stress matrix (Eq. 2.4), the mean effective stress, p', and deviator stress, q, are defined by:

$$p' = \frac{1}{3}\left(\sigma_1' + \sigma_2' + \sigma_3'\right) \qquad 2.9$$
$$q = \sqrt{\frac{1}{2}\left[\left(\sigma_1' - \sigma_2'\right)^2 + \left(\sigma_2' - \sigma_3'\right)^2 + \left(\sigma_3' - \sigma_1'\right)^2\right]}$$

Stress and strain invariants should be work-conjugate, meaning that the stresses and strains components and the invariants can be used interchangeably in the equation of work. Hence:

$$\text{Work done per unit volume} = q\dot{\varepsilon}_q + p'\dot{\varepsilon}_v = \sigma'_1\dot{\varepsilon}_1 + \sigma'_2\dot{\varepsilon}_2 + \sigma'_3\dot{\varepsilon}_3 \qquad 2.10$$

Where $\dot{\varepsilon}_q$ and $\dot{\varepsilon}_v$ are the shear strain increment and volumetric strain increment, respectively.

Special care is needed when choosing the shear strain component in 3-D. As the volumetric and shear strains are separated, it is necessary to find a work conjugate expression for the shear strain increment, as the volumetric strain increment is already a strain invariant (Eq. 2.8). Rearranging Equation 2.10, the shear strain increment is given by Equation 2.11:

$$\dot{\varepsilon}_q = \frac{s_1 \dot{\varepsilon}_1 + s_2 \dot{\varepsilon}_2 + s_3 \dot{\varepsilon}_3}{q'} \qquad 2.11$$

where $s_1 = (2\sigma_1' - \sigma_2' - \sigma_3'/3)$ and s_2 and s_3 are found by cycling rotation.

By replacing the principal stresses, the work-conjugate shear strain can be written as:

$$\dot{\varepsilon}_q = \frac{1}{3}\left[\left(\sin\theta + \sqrt{3}\cos\theta\right)\dot{\varepsilon}_1 - 2\sin\theta\,\dot{\varepsilon}_2 + \left(\sin\theta - \sqrt{3}\cos\theta\right)\dot{\varepsilon}_3\right] \qquad 2.12$$

Where θ is the Lode angle. For triaxial compression, $\theta = 30^o$. This thesis invokes stresses and strains found in triaxial compression, where $\sigma_2' = \sigma_3'$. Hence, the mean effective stress and deviator stress are given by:

$$p' = \frac{\sigma'_1 + 2\sigma'_3}{3} \qquad 2.13$$
$$q = \sigma'_1 - \sigma'_3$$

Similarly, the volumetric strain for triaxial compression is given by:

$$\varepsilon_v = \varepsilon_1 + 2\varepsilon_3 \qquad 2.14$$

The total mean stress and deviator stress are given by:

$$p = p' + u \qquad 2.15$$
$$q = q'$$

where u is the pore water pressure.

The bulk modulus, K, is defined as the ratio between the change in mean stress and change in volumetric strain. It represents the change of size at constant shape and is given by:

$$K = \frac{\dot{p}'}{\dot{\varepsilon}_v} \qquad 2.16$$

where $\dot{p}'$ is the mean effective stress rate (from Eq. 2.13) and $\dot{\varepsilon}_v$ is the volumetric strain rate (from Eq. 2.8).

The shear strain is given by:

$$\varepsilon_q = \frac{2}{3}(\varepsilon_1 - \varepsilon_3) \qquad 2.17$$

The shear modulus represents the distortional part, ie, the change in shape at constant volume and it is independent of drainage conditions. G is given by:

$$3G = \frac{\dot{q}}{\dot{\varepsilon}_q} \qquad 2.18$$

Finally, the stress ratio, η is defined by:

$$\eta = q/p' \qquad 2.19$$

Figure 2.2 shows a typical stress-path in the q-p' space for the drained and undrained triaxial compression test. Replacing the deviator stress in the mean effective stress, the equation for the drained stress-path is:

$$p' = \frac{q}{3} + \sigma_3' \qquad 2.20$$

This equation corresponds to a slope of 1:3 for drained triaxial compression tests (A -> C).

For an undrained condition, as the sample is loaded, the pore water pressure starts increasing, and the stress path follows A -> B. The difference between the drained and the undrained mean stress (D –> B) is equal to the pore water pressure, u.

At failure, a relation is found between the mean effective stress and the deviator stress given by:

$$q = Mp' \qquad 2.21$$

The friction angle in triaxial compression, ϕ_{tc}, associated with M is given by:

$$\sin\phi_{tc} = \frac{3M}{6+M} \qquad 2.22$$

2.1.3. Triaxial behaviour of sands

Figure 2.3 shows a typical response of (a) loose and (b) dense sand specimens, under drained and undrained loading.

For the loose specimen, the void ratio-confining pressure combination is above the critical state line, which will be defined in details later in this chapter, (point A). If the specimen is tested in the drained condition, the stress-path follows a 1:3 slope and ends in the critical state line (from A to C). For an undrained condition, the stress-path goes from A to B. The difference between the drained and the undrained stress-path corresponds to the pore pressure generated during undrained shear. As seen in Figure 2.3 the drained strength is higher than the undrained strength. For dense sand specimen, the drained stress path follows the same 1:3 slope and exhibits a peak friction angle, and then goes back (following the same path) and stops at the critical state (point F). The undrained stress path ends at point E showing, in this case, a higher strength than the drained case.

Finally in the υ-lnp' space, a loose specimen starts above the critical state line (point A) and finishes at C for a drained condition and at B for an undrained condition. A dense sample starts at the left of the critical state line (point D), shows a decrease in void ratio as the specimen contracts and then an increase in void ratio as the specimen dilates and ends up in the critical state line (point F).

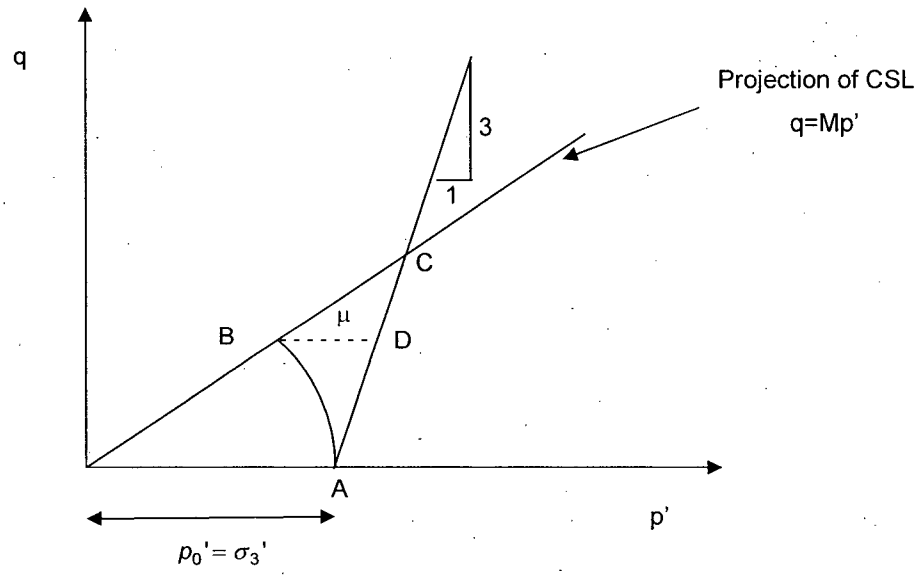

Figure 2.2: Drained and undrained stress path for compression triaxial test

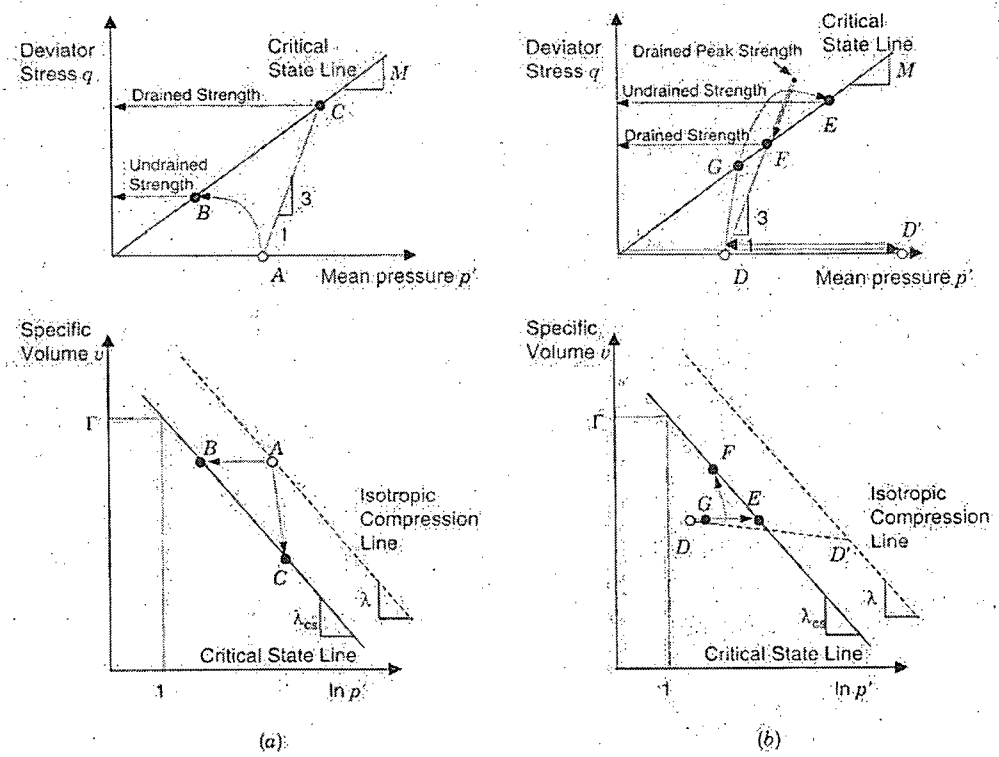

Figure 2.3: Drained and undrained stress-strain response for (a) loose sand specimens (b) dense sand specimens (from Mitchell and Soga, 2005)

2.2. Definition of friction angles for sands

As sand specimens are sheared, different friction angles are mobilized at each state; peak or residual friction angle for dense sands, critical state friction angle, and phase transformation, among others. Some authors have given conflicting definitions to these angles. Hence some confusion exists when trying to determine them from laboratory testing. The intent of this section is to define each of these angles and clearly identify them in order to be able to obtain the values from laboratory testing programs. Consider first the most commonly reported friction angles, namely, angle of repose, constant volume friction angle and peak friction angle. Thereafter a description follows of the maximum contraction friction angle, phase transformation friction angle and maximum obliquity friction angle.

2.2.1. Angle of repose (ϕ_{rep})

Little information is found in the literature about the angle of repose. Some authors have given definitions and have tried to establish which factors influence its value.

After the Dictionary of Earth Sciences (2003) the angle of repose is defined as the "maximum angle at which unconsolidated material can stand. Various factors determine this angle, including particle size and angularity, the degree of interlocking between particles, and pore water pressure."

In order to measure the angle of repose, dry material is deposited as loose as possible through a funnel and the angle of the resulting heap is then calculated. Miura et al (1997) performed several tests to determine the angle of repose (ϕ_{rep}) of four granular materials (two sub angular sands and two rounded materials, glass beads) and the factors influencing its value. They found it decreases as the volume of material used increases, increases with the time elapsed to form the heap and increases with the roughness of the base plate upon which the heap is formed. The latter finding was corroborated by Chik and Vallejo (2005).

The relation between the angle of repose and the angle of internal friction of granular materials is somewhat intriguing. Miura et al (1997) demonstrated that "the angle of repose of sand is equivalent to the angle of internal friction mobilized under low confining pressure within a thin surface sliding layer which is at the loosest state." This statement is in accordance with the observation of Lambe and Whitman (1979) that the angle of repose is approximately equal to the internal friction angle for very loose sands at very low confining pressures.

2.2.2. Critical state or steady state friction angle (ϕ_{cv})

Roscoe et al (1958) defined the critical state as "the state at which a soil continues to deform at constant stress and constant void ratio". Similarly, Poulos (1981) defined the steady state as "the state in which a mass of particles continuously deforms at constant volume, constant normal effective stress, constant shear stress and constant velocity". Independent of the given definition, the critical state or steady state friction angle can be seen as a material property; it is a combination of the particle-to-particle friction angle and the degree of interlocking that can occur with zero overall volume change during continued shear deformation. This angle is related to the critical void ratio, e_c (Lambe, 1979).

Negussey et al (1988) performed ring shear tests on Ottawa sand, a tailings sand, granular copper, lead shot and glass beads in order to determine the effects of initial density, particle size and shape, gradation and confining stress, on the value of ϕ_{cv}. They found that value of the critical state friction angle is independent of the previously mentioned factors. This finding is supported by Verdugo (1992) who found that the critical state friction angle is independent of the initial state of the soil. Also Chu (1995) concluded from his tests on Sydney sand that the critical state friction angle is independent of the initial void ratio, but claimed it is a stress level dependent parameter, specially at low confining pressures; the higher the confining pressure, the lower the critical state friction angle.

2.2.3. Peak friction angle (ϕ_p)

A peak friction angle is obtained from tests on dense samples (as shown in Figure 2.3). Grain properties, including angularity and grading, exert an influence on the values of ϕ_p (see Table 2.1). A more angular and well graded soil has a higher peak friction angle.

Table 2.1: Effect of angularity and grading on peak friction angle (from Lambe and Whitman, 1979)

Shape and Grading	Loose	Dense
Rounded, uniform	30°	37°
Rounded, well graded	34°	40°
Angular, uniform	35°	43°
Angular, well graded	39°	45°

The peak friction angle is the sum of the interparticle friction, rearrangement, crushing and dilation as shown in Figure 2.4 (Mitchell and Soga, 2005). This angle is not a material property since it depends on the density of the sample and stress-path (Bolton, 1986). Peak friction angle increases when the void ratio and the mean effective stress decrease. Also, the peak friction angle is related to the rate of dilation of the soil. By correlating data of peak friction angle and constant volume friction angle, for 17 soils, Bolton (1986) found a relation between relative density (Dr) and the mean confining pressure, expressed as the relative dilatancy index, I_R, given by:

$$I_R = Dr(Q - \ln p') - R \qquad 2.23$$

where values of Q=10 and R=1 give the best fit. Further in triaxial compression he found that the peak friction angle and the constant volume friction angle are related through 2.24.

$$\phi_p - \phi_{cv} \approx 3I_R \qquad 2.24$$

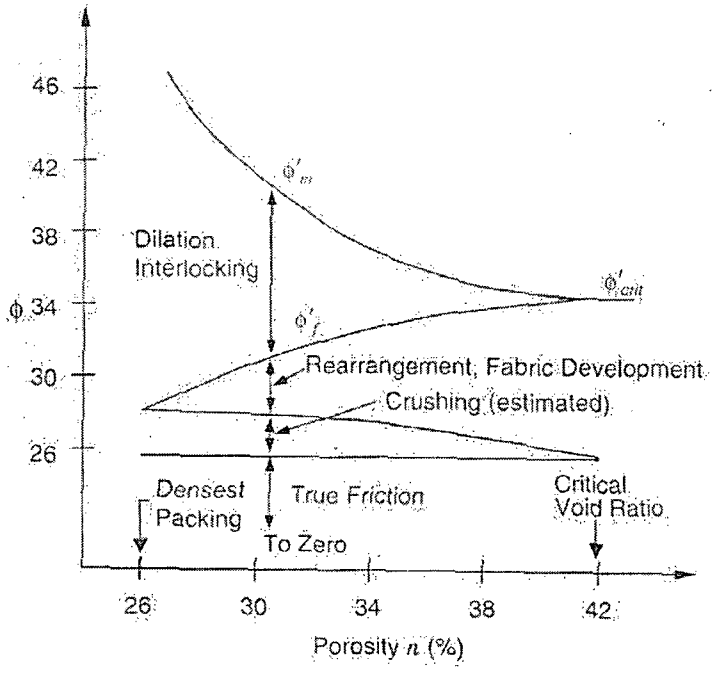

Figure 2.4: Contributions to shear strength of granular soils (from Mitchell and Soga[1], 2005)

[1] In the figure, ϕ'_{crit} corresponds to ϕ_{CV}, ϕ'_m corresponds to ϕ'_p, and ϕ'_f corresponds to the interparticle friction angle

2.2.4. Maximum contraction friction angle (ϕ_{MC})

The term "characteristic state" was proposed by Luong (1980) to define the point where the volumetric deformation passes from contraction to dilation, ie, $\dot{\varepsilon}_v = 0$. This state was also defined as "maximum contraction state" by Negussey et al (1988). Kirkpatrick (1961) found that the maximum contraction friction angle is unique for each sand. However, Negussey et al (1988) found that this angle is not unique and varies with density and confining stress level; this last finding is further confirmed by Chu (1995).

The stress ratio at the characteristic state is given by:

$$\frac{\sigma_1'}{\sigma_3'} = tg^2\left(\frac{\pi}{4} + \frac{\phi_{MC}}{2}\right) \qquad 2.25$$

where ϕ_{MC} is the friction angle mobilized at the characteristic state or maximum contraction state and it is an intrinsic property of the material tested. The subscript "MC" (for maximum contraction) was chosen instead "CS" (characteristic state) for a better distinction with the critical state or constant volume friction angle defined later in this chapter. It is attributed to the point at which interlocking between particles ceases and the disruption of interlocking starts. The characteristic state is independent of the initial void ratio, anisotropy and grain size (Luong, 1980). More studies performed by Luong in monotonic triaxial tests, showed that the characteristic state is also independent of the stress path imposed on the specimen.

For drained triaxial tests under constant confining pressure, the characteristic state separates two regions in the behaviour of sands. A "subcharacteristic" region (or contraction), where the stress ratio η=q/p' is smaller than η_{MC}, which is the stress ratio at maximum contraction, and a "surcharacteristic" region (or dilation), where $\eta > \eta_{MC}$. In the subcharacteristic region, as the soil is loaded, the change in volume is due to interlocking of the sand particles. In the surcharacteristic region, Luong states that "the characteristic state merges with the critical state", a claim that is discussed, together with the concept of a phase transformation angle, in Chapter V with reference to the results obtained in this research.

2.2.5. Phase transformation friction angle (ϕ_{PT})

The state at which the response of the sand, in undrained tests, transforms from positive excess pore water pressure to negative excess pore water pressure is termed phase transformation by Ishihara et al (1975), see Figure 2.5. It corresponds to the maximum excess pore water pressure. The phase transformation state is very important for assessing the risk of liquefaction and limited liquefaction in loose (contractive) sand samples.

Several authors have shown the stress ratio at the phase transformation point is independent of the initial void ratio (Vaid and Chern, 1985), confining stress and loading, and hence it is unique for a sand. This finding is confirmed by Negussey et al (1988) who showed that the phase transformation friction angle is independent of the density of the specimen. However, in contrast Chu (1995) showed that the phase transformation state changes with the initial confining stress and the initial void ratio of soil.

Finally Luong (1980) suggested that the maximum contraction friction angle established in drained tests is the same as the phase transformation friction angle from undrained tests. These findings are confirmed by Chu (1995). However, Negussey et al (1988) suggested that this condition is valid only for loose specimens.

2.2.6. Maximum obliquity friction angle (ϕ_{MO})

The failure envelope or maximum obliquity friction angle corresponds to the state where the effective stress ratio is maximum, ie, $(\sigma_1'/\sigma_3')_{max}$. In undrained tests, at strains larger than that at the phase transformation friction angle, the stress path climbs up and approaches the maximum obliquity line tangentially until the end of the test. It has been shown that the maximum obliquity friction angle is dependent on the angularity of the sand grains and the depositional structure (Al Hattamleh, 2005). Vaid and Chern (1985) observe the failure envelope "represents the upper limit of all undrained effective stress paths, excluding cases when liquefaction occurred". They suggested that the maximum obliquity friction angle is unique for each sand and that it is independent of the initial state before undrained shearing. Vaid and Eliadorani (1998) suggested that the maximum obliquity state in drained triaxial tests is the instant of instability. Figure 2.5 shows a schematic representation on the maximum obliquity friction angle and the phase transformation friction angle.

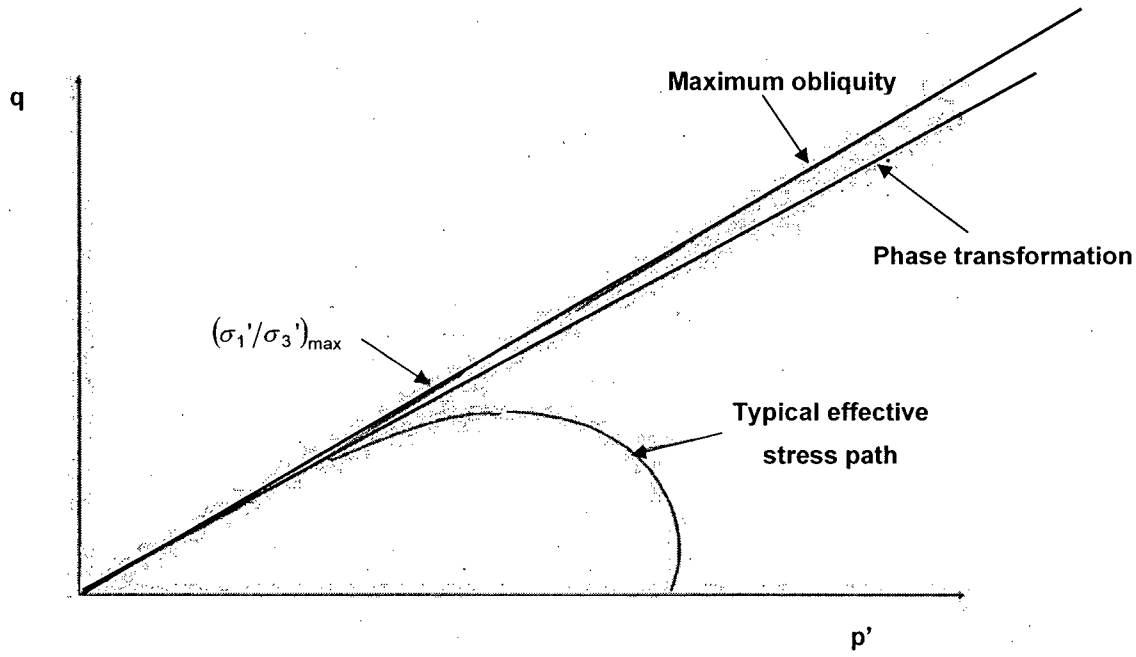

Figure 2.5: Maximum obliquity friction angle and phase transformation friction angle

2.3. Definition of roundness and sphericity

In this section, two concepts are introduced; sphericity (a 3-D phenomenon) and roundness (a 2-D phenomenon). These terms have been in use for many years, and different definitions can be found in the literature.

2.3.1. Sphericity

From the Dictionary of Earth Sciences (2003), *"Sphericity can be determined by examining the relation between the long (L), intermediate (I), and short (S) axes of the particle, the maximum projection Sphericity, ψ , being given by the expression:*

$$\psi = \sqrt[3]{\left(S^2/LI\right)} \qquad 2.26$$

Krumbein (1941) observed sphericity (S) as: *"Fundamentally the shape is a measure of the ratio of the surface area of a particle to its volume. For practical purposes this ratio is difficult to measure, and the actual measurement is expressed in terms of the ratio of the volume of the particle to the volume of its circumscribing sphere. The cube root of this ratio is called the sphericity of the particle."* He considered the long (a), intermediate (b) and short (c) axes as mutually perpendicular intercepts, as shown in Figure 2.6, which yields:

$$S = \sqrt[3]{\frac{(\pi/6)abc}{(\pi/6)a^3}} = \sqrt[3]{\frac{bc}{a^2}} \qquad 2.27$$

Eq. 2.26 and 2.27, for a volumetric calculation of sphericity, are different. However, taking the particular cases of a perfect sphere and an elongated grain, the values of S are equal and both between 0 and 1.

- For a perfect sphere: L = I = S = a = b = c ,

$$S = \sqrt[3]{\frac{S^2}{S^2}} = 1 \text{ and } \psi = \sqrt[3]{\frac{c^2}{c^2}} = 1$$

- For an elongated grain: L = 2I = 4S and a = 2b = 4c,

$$S = \sqrt[3]{\frac{1}{8}} = 0.5 \text{ and } \psi = \sqrt[3]{\frac{1}{8}} = 0.5$$

Santamarina and Cho (2004), defined sphericity as a two-dimensional problem: *"Sphericity is quantified as the diameter ratio between the largest inscribed and the smallest circumscribing sphere".* This latest expression was defined by Mitchell and Soga (2005) as an "Inscribed circle sphericity" given by:

$$S = \frac{r_{max}}{R_{min}} \qquad 2.28$$

2.3.2. Roundness

From the Dictionary of Earth Sciences (2003), the Roundness Index (RI) is defined as *"the average radius of curvature of the corners of a particle, divided by the radius of the maximum inscribed circle for a two-dimensional image of the particle."*

Krumbein (1941) defined the roundness (R) of a particle as "*a measure of the curvature of the corners and edges expressed as a ratio to the average curvature of the particle as a whole, independent of its form. For practical purposes the "average curvature" is expressed in terms of the inscribed circle drawn on a projection of the particle in a plane."*

Santamarina and Cho (2004), defined roundness as*: Roundness is quantified as the average radius of curvature of surface features relative to the radius of the maximum sphere that can be inscribed in the particle."*

The three previous definitions are the same and are given by:

$$R = \frac{\sum \frac{r_i}{N}}{r_{max}} \qquad 2.29$$

Other definitions for roundness are also available but are less used; they are presented for completeness in Equations 2.30 and 2.31 (Mitchell and Soga, 2005):

$$\frac{\text{Radius of curvature of the most convex part}}{0.5(\text{longest diameter through the most convex part})} \qquad 2.30$$

$$\frac{\text{Radius of curvature of the most convex part}}{\text{Mean radius}} \qquad 2.31$$

Powers (1953) proposed a classification table with six intervals to define the roundness of particles, as shown in Table 2.2.

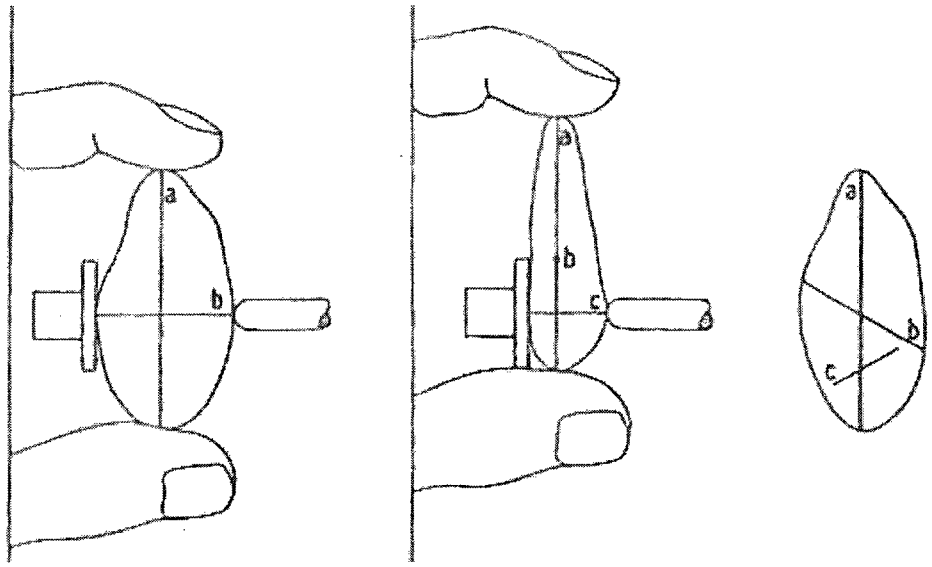

Figure 2.6: Measurement of pebble diameters. Left, the b-axis in position; center, the c-axis in position; right, the pebble in perspective (from Krumbein, 1941)

Table 2.2: Categories of roundness (from Powers, 1953)

Grade Terms	Class Interval	Geometric Means
Very Angular	0.12 – 0.17	0.14
Angular	0.17 – 0.25	0.21
Subangular	0.25 – 0.35	0.30
Subrounded	0.35 – 0.49	0.41
Rounded	0.49 – 0.70	0.59
Well Rounded	0.70 – 1.00	0.84

Several authors have studied the influence of particle shape on material properties such as minimum and maximum void ratios. It has been observed that e_{min} and e_{max} decrease with increasing roundness of the particles. Superimposed in Figure 2.7 are the relations found by Youd (1973), Shimobe and Moroto (1995) and Santamarina and Cho (2004). All three of them obtained the values of roundness using the method described by Powers (1953), corresponding to Equation 2.29. Inspection shows that the values found by Santamarina and Cho define an upper limit for the void ratios and the values of Youd define a lower limit.

Youd (1973) reported the values of e_{min}, e_{max} and R for specimens of Ottawa Sand, Del Monte White Sand, Monterey Sand, Lapis Lacustre Sand and Crushed Basalt, all of them having a coefficient of uniformity $C_u = 1.4$.

Shimobe and Moroto (1995) found a relation between e_{max} and R for uniform samples with a coefficient of uniformity $C_u \leq 2$ based on results obtained with materials as sand, gravel, glass beads and sand mixed with glass beads, given by:

$$e_{max} = 0.642R^{-0.354} \qquad 2.32$$

Based on observations of 54 specimens of angular-crushed and natural-rounded sands, Santamarina and Cho (2004), proposed a relation between the roundness of the particles and the values of e_{min} and e_{max}, defined in Equation 2.33.

$$e_{max} = 0.554 + \frac{0.154}{R} \quad \text{and} \quad e_{min} = 0.359 + \frac{0.082}{R} \qquad 2.33$$

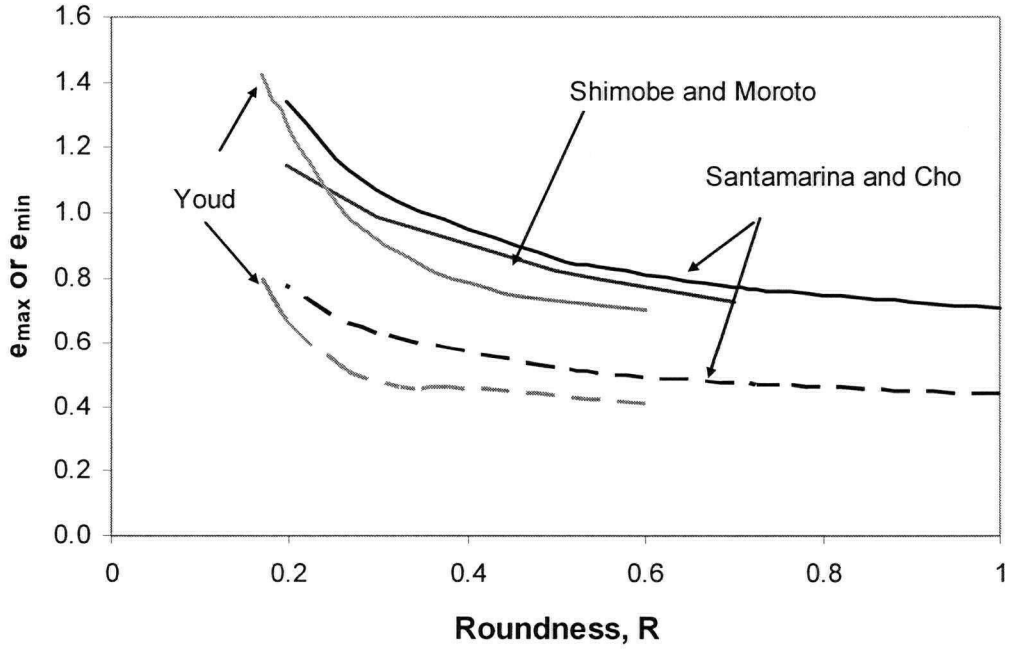

Figure 2.7: Relations between roundness and minimum and maximum void ratios

2.4. Critical State Soil Mechanics

Soil exists in a large variety of densities, going from very loose to very dense, and the stress-strain and volumetric behaviour depend on those variations. Many constitutive models for soils exist where for each density, the model has to recalibrate, (ie, each soil density has a different parameter set). It is more convenient to introduce a constitutive model able to capture and predict the behaviour of soils at different void ratios. This section introduces the concept of Critical State Soil Mechanics (CSSM) and two of the most important and well known constitutive models, Original Cam Clay (Roscoe, Schofield and Thurairajah, 1963) and Modified Cam Clay (Roscoe and Burland, 1968). For convenience, before discussing CSSM consider first general concepts of plasticity.

2.4.1. General plasticity concepts

All elasto-plastic models comprise four main components:

i) elastic properties,
ii) a yield surface which is the locus of stresses leading to plastic strain,
iii) a hardening/softening rule, which determines the size of the yield surface, and
iv) a flow rule which specifies the direction of the plastic strain increment vector.

Each of these terms is considered separately together with other plasticity concepts. The definitions are given below:

- Elasticity:

All plasticity models assume elasticity at very small strains. Elasticity is associated with recoverable strains and a 1:1 relation between stresses and strains, ie, if we know the strain level we also know the stress level.

- Yield surface, F:

In simple words, the yield surface is the interface between an elastic and an inelastic region. Yielding is associated with the occurrence of an irrecoverable, ie plastic, volumetric strain increment $\dot{\varepsilon}_v^p$ and an irrecoverable, plastic, shear strain increment $\dot{\varepsilon}_q^p$.

It was proposed that the yield surface must intersect the NCL in order to have an end, or cap. A cap implies that the model yields in isotropic compression. Hence, the Mohr-Coulomb criterion could not be seen as a yield surface. Finally a curved yield surface which closes was proposed as for example, Figure 2.15. That is the start of critical state soil mechanics.

- Normality:

Taking a point A on the yield surface, as shown in Figure 2.9, there exist three options. When a stress increment is applied, the first option is that a stress increment combination $\left(\dot{q}, \dot{p}'\right)$ moves toward E in the elastic zone. In this case all strains are elastic and no plastic work is done. The second option is that the stress increment combination moves from A toward P into the plastic zone. In that case plastic work is done and energy is dissipated. Finally, the third option is that the stress increment makes A move toward Y, along the tangent to the yield surface. In this case no work is dissipated. Equation 2.34 is the definition of normality.

$$W = \dot{p}' \dot{\varepsilon}_v^p + \dot{q} \dot{\varepsilon}_q^p = 0$$

$$\frac{\dot{\varepsilon}_v^p}{\dot{\varepsilon}_q^p} = -\frac{\dot{q}}{\dot{p}'} \qquad 2.34$$

Figure 2.10 shows the normality condition. With normality, the principal stress and principal strain increment are aligned and the net strain increment vector is normal to the yield surface at the stress state corresponding to the present yielding.

- Plastic potential surface, Q:

For each combination of stresses a vector of plastic strains can be drawn. The curves formed by orthogonal plastic strain increment vectors $\dot{\varepsilon}_v^p : \dot{\varepsilon}_q^p$ are called plastic potentials. After Poorooshasb et al (1966), "the plastic potential curves for a given value of e should form a family of geometrically similar curves." The plastic strain increments are defined as:

$$\dot{\varepsilon}_v^p = \lambda_s \frac{\partial Q}{\partial p'} \quad \text{and} \quad \dot{\varepsilon}_q^p = \lambda_s \frac{\partial Q}{\partial q} \qquad 2.35$$

where λ_s is a scalar which depends on the mode of yielding and determines the incremental magnitude and Q is the plastic potential surface.

If the yield surface (F) and the plastic potential surface (Q) are the same, then the material is obeying the postulate of normality or associated flow.

- Hardening rule:

The hardening rule defines how the size of the yield surface changes with increasing plastic shear strain $\left(\dot{\varepsilon}_q^p\right)$. If the yield surface becomes larger, the material is hardening and if the yield surface becomes smaller, the material is softening.

- Dilatancy:

Stress-dilatancy (or flow rule) relates the stresses and strains increments of a soil. Dilatancy was first defined by Reynolds in 1885 as "dilatancy consists in a definite change of bulk, consequent on a definite change of shape or distortional strain, any disturbance whatever causing a change of volume and generally dilatation. ... A medium composed of grains of any possible shape, possessed this property of dilatancy, so as long as one important condition was satisfied.... This condition is, that the medium should be continuous, infinite in extent, or the grains at the boundary should be so held as to prevent a rearrangement commencing". Two definitions of dilatancy are widely used in North America, the absolute and the rate of dilatancy. Jefferies and Been (2005) defined the absolute dilatancy as "dilation is the change in volumetric strain incurred since the initial condition" given by:

$$D^{ABS} = \frac{\varepsilon_v}{\varepsilon_q} \qquad 2.36$$

The rate of dilatancy is defined as "dilation is the ratio of rate (or increment) of volume change with rate (or increment) of shear strain and given by $\dot{D}$. This is shown in Figure 2.11.

When normality was applied to the Mohr-Coulomb yield surface, dilatancy larger than the ones measured in real soils were found, given that the dilation angle was equal to the friction angle, as shown in Figure 2.8.

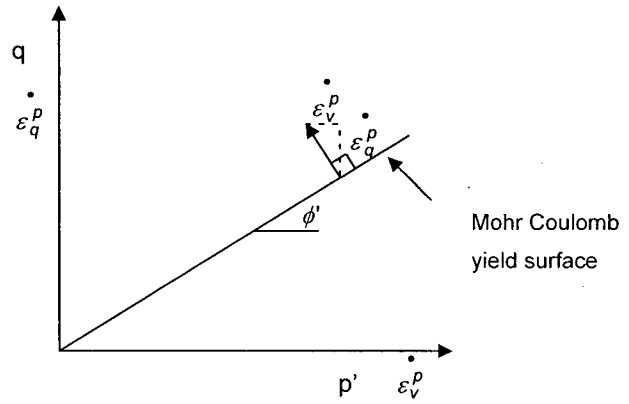

Figure 2.8: Mohr-Coulomb yield surface with an associated flow rule

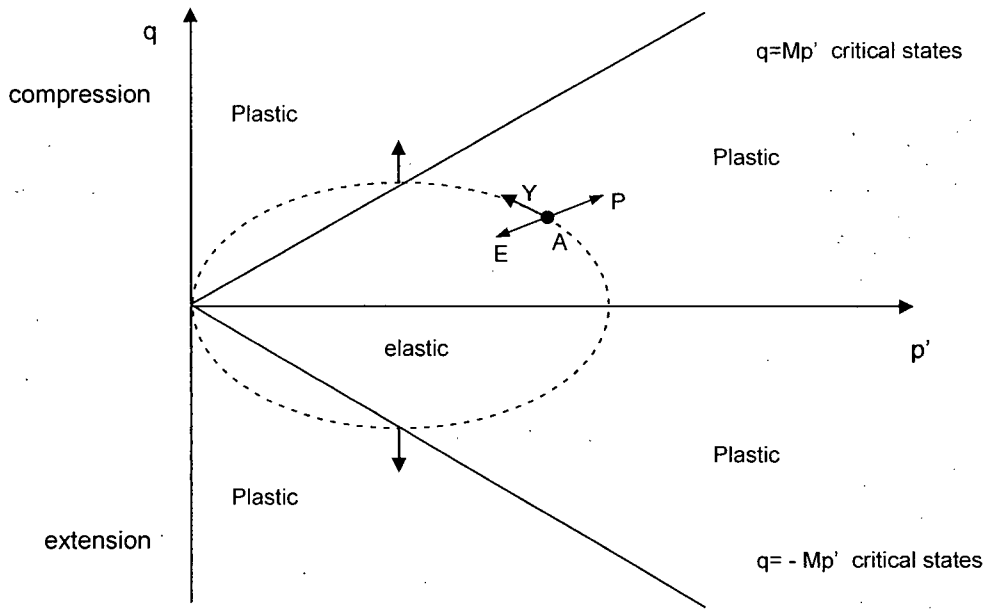

Figure 2.9: Zones on the q-p' diagram (from Bolton, 1979)

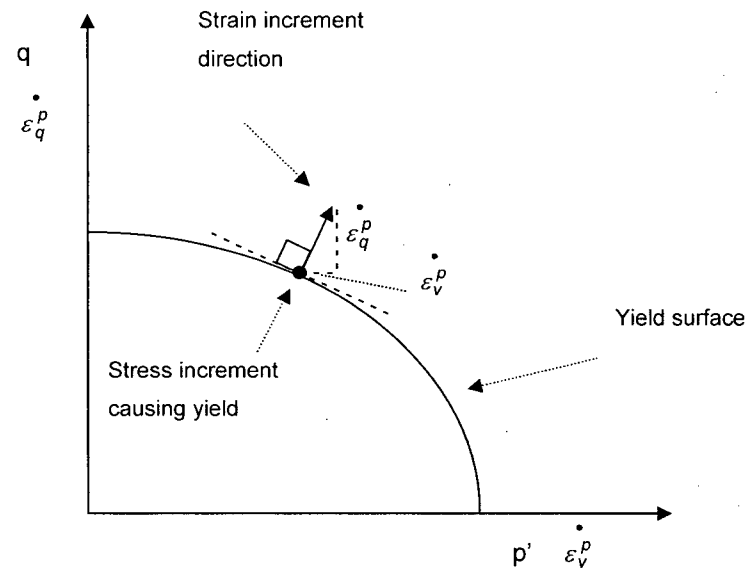

Figure 2.10: Definition of normality

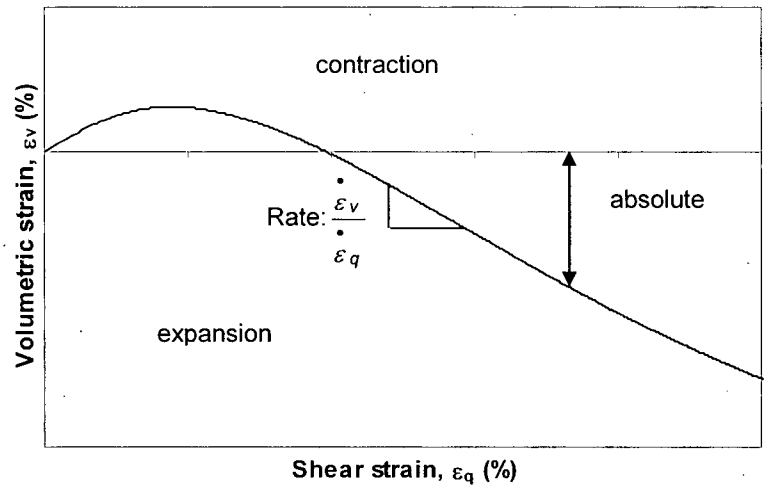

Figure 2.11: Difference between rate and absolute definitions of dilatancy (adapted from Jefferies and Been, 2005)

2.4.2. The critical state

Before the soil mechanics was established as a subject, Reynolds (1885), found that by placing sand and water into "thin india-rubber balloons", the sand tended to change in volume as the bag was squeezed. This observation was reproduced by Casagrande (1936) at MIT in Cambridge MA, who showed experimentally doing drained shear box tests in sands, that "dense sand expands and very loose sand reduces its volume". In addition, Casagrande found that irrespective of the initial density of the sand, loose and dense sands ended up at the same ultimate shear resistance (τ_{ult}) and void ratio. He defined this ultimate void ratio as the "critical void ratio". Later on, Roscoe et al (1958) took Casagrande's idea of "critical void ratio" and defined the critical state of soils as "the state at which a soil continues to deform at constant stress and constant void ratio". Two ideas appeared from this definition, the first is that at the critical state the soil reaches a constant void ratio (or the "critical void ratio") and the second is that this constant void ratio does not change as shearing continues. 10 years later, supervised by Casagrande, Castro (1969) preformed stress controlled triaxial tests on loose sand samples achieving systematically a steady state of deformation at the end of the tests. He defined this state as "steady state line". Finally, Poulos (1981) formalized Castro's idea and defined the steady state as "the state in which a mass of particles continuously deforms at constant volume, constant normal effective stress, constant shear stress and constant velocity". The locus of mean effective stress and void ratio combination at the steady state is referred as the steady state line for undrained tests.

There has been much discussion on whether the critical and steady state are the same (Alarcon-Guzman et al (1988), Oyenuga and Tisot (1989), Been et al (1991), Chu and Lo (1992), Verdugo (1992), and Negussey and Islam (1993), among others). Review of the literature seems to suggest that the only difference between them is in how they are measured; Poulos (1981) suggested that the steady state is measured in undrained tests on fully saturated contractive sand samples and the critical state is obtained from drained tests on dilative sand samples. Been et al (1991) showed that for Erksak 330/0.7 sand, the critical and steady state are the same. This finding is confirmed by Chu (1995).

For critical state soil mechanics, it is assumed that the critical state and the steady state are the same and unique (as discussed later in this Chapter). The concept that when sheared, soils reach the already defined critical state locus is the framework for CSSM.

CSSM models are based on two ideas, formally termed axioms:

- Axiom 1: "A unique locus exists in q, p', e space such that soil can be deformed without limit at constant stress and constant void ratio; this locus is called the critical state locus (CSL)". This axiom can be mathematically represented by Equation 2.37. In simple words, Eq. 2.37 means that there exists ($\exists$) a function C, at a constant mean effective stress, such that ($\ni$) the volumetric strain rate and ($\wedge$) the change in volumetric strain rate must be zero in order to be in the CSL for every ($\forall$) shear strain.

$$\exists C(e,q,p')\Big|_{p'=0} \ni \dot{\varepsilon}_v \equiv 0 \wedge \ddot{\varepsilon}_v \equiv 0 \qquad \forall \varepsilon_q \tag{2.37}$$

where C( ) is the function that defines the CSL which at the critical state has a unique value function of the void ratio and the mean effective stress. This condition is equivalent to the one proposed by Roscoe et al (1958) in terms of dilatancy, where the dilatancy and the rate of dilatancy must be zero $(D = 0)$ and $(\dot{D} = 0)$ at the critical state.

The Second Axiom is stated as:

- Axiom 2: "The CSL forms the ultimate condition of all distortional processes in soil, so that all monotonic distortional stress state paths tend to this locus".

$$e \to e_c \text{ as } \varepsilon_q \to \infty \quad \forall \quad \eta \geq M \tag{2.38}$$

This condition is equivalent to Casagrande's idea that as shear strains develop, the void ratio tends to the critical void ratio.

It is usual to idealise the critical state locus (CSL) as a straight line in the e-lnp' space, however this is not a condition. It is just a mathematical simplification; the critical state locus can be curved.

The CSL in the e-lnp' space is usually written as:

$$e_c = \Gamma - \lambda \ln p_c' \tag{2.39}$$

where Γ corresponds to the void ratio at p' = 1kPa, λ is the slope of the CSL and p_c' is the mean effective stress at the critical state. This is shown in Figure 2.13.

Data on Erksak sand (Been et al 1991) and Toyoura sand (Ishihara, 1993) suggest that the CSL is not a straight line in the e-ln(p') plane. Figure 2.12 shows data on Erksak sand where the critical state line curves at around 1MPa. Been et al (1991) suggested that this break point is given by some breakage of the grains. Verdugo (1992) discusses this idea by showing that if the critical state line is plotted in a bi-linear manner, the curvature of the CSL happens at a lower stress. In addition Verdugo shows that the critical state line is linear at higher stresses when plotted in a linear scale. The shape of the critical state line is not of real importance for the void ratio-mean stress combinations used in practice.

For CSSM the important condition is that the CSL has to be unique. Authors such as Been et al (1991), Verdugo (1992) and Ishihara (1993) found an apparent unique CSL for Erksak and Toyoura sand. However, some authors have suggested that the CSL is not unique and depends on triaxial compression or extension, or initial fabric (for example, Vaid et al, 1990, Negussey and Islam, 1994). Been (1999) discussed the arguments given by the different authors in order to clarify the non-uniqueness of the CSL. He suggests that special care is needed when defining the critical state. The confusion arises when considering the critical state at the phase transformation point, defined by Ishihara et al (1975) also called pseudo or quasi steady state (Alarcon et al, 1988 and Zhang and Garga, 1997). As well, Jefferies, 1999, states that the critical state is defined by dilatancy equal zero but also the rate of dilatancy must be zero, and that choosing the phase transformation point as the critical state is a mistake given that this second condition is not satisfied. This topic is not the intent of this thesis, but it is important to recognize that the uniqueness of the CSL is not universally accepted. For the development of CSSM constitutive models, a unique CSL has been assumed.

As shown in Figure 2.2, in the stress space, the CSL is also unique and defined as:

$$q = Mp' \qquad 2.40$$

where, for triaxial condition, M is given in terms of the friction angle by Eq. 2.22. Note that uniqueness requires a unique locus, not constant M in the π-plane or with p'.

It is important to state that constant M does not mean a constant friction angle. For constant friction angle M varies with the Lode angle, θ, which represents the intermediate principal stress, σ_2'. For triaxial compression, θ has a value of 30° and for triaxial extension θ = -30°. Plotting the Lode angle against the dilatancy for plane strain condition, it is found that θ is not constant. Hence, there is no unique M_{ps} (Jefferies and Shuttle, 2002). The question is how M varies with the Lode angle. Data on Brasted sand shows that for plane strain, M varies between the Mohr-

Coulomb criterion and the Matsuoka-Nakai criterion. For constant friction angle, the Mohr-Coulomb criterion is given by Equation 2.41.

$$M = \left(3\sqrt{3}\right) / \left[\cos\theta\left(1 + 6/M_{tc}\right) - \sqrt{3}\sin\theta\right] \qquad 2.41$$

For triaxial tests, there are different ways to find the value of M. For loose sand specimens, M is found as the value of the stress ratio at the end of the test. However, for dense sand specimens, as they dilate, the critical state can be reached only at very large strains. A different approach to find the critical stress ratio, M, for dense samples was proposed by Bishop (1966). M can be obtained by plotting the maximum stress ratio, η_{max} against the dilation, D_{min}[2], of several drained tests. At the critical state $D_{min}=0$, hence, taking the best fit between the points and projecting to $D_{min}=0$, M is obtained as the value of η_{max} at $D_{min}=0$.

2.4.3. Original Cam Clay formulation

Original Cam Clay was first introduced by Roscoe, Schofield and Thurairajah (1963) and is based on plastic work dissipation. Consider an element where the only stresses acting on it are the principal effective stresses, σ_1', σ_2' and σ_3'. If the sides of this element shorten by the strains ε_1, ε_2 and ε_3, respectively, due to the applications of these stresses (Figure 2.14), then the work per unit volume is given by:

$$W = \sigma_1'\varepsilon_1 + \sigma_2'\varepsilon_2 + \sigma_3'\varepsilon_3 \qquad 2.42$$

Here, two assumptions have been made. The first is that the effective stresses are constant during the strain increment and that the change of area and volume of the element is not affected by the small strains.

Using work conjugate stress and strain invariants:

$$\text{Work done per unit volume} = q\dot{\varepsilon}_q + p'\dot{\varepsilon}_v = \sigma'_1\dot{\varepsilon}_1 + \sigma'_2\dot{\varepsilon}_2 + \sigma'_3\dot{\varepsilon}_3 \qquad \text{(Eq. 2.10)}$$

and translating Equation 2.42 for a triaxial condition, the total rate of working per unit volume on the soil skeleton can be divided in an elastic and a plastic component as:

---

[2] Peak dilatancy is D_{min} because of the dilation-negative convention

$$\dot{W} = \dot{W}^e + \dot{W}^p = q\,\dot{\varepsilon}_q + p'\,\dot{\varepsilon}_v \qquad 2.43$$

where the subscript "e" means elastic and "p" means plastic. Here, the elastic part of the work is stored as strain energy (as long as the soil remains in the the κ-line (Figure 2.13)) and the plastic part is dissipated. Another assumption is made here for Original Cam Clay, all deviatoric energy is dissipated, ie, the elastic shear modulus is infinite.

In Figure 2.13, assuming a movement from A to Q, there is a plastic part (A to P) and an elastic part (P to Q). The change in volumetric strain can be written as:

$$\dot{\varepsilon}_v = \frac{e_A - e_Q}{1+e} = \frac{\dot{e}}{1+e} \qquad 2.44$$

Considering the equation of the κ-line as:

$$e = e_\kappa - \kappa \ln p' \qquad 2.45$$

where e_κ is the void ratio for a particular κ-line taken at 1 kPa.

Differentiating Equation 2.45 and replacing in Equation 2.44,

$$\dot{\varepsilon}_v = \frac{\kappa}{p'}\frac{1}{1+e}\dot{p}' \qquad 2.46$$

The elastic bulk modulus is given by:

$$\frac{K}{p'} = \frac{1+e}{\kappa} \qquad 2.47$$

As shown in Equations 2.8 and 2.17, the volumetric and shear strains are linear and can also be decomposed in elastic (P to Q) and plastic (A to P) components. Hence, the plastic rate of working can be written as:

$$\dot{W}^p = q\,\dot{\varepsilon}_q^p + p'\,\dot{\varepsilon}_v^p \qquad 2.48$$

Dividing by the mean effective stress and the plastic shear strain increment in order to make the plastic work rate dimensionless, we have that the dimensionless plastic work rate is just the sum of the plastic dilation rate (D^P) and the stress ratio (q/p'), as shown in Equation 2.49:

$$\frac{\dot{W}^P}{p'\dot{\varepsilon}_q^p} = M = \frac{\dot{\varepsilon}_v^p}{\dot{\varepsilon}_q^p} + \frac{q}{p'} = D^P + \eta \qquad 2.49$$

Original Cam Clay assumes that the dimensionless plastic energy dissipation rate is constant and equal to M.

Equation 2.49 is consistent with the idea that at the critical state, dilatancy , $\dot{\varepsilon}_v^p / \dot{\varepsilon}_q^p$, is equal to zero and the stress ratio η is equal to M.

Hence, rearranging Equation 2.49 gives a stress-dilatancy relation for Original Cam Clay:

$$D^P = M - \eta \qquad 2.50$$

In order to know when the plastic yielding occurs, a yield surface is needed. To derive the yield surface, two assumptions are needed; normality and the previous stress-dilatancy relation (Eq. 2.50).

From the definition of stress ratio $q = \eta p'$ (Eq. 2.19) and taking the differential, the change in shear stress can be written as:

$$\dot{q} = p'\dot{\eta} + \eta\dot{p}' \qquad 2.51$$

Where $\dot{\eta}$ is the change in stress ratio. From normality:

$$\dot{q} = -D^P\dot{p}' \qquad 2.52$$

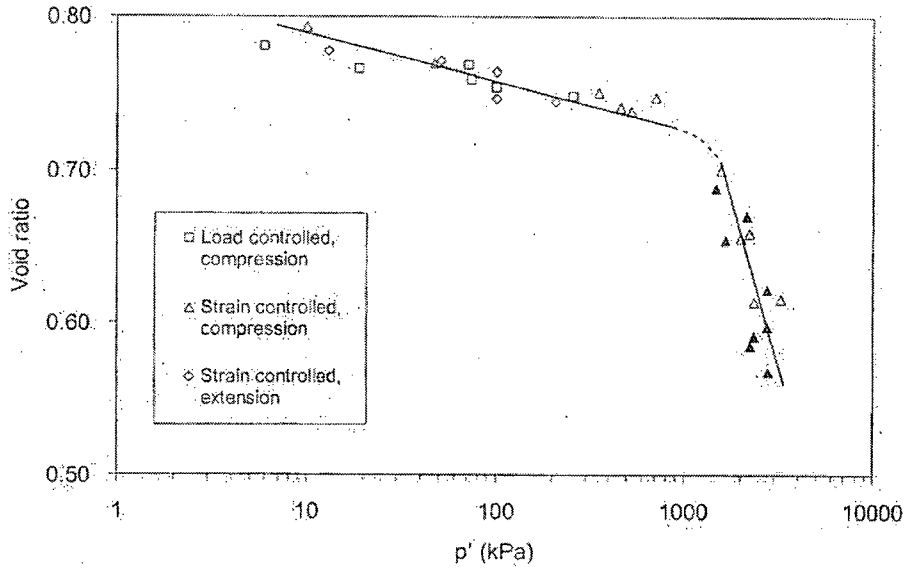

Figure 2.12: Shape of the CSL (from Jefferies and Been, 2005)

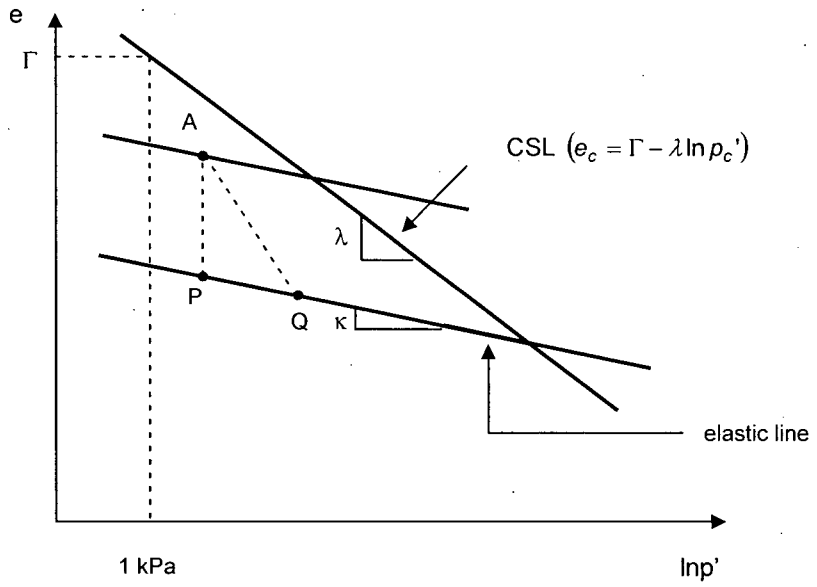

Figure 2.13: CSL in the e-lnp' space (from Bolton, 1979)

Substituting Equation 2.51 in Equation 2.52 and rearranging:

$$\frac{\dot{p'}}{p'} + \frac{\dot{\eta}}{D^P + \eta} = 0 \qquad 2.53$$

Substituting Equation 2.50 in Equation 2.53 and integrating,

$$\ln(p') + \frac{\eta}{M} = C \qquad 2.54$$

The value of the constant C can be determined by substituting the value of ln(p') when η=M (ie, the critical state), the yield surface for Original Cam Clay can be written as:

$$\frac{\eta}{M} = 1 - \ln\left(\frac{p'}{p_c'}\right) \qquad 2.55$$

where p_c' is the pressure where the current elastic line meets with the CSL. p_c' indicates the size of the yield surface. The shape of the yield surface for Original Cam Clay is shown in Figure 2.15.

Equation 2.55 can be written as:

$$F = \ln\left(\frac{p'}{p_c'}\right) + \frac{q}{p'M} - 1 \qquad 2.56$$

The condition F=0 means that the stresses are on the yield surface.

2.4.4. Modified Cam Clay formulation

Original Cam Clay was the first mathematical model able to predict the behaviour of clays. Only three material properties are needed which makes it very simple to use. However, in the late 1960's some problems were found with the predictions given by OCC. First of all, for a condition of isotropic consolidation, OCC predicts shear strains. Secondly, OCC overestimates the values of the strain increments for changes of the stress ratio at small strains and finally OCC seems to overpredict the values of the coefficient of earth pressure at rest (Roscoe and Burland, 1968).

Because of that Modified Cam Clay was developed. Nowadays, Modified Cam Clay is the most widely used advanced constitutive model. Commercial codes as ABAQUS, PLAXIS, CRISP and FLAC have MCC as built-in constitutive models.

To obtain the expressions for MCC, Roscoe and Burland (1968), proposed a new expression for the work dissipation. Assuming that under isotropic stress there is no shear strain and that at the critical state the plastic volumetric strain is equal to zero, they defined:

$$\dot{W} = p' \sqrt{\left[\left(\dot{\varepsilon}_v^p\right)^2 + \left(M\,\dot{\varepsilon}_q^p\right)^2\right]} \qquad 2.57$$

Equation 2.57 ensures that at the critical state the work dissipation rate with respect to total plastic strain is equal to the isotropic state for a given mean effective stress (Burland, 1965).

Combining Equation 2.57 and the work equation for OCC (Eq. 2.48),

$$q\,\dot{\varepsilon}_q^p + p'\,\dot{\varepsilon}_v^p = p' \sqrt{\left[\left(\dot{\varepsilon}_v^p\right)^2 + \left(M\,\dot{\varepsilon}_q^p\right)^2\right]} \qquad 2.58$$

and rearranging, the stress-dilatancy relation for Modified Cam Clay is given by:

$$D^P = \frac{\dot{\varepsilon}_v^p}{\dot{\varepsilon}_q^p} = \frac{M^2 - \eta^2}{2\eta} \qquad 2.59$$

The same procedure used to find OCC yield surface can be used to find the yield surface of Modified Cam Clay. Applying normality and integrating Equation 2.59, we have:

$$\frac{p'}{p_c'} = \frac{M^2}{M^2 + \eta^2} \qquad 2.60$$

MCC yield surface is an ellipse passing through the origin and the size is controlled by p_c'.

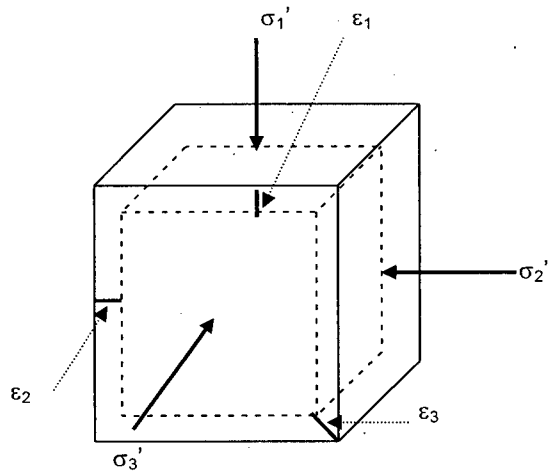

Figure 2.14: Work done in a quadrilateral element

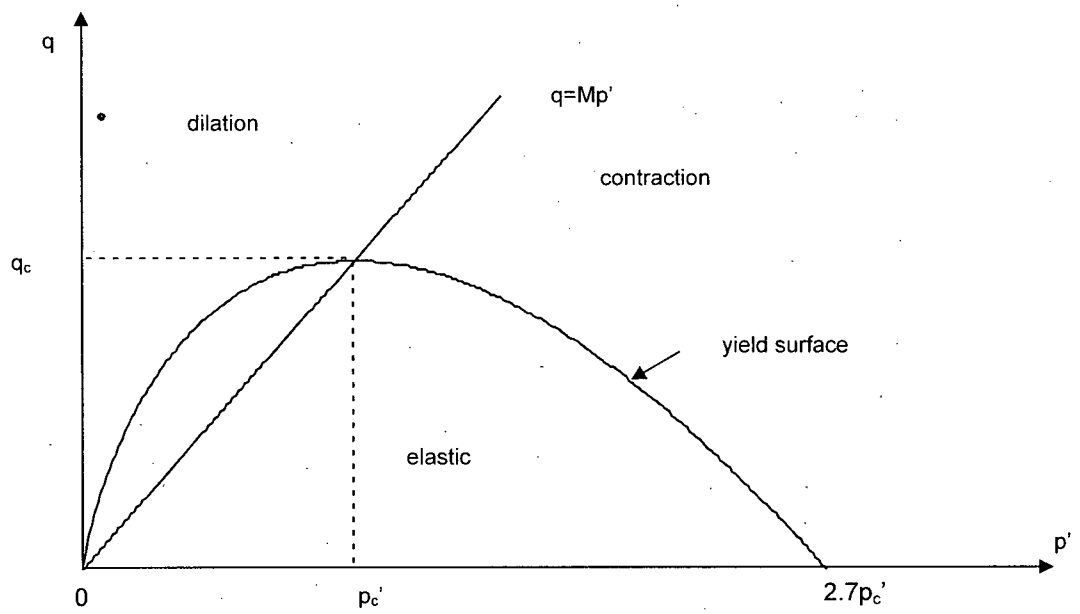

Figure 2.15: Original Cam Clay yield surface

Figure 2.16 shows the shape of Modified Cam Clay yield surface. This new yield surface takes into account the shear distortion without plastic volumetric change.

Work hardening or softening plastic models change the size of their yield surface with plastic strain. The stresses must stay on the yield surface during plastic strain or else the stress point would be in illegal space (ie, beyond the yield surface). The consistency condition is the name given to the condition that a loading stress starts and finishes on the yield surface, and is given by:

$$\dot{F} = 0 \qquad 2.61$$

This is shown in Figure 2.17.

Differentiating the equation of the yield surface, F, (Eq. 2.55), the consistency condition is given by:

$$\dot{\eta} = M\left(\frac{\dot{p_c}'}{p_c'} - \frac{\dot{p}'}{p'}\right) \qquad 2.62$$

The first term of the previous equation is the hardening rule as it controls the size of the yield surface via p_c'. It is obtained by differentiating the CSL:

$$e_c = \Gamma - \lambda \ln p_c' \qquad \text{(Eq. 2.39)}$$

$$\frac{\dot{p_c}'}{p_c'} = \frac{(1+e)\dot{\varepsilon}_v^p}{\lambda - \kappa} \qquad 2.63$$

Figure 2.18 shows a four steps-loop in order to solve plasticity models.

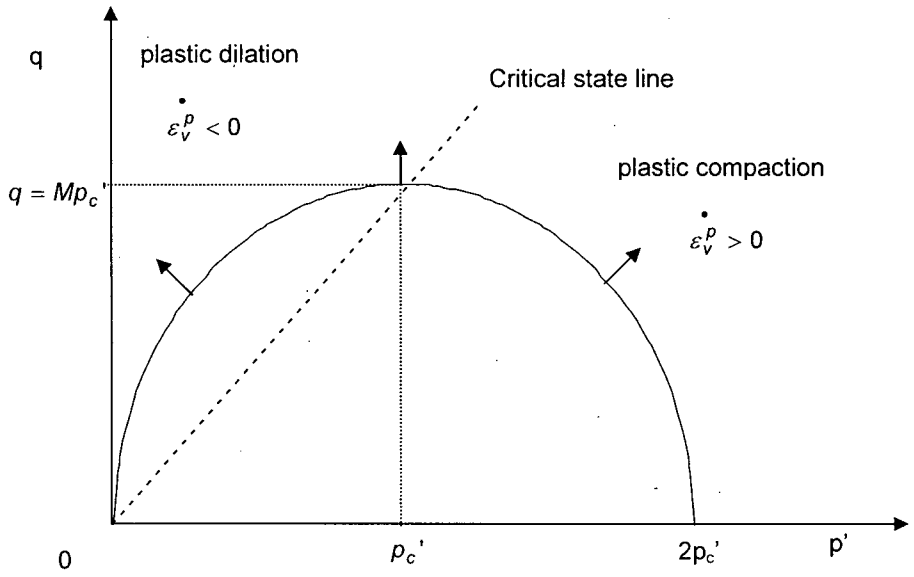

Figure 2.16: Modified Cam Clay yield surface

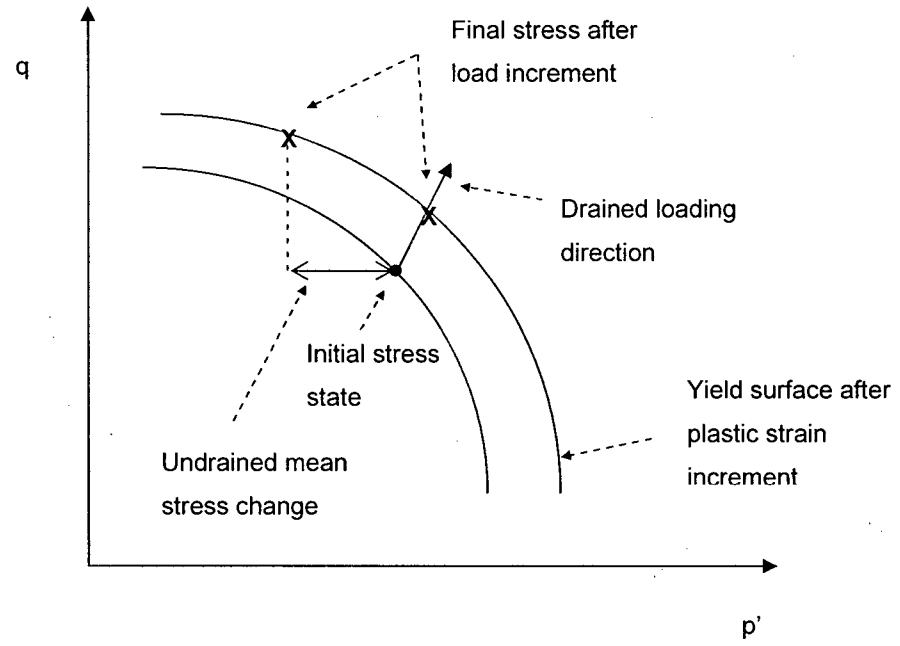

Figure 2.17: Illustration of consistency condition (from Jefferies and Been, 2005)

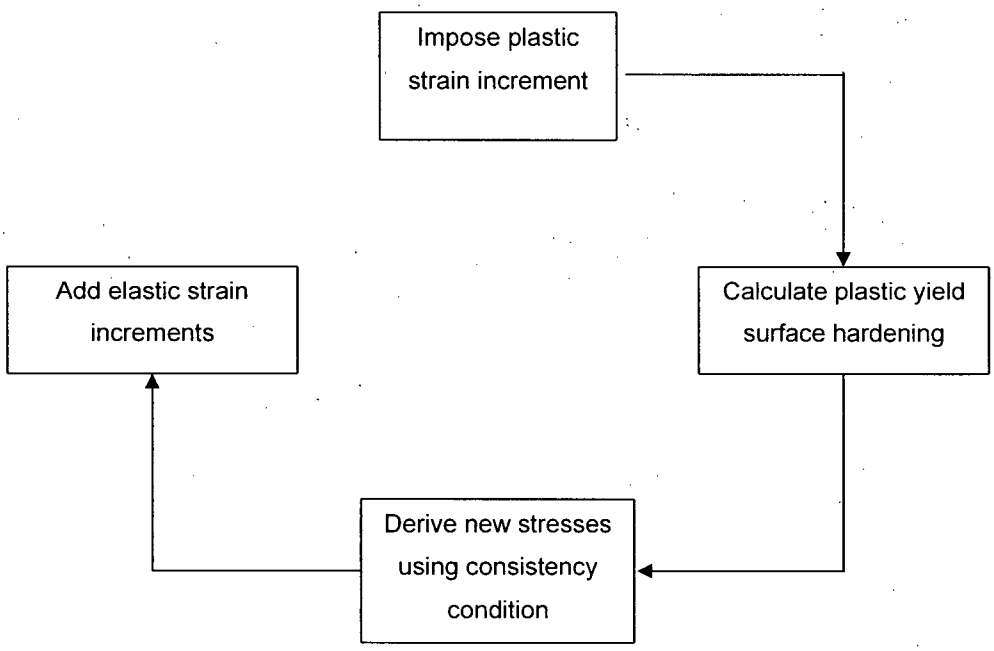

Figure 2.18: Four-step loop to solve plasticity models

2.4.6. Stress – dilatancy

The stress-dilatancy definition was presented earlier and the relations for Original Cam Clay (Eq. 2.50) and Modified Cam Clay (Eq. 2.59) have already been discussed; OCC has a linear relation between stress and strains and MCC has a nonlinear form. However this topic must be discussed in more detail.

Taylor (1948) examined shear box tests on sands, and first attempted to separate the strength of soils into the true friction angle between particles, ϕ_μ, and the dilation produced by the shearing. ϕ_μ was found to be a function of the mineralogy of the material, the properties and roughness of the surface and the size of the load per particle. Rowe (1962) by means of idealized packing of rods and spheres, proposed a stress-dilatancy (for triaxial compression) relation given by:

$$\frac{\sigma_1'}{\sigma_3'} = K\left(1 - \frac{\dot{\varepsilon}_v}{\dot{\varepsilon}_1}\right) \qquad 2.64$$

where K is given by:

$$K = \frac{1+\sin\phi_f}{1-\sin\phi_f} \qquad 2.65$$

where ϕ_f is an angle of soil friction, given by: $\phi_\mu \le \phi_f \le \phi_{cv}$. Rowe showed that ϕ_f was equal to ϕ_μ at the minimum porosity and increased towards ϕ_{cv} at the maximum porosity. When Rowe's theory was applied to real soils, it was found that when K was computed using $\phi_f = \phi_\mu$, the predicted strains were too small, and when K was computed using $\phi_f = \phi_{cv}$, they were too large. Hence, K has to be related to ϕ_f and not to ϕ_μ because K has to evolve with strain, ie, has to relate the stress ratio to strain increment ratio.

Rewriting Equation 2.64 in terms of the stress ratio (q/p'),

$$\frac{\dot{\varepsilon}_v}{\dot{\varepsilon}_q} = \frac{3\eta(2+K)-9(K-1)}{2\eta(K-1)-3(2K+1)} \qquad 2.66$$

Using the expression of the friction angle, ϕ, as a function of M (Eq. 2.22) and rewriting Equation 2.65 as,

$$K = \frac{3+2M}{3-M} \qquad 2.67$$

the stress-dilatancy relation proposed by Rowe can be written as:

$$\frac{\dot{\varepsilon}_v}{\dot{\varepsilon}_q} = \frac{9(M-\eta)}{9+3M-2M\eta} \qquad 2.68$$

As well, Wroth (1965) performed simple shear tests on 1mm steel balls and assumed a work dissipation postulate. He suggested that work has to be done by some external force in order to deform a sample. This energy has to be enough to supply three components; a frictional component, a volume change component and a pressure change component. In his work, the relation between the input and the output work is related to a constant M which is given by Equation 2.22 but the angle of friction is ϕ_{cv}.

Based on experimental observations, the simple OCC dilatancy D^P = M-η did not match sand well. Nova (1982) proposed a new stress-dilatancy relation given by:

$$D^P = \frac{M-\eta}{1-N} \qquad 2.69$$

He introduces a new material property, a volumetric coupling coefficient, N, found by plotting the maximum stress ratio against the minimum dilatancy. The slope of the line is equal to (1-N) as shown in Figure 2.19. Values of N have been found to be equal to 0.37 for Erksak sand and 0.30 for Brasted sand. It is important to note that for N=0 the previous flow rule reduces to the Cam Clay one.

Recently, Li and Dafalias (2000) proposed a stress-dilatancy relation given by:

$$D^P = D_o(M_i - \eta)/M \qquad 2.70$$

Replacing D_o by $M/(1-N)$, the previous equation is the same as the flow rule proposed by Nova, but using a changing M_i rather than a constant M. In this case, M_i is used to follow the same principle than Rowe with his evolving friction angle ϕ_f. Table 2.3 shows a summary of the described flow rules.

Table 2.3: Stress-dilatancy relations (from Been and Jefferies, 2004)

Theory	Relation
Cam Clay	$D^P = M_i - \eta$
Modified Cam Clay	$D^P = (M_i^2 - \eta^2)/2\eta$
Nova 1982	$D^P = (M-\eta)/(1-N)$
Li and Dafalias 2000	$D^P = D_o(M_i - \eta)/M$
Rowe 1962	$D^P = 9(M_i - \eta)/(9 + 3M_i - 2M_i\eta)$

The idea of a M_i in the flow rule that evolves with strain has been adopted by many recent authors. Table 2.4 shows the expressions found for the changing M_i by different authors.

Table 2.4: Relations of M_i after different authors (from Been and Jefferies, 2004)

Originator	Relation
Manzari and Dafalias 1997	$M_i = M + m\psi$
Li and Dafalias 2000	$M_i = M\exp(m\psi)$
Jefferies and Shuttle 2002	$M_i = M - \lvert\psi\rvert$

The NorSand constitutive model will be used in this thesis, then the relation obtained by Jefferies and Shuttle, 2002, will be explained in details later in this chapter.

Figure 2.20 shows the comparison of these four flow rules for a value of M_i=1.25.

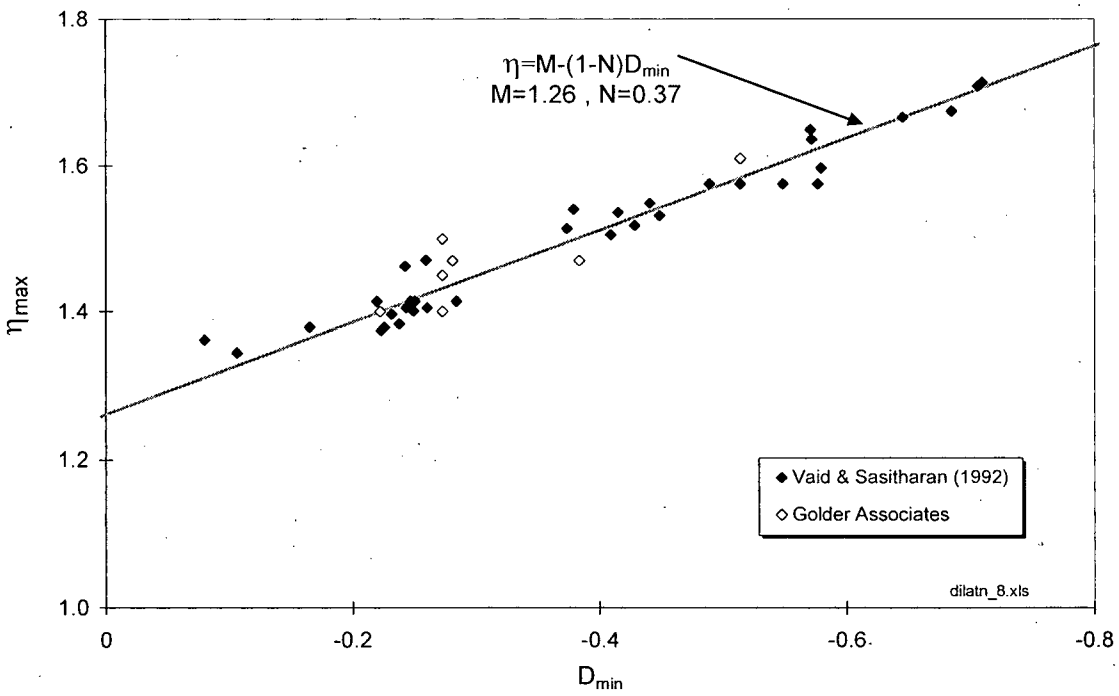

Figure 2.19: Nova's stress-dilatancy rule (from Been and Jefferies, 2004)

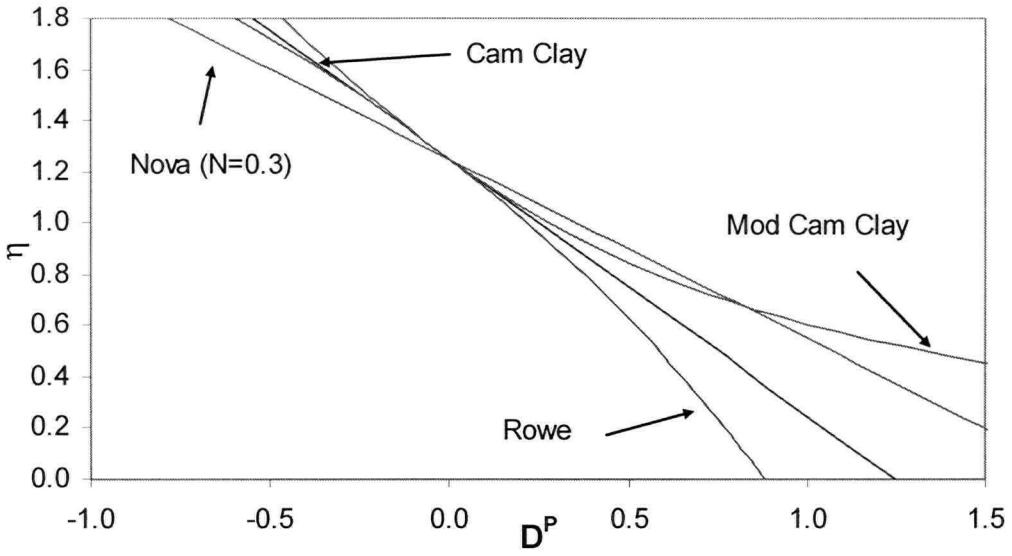

Figure 2.20: Comparison of stress-dilatancy relations

2.5. Critical state model for sands

Many constitutive models must be calibrated at the in situ void ratio. Hence, every time density changes, another set of parameters is needed and the model has to be re-calibrated. In CSSM models, the parameters are not associated to any particular value of initial void ratio. Hence the same set of parameters is able to capture the behaviour of soils regardless of the initial void ratio. However, CSSM as Original Cam Clay and Modified Cam Clay primarily work for "well-behaved, insensitive" clays (Lade, 2005) and they are not able to predict dilation and strain softening as it occurs in dense sands. Hence to model sands, new constitutive models were developed. The intent of this section is to briefly describe the main model groups and the new constitutive models for sands, between the 1970's and 1993 where Jefferies developed NorSand, the first CSSM for sands.

Lade (2005) divided the available constitutive models in eight groups. The characteristics of the best known groups will be briefly described next.

Elastic models are probably the simplest models available, and the simplest elastic models are based on isotropic elasticity. Isotropic elasticity is defined by a single value of Young's Modulus and a single value of Poisson's Ratio. More complex elastic models are the Transversely isotropic, Orthotropic and Hyperbolic (in these type of models, principal strains are in the same direction as the principal stress increments).

Elastic-plastic models comprise elasticity, a yield surface, a hardening rule and a flow rule. These models are associated with irrecoverable strains. The most popular plasticity model is Mohr-Coulomb, followed by Tresca and Von Mises. Only Mohr-Coulomb is suitable to model sands.

Critical state models have already been presented and discussed. Typical critical state models are Original Cam Clay and Modified Cam Clay for clays, and NorSand for sands.

Double hardening models comprise two yield surfaces; one yield surface yields in shear and the other yields in isotropic compression.

A summary of the constitutive models for sands is presented in Table 2.5a and Table 2.5b. In Table 2.5a the different attributes of the models, such as shape of failure surface and yield surface, associated or non-associated flow rule and type of hardening parameter are presented. In Table 2.5b the capabilities of each model, such as, prediction of drained softening, large stress reversals, cyclic loading, pore pressure and 3D behaviour are presented. In addition the type of tests needed to obtain the input parameters and the number of parameters needed for the model are presented.

Table 2.5a: Constitutive models for sands (extracted from Lade, 2005)

Model	Failure surface	Yield surface	Plastic potential	Hardening parameter
Hyperbolic	Mohr-Coulomb	NA	NA	NA
Mohr-Coulomb	Mohr-Coulomb	= failure surface	Non-associated	None
DiMaggio-Sandler	Curved extended von Mises	Elliptical cap	Associated	Plastic volumetric strain
Lade and Duncan	Smooth triangular, conical	Smooth triangular, conical	Non-associated	Plastic work
Darve	Mohr-Coulomb	NA	NA	NA
Hypoplastic	Smooth triangular, conical	NA	NA	NA
Fuzzy set plasticity	Smooth triangular, conical	Smooth triangular, conical & oct. plane	Non-ass. and associated	Plastic work
Lade	Smooth triangular, conical	Smooth triangular, conical & sphere. cap	Non-ass. and associated	Plastic work
PLAXIS hardening	Mohr-Coulomb	Curved Mohr-Coulomb & ellipt. cap	Non-ass. and associated	Plastic vol. & shear strain
MONOT	Smooth triangular, conical	Smooth triangular, conical & sphere. cap	Non-ass. and associated	Plastic vol. & shear strain
MIT-S1	Smooth triangular, conical	Distorted lemniscate	Non-associated	Plastic vol. & shear strain
Single hardening	Smooth triangular, conical	Tear-drop shaped	Non-associated	Plastic work
Sinfonietta classica	Smooth triangular, conical	Tear-drop shaped	Non-associated	Plastic vol. & shear strain
Disturbed state concept/hierarchical	Smooth triangular, conical	Tear-drop shaped	Non-ass. or associated	Plastic vol. & shear strain
Generalized plasticity	Smooth triangular, conical	Elliptical cap	Non-associated	Plastic vol. & shear strain
NorSand	Smooth triangular, conical	Bullet-shaped (OCC)	Associated	Plastic work

Table 2.5b: Constitutive models for sands (extracted from Lade, 2005)

Model	Drained softening	Large stress reversal	Cyclic loading	Realistic pore pressures	Realistic 3D behaviour	Experiments for parameter determination	Number of parameters
Hyperbolic	No	No	No	No	Yes, away from failure	3 triaxial compression	7
Mohr-Coulomb	No	No	No	No	No	3 triaxial compression	5
DiMaggio-Sandler	No	No	No	No	No	3 triax. comp., 1 Iso. comp	10
Lade and Duncan	No	No	No	No	Yes	3 triaxial compression	9
Darve	No	Yes	Yes	No	No	Triax. comp & ext., cyclic tests	16
Hypoplastic	Yes	Yes	Yes	Yes	Yes	Triax. comp & K_0-comp.	8
Fuzzy set plasticity	Yes	Yes	Yes	Yes	Yes	Triax. comp. & Iso. Comp.	13-20
Lade	Yes	No	No	Yes	Yes	3 triax. comp., 1 Iso. comp.	14
PLAXIS hardening	No	No	No	Yes	Yes	3 triax. comp., 1 Iso. comp.	11
MONOT	No	Yes	Yes	Yes	Yes	3 triax. comp., 1 Iso. comp.	21
MIT-S1	Yes	Yes	Yes	Yes	Yes	CU Triax. comp. CD Triax. comp. Iso./K_0-comp. K_0-comp. with meas. lateral stresses	13
Single hardening	Yes	Yes	Yes	Yes	Yes	3 triax. comp., 1 Iso. comp.	12
Sinfonietta classica	No	No	No	Yes	Yes	3 triax. comp., 1 Iso. comp.	17
Disturbed state concept/hierarchical	Yes	No	No	Yes	Yes, requires 3D test	3 triax. comp., 1 Iso. comp.	15
Generalized plasticity	Yes	Yes	Yes	Yes	Yes	2CD or CU triax. comp. & 1 cyclic test	15
NorSand	Yes, for OC soil	No	Yes, undrained	Yes	Yes	2 CD triax. comp 2CU triax. comp. with Iso. comp.	7

2.6 Critical state models for sands and NorSand

Critical state constitutive models such as Original Cam Clay and Modified Cam Clay are able to capture the behaviour of soils, mostly clays, at different densities. However, those models are not able to predict the dilation and softening as it occurs in dense sands. NorSand is a CSSM constitutive model, developed by Jefferies in 1993, able to capture the softening and dilatancy behaviour of sands by introducing a new parameter, the state parameter and by postulating an infinity of normal consolidation loci (NCL).

NorSand is used later in the thesis to simulate triaxial compression tests. This model was chosen because it is convenient given that it needs only few parameters (7) compared with other more advanced soil models, as shown in Table 2.5a and Table 2.5b. Also, as with all CSSM models, NorSand is developed from ideas rather than curve fits, which enables new concepts and ideas to be tested. However, sometimes some fits may not be as good as from models based on curve fits, as the predictions are constrained by its rules.

The idea of Infinity of NCL was first introduced by Ishihara et al (1975). They suggested that given that in a sand an infinity of void ratios can be obtained, an infinity of NCL exist. Jefferies and Been (2000) supported the idea with experimental data. Four samples of Erksak sand were tested at different void ratios. They performed load/unload tests for each sample and found that each isotropic loading line can be seen as a true NCL. Figure 2.21 shows the concept of infinity of NCL. Infinity of NCL can be viewed as infinity of yield surfaces and each NCL can be viewed as a hardening law for an associated yield surface. This means that instead of one NCL, as used in OCC and MCC, with an infinity of NCL, the void ratio e and the CSL are uncoupled in NorSand.

Hence, as any soil can exist over a wide spectrum of NCL, the void ratio is no longer sufficient to define the state of a soil, two parameters are introduced in NorSand, the state parameter, ψ, and the overconsolidation ratio, R.

2.6.1. The state parameter and overconsolidation

The use of void ratio or relative density does not tell us how the soil is going to behave, given that dilation or contraction depends not only on the void ratio, or relative density, but also on the stress level. That is why the state parameter is so useful in determining whether the soil sample will dilate or contract when sheared. Been and Jefferies (2004) showed that samples with similar relative densities and different stress levels behaved differently, while samples with same state

parameter but different void ratios and stress level, had similar behavior, confirming that the behaviour of sands under shear loading depends on the state parameter.

The state parameter, ψ, relates the void ratio of the soil in e-ln(p') space with the void ratio at critical state. ψ is defined as the distance between the actual void ratio and the void ratio at the critical state for the same p', and is given by;

$$\psi = e - e_c \qquad 2.71$$

where e is the actual void ratio and e_c is the critical void ratio at the same p'. If the state parameter is positive, then the soil sample will contract with shear and if the state parameter is negative the soil will dilate with shear.

From stress-dilatancy theory and experimental observation it is evident that peak dilatancy is related to the state parameter. This will be shown later when the parameter χ will be defined and determined for the NorSand constitutive model.

While NorSand was the first CSSM for sand, many models are now based on the state parameter, implicitly or not, such as Manzari and Dafalias (1997), Wan and Guo (1998), Gajo and Wood (1999) and Collins and Muhunthan (2003).

For completeness the over-consolidation ratio, R, is also defined. R represents how close the soil is to its yield surface. It is important to note that here, R is defined using the mean stress, typical for constitutive models, and not the vertical stress, more usual in engineering practice.

Figure 2.21 shows the difference between overconsolidation and state.

2.6.2. NorSand formulation

This section introduces the original 1993 version of NorSand for triaxial compression. The later modifications incorporated into the simulations shown in Chapter V are described later.

The NorSand and Original Cam Clay formulations are very similar; they both lie in stress dilatancy. NorSand uses the plastic shear strains to control the hardening rule. As explained before, this does not work with MCC because for a q=0 condition there is no shear strain.

NorSand uses the two axioms of CSSM described above. However with the introduction of the state parameter, Axiom 2 can be re-stated as:

$$\psi \to 0 \quad \text{as} \quad \varepsilon_q \to \infty \tag{2.72}$$

The deduction of the yield surface equation is the same as for Cam Clay. From Nova's flow rule and substituting in Equation 2.53,

$$\frac{\dot{p'}}{p'} + \frac{(1-N)\dot{\eta}}{M - \eta N} = 0 \tag{2.73}$$

Integrating Equation 2.73, it is possible to obtain again Equation 2.54, by taking N=0. In this case, the integration constant C is taken as the value of p' when η=M. Here, p' is taken as the image condition (denoted by p_i', see Figure 2.22) and it is used to scale the size of the yield surface, similar to the use of p_c', to size the yield surface in OCC. Hence,

$$\frac{\eta}{M} = 1 - \ln\left(\frac{p'}{p_i'}\right) \tag{2.74}$$

The introduction of p_i' is required as with the introduction of the state parameter, ψ, the yield surfaces no longer intersect the critical state (see Figure 2.22) as they did with OCC.

For convenience, the yield surface is written as:

$$F = \ln\left(\frac{p'}{p_i'}\right) + \frac{q}{p'M} - 1 \tag{2.75}$$

for N=0 and as:

$$F = \eta - \frac{M}{N}\left[1 + (N-1)\left(\frac{p'}{p_i'}\right)^{(N/N-1)}\right] \tag{2.76}$$

for N≠0.

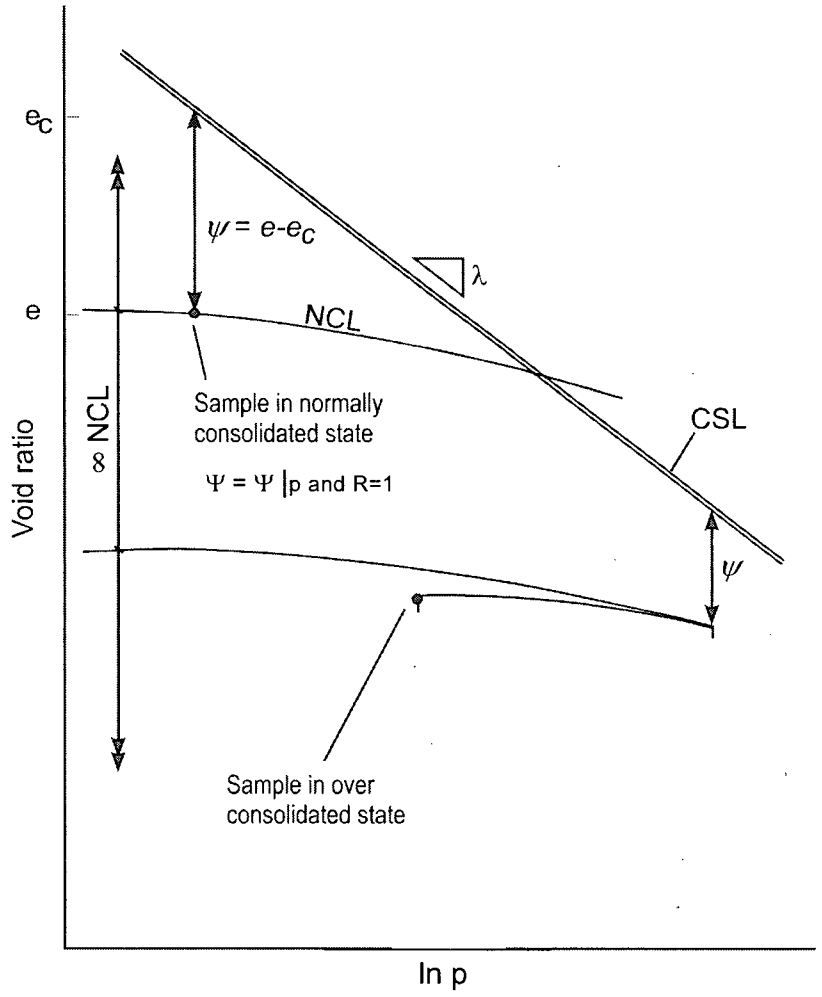

Figure 2.21: Difference between state parameter and overconsolidation, and infinity of NCL (from Jefferies, 1993)

The original version of NorSand (Jefferies, 1993) uses Nova's flow rule (Eq. 2.69)

$$D^P = \frac{M - \eta}{1 - N} \qquad \text{(Eq. 2.69)}$$

To relate the image stress with the soil's void ratio, NorSand uses the Second Axiom of critical state theory. Rearranging the equation of the yield surface and differentiating, for N=0, the consistency condition is given by:

$$\dot{\eta} = M\left(\frac{\dot{p_i}'}{p_i'} - \frac{\dot{p}'}{p'}\right) \qquad 2.77$$

From Axiom 2, the hardening law expressed in dimensionless form is:

$$\frac{\dot{p_i}'}{p'} = H\left(\left(\frac{p_i'}{p'}\right)_{max} - \left(\frac{p_i'}{p'}\right)\right)\dot{\varepsilon}_q^p \qquad 2.78$$

where,

$$\left(\frac{p_i'}{p'}\right)_{max} = \exp\left(-D_{min}^P / M\right) \qquad 2.79$$

for N=0 and:

$$\left(\frac{p_i'}{p'}\right)_{max} = \left(1 + \chi\psi_i N / M\right)^{(N-1/N)} \qquad 2.80$$

for N≠0.

It has been found that there exists a strong relation between the minimum dilatancy, D_{min}^P (ie, value close to the peak stress ratio) and ψ_i, the value of ψ at the image state, shown in Figure 2.23 and given by:

$$D_{min}^P = \chi\psi_i \qquad 2.81$$

where χ is a model property and it usually lies between 2.5 and 4.5 for triaxial compression (with a common value of 3.5), the image state is related to ψ by:

$$\psi_i = \psi + \lambda \ln\left(p_i'/p'\right) \qquad 2.82$$

Rearranging the yield surface equation (Eqs. 2.75 and 2.76), for N=0:

$$\left(\frac{p_i'}{p'}\right) = \exp(\eta/M - 1) \qquad 2.83$$

and for N≠0:

$$\left(\frac{p_i'}{p'}\right) = \left(\frac{1 - N\eta/M}{1 - N}\right)^{(N-1)/N} \qquad 2.84$$

From Equation 2.81 and substituting the value of χ by 3.5, Equation 2.79 can be written as:

$$\left(\frac{p_i'}{p'}\right)_{max} = \exp(-3.5\psi_i/M) \qquad 2.85$$

for N=0 and for N≠0 as:

$$\left(\frac{p_i'}{p'}\right)_{max} = (1 + 3.5\psi_i N/M)^{(N-1/N)} \qquad 2.86$$

By reproducing experimental data, a better fit has been found if the hardening rule depends on the shear stress level using an exponential function (Jefferies and Shuttle, 2002),

$$\frac{\dot{p_i}'}{p_i'} = H\exp(1 - \eta/M)\left(\left(\frac{p_i'}{p'}\right)_{max} - \left(\frac{p_i'}{p'}\right)\right)\dot{\varepsilon}_q^p \qquad 2.87$$

where H is a model parameter, which is a function of the state parameter.

In NorSand, isotropic elasticity is assumed. Elasticity parameters are defined by a shear rigidity I_r and a constant Poisson's ratio as:

$$I_r = \frac{G}{p'}$$
$$\frac{K}{p'} = I_r \frac{2(1+\nu)}{3(1-2\nu)} \qquad 2.88$$

Table 2.6 shows a summary with the equations of the original version of NorSand.

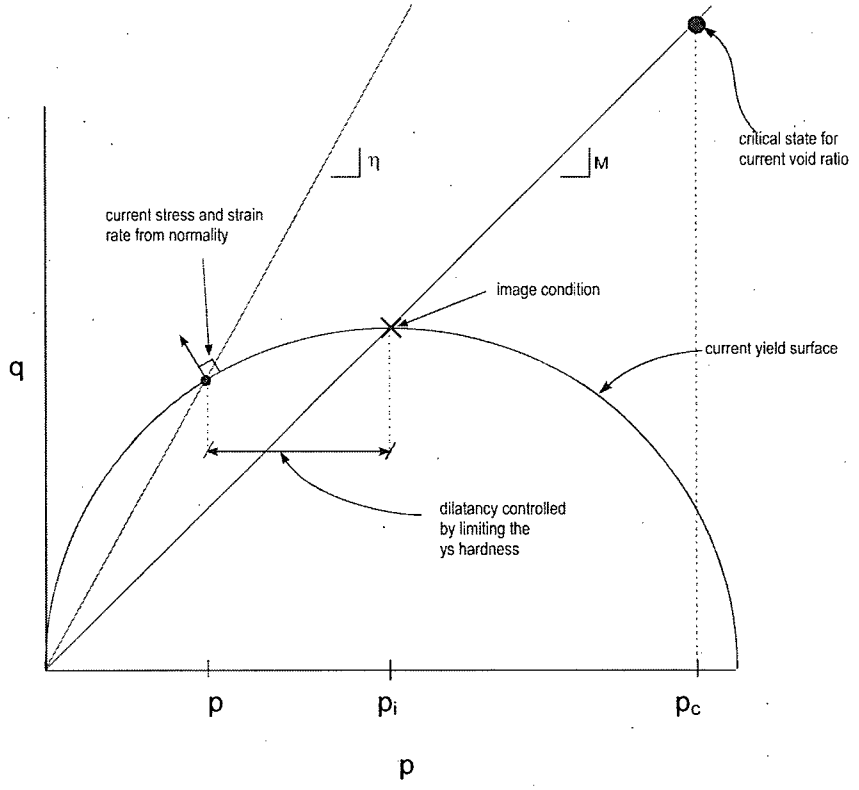

Figure 2.22: NorSand image condition on yield surface (ys) (from Jefferies and Shuttle, 2002)

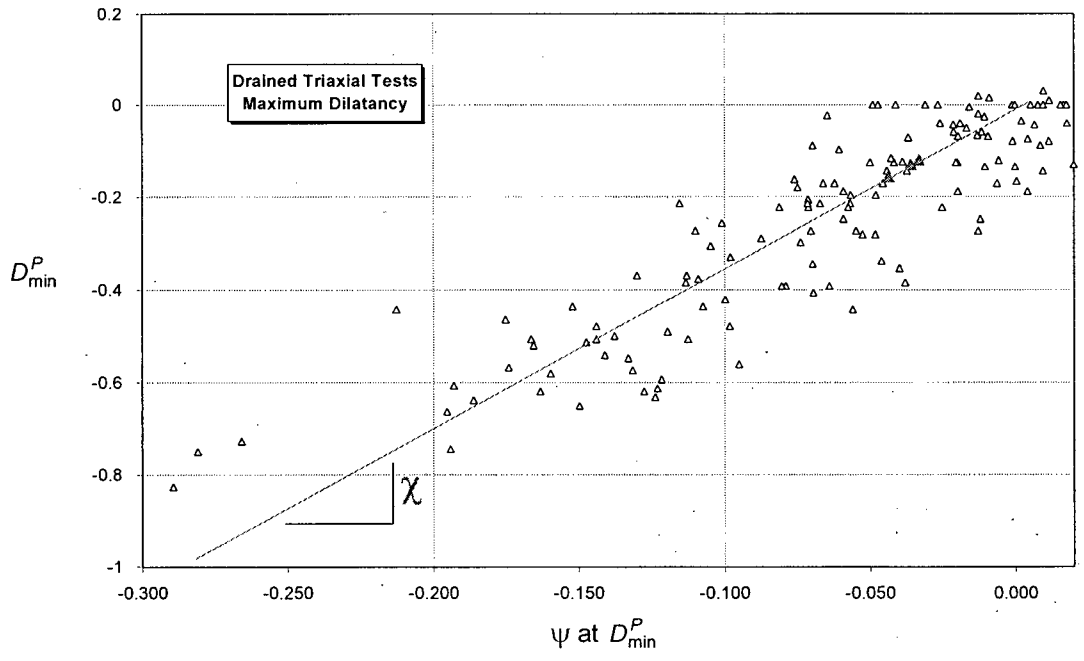

Figure 2.23: Definition of χ: D^P_{min} versus ψ

Table 2.6: Summary of equations for NorSand (from Jefferies and Been, 2005)

Aspect of NorSand	Equations
Internal model parameters	$\psi_i = \psi + \lambda \ln(p_i'/p')$ where $\psi = e - e_c$
Critical state	$e_c = \Gamma - \lambda \ln p'$
Yield surface	$F = \ln\left(\frac{p'}{p_i'}\right) + \frac{q}{p'M} - 1$ for N=0 $F = \eta - \frac{M}{N}\left[1 + (N-1)\left(\frac{p'}{p_i'}\right)^{(N/N-1)}\right]$ for N≠0
Hardening rule	$\frac{\dot{p_i}'}{p_i'} = H \exp(1-\eta/M)\left(\left(\frac{p_i'}{p'}\right)_{max} - \left(\frac{p_i'}{p'}\right)\right)\dot{\varepsilon}_q^p$ $\left(\frac{p_i'}{p'}\right)_{max} = \exp(-\chi\psi_i/M)$ for N=0 $\left(\frac{p_i'}{p'}\right)_{max} = (1+\chi\psi_i N/M)^{(N-1/N)}$ for N≠0
Stress dilatancy	$D^P = \frac{M-\eta}{1-N}$
Elasticity	$I_r = \frac{G}{p'}$

A modification of the original version of NorSand was suggested (Jefferies and Shuttle, 2002) where the N parameter was equal to zero. The incorrect sand dilatancy from N=0 is accounted for by allowing M to evolve with shear strain, similar to the idea of Rowe where ϕ_f evolves from ϕ_μ to ϕ_{CV} with shear strain.

Rearranging Equation 2.69 the expression for M_i is given by:

$$M_i = M + ND_{min}^P \qquad 2.89$$

Substituting the relation for maximum dilatancy (Eq. 2.81) in Equation 2.89,

$$M_i = M/\left(1 - \chi_{tc} N|\psi_i|/M_{tc}\right) \qquad 2.90$$

Typical values of N and χ_{tc} are found to be around 0.3 and 3.5 respectively. Hence M_i is finally given by:

$$M_i = M\left(1 - |\psi_i|/M_{tc}\right) \qquad 2.91$$

This later modification of the flow rule is used in this thesis.

2.6.3. Determination of NorSand parameters

In order to describe the NorSand constitutive model, 7 properties are needed and 2 initial soil state parameters. The properties needed to describe the model are shown in Table 2.7 and the procedure to obtain them is summarized next. More detail is given in Jefferies and Shuttle, 2005.

Table 2.7: Properties needed to describe the NorSand constitutive model and their typical range for sand (from Jefferies and Been, 2005)

Property	*Typical Range*	*Remark*
CSL		
Γ	0.9 - 1.4	Altitude of CSL, defined at 1 kPa
λ	0.01 - 0.07	Slope of CSL, defined on base e
Plasticity		
M_{tc}	1.2 - 1.5	Critical friction ratio, triaxial compression as reference condition
H	50 - 500	Plastic hardening modulus for loading
χ	2.5 - 3.5	Relates minimum dilatancy to ψ at D_{min}
Elasticity		
Ir	200 - 800	Dimensionless shear rigidity
ν	0.1 - 0.3	Poisson's ratio
Initial Soil State		
R		Overconsolidation ratio (R=1 for NC soils)
ψ	-0.3 - 0.15	State parameter

The critical state parameters in the e-ln(p') space, Γ and λ are obtained from drained and undrained tests on very loose reconstituted sand samples at different confining pressures. In that case, the samples will contract and reach the CSL in the e-ln(p') space at strains within the limits of the triaxial device. As the critical state of sands is an intrinsic state and does not depend on the initial soil structure, using reconstituted samples is fine. Loose samples are preferred instead of dense samples, given that these later dilate and do not reach the critical state, sometimes at 25% strain and are prone to localize. M_{tc} is obtained from the end of test condition of the drained tests and can be confirmed by the stress-dilatancy plots.

A couple of very dense drained test are necessary to estimate the maximum dilatancy of the soil (D_{min}). As the incremental elastic strains are zero at peak strength, from a stress-dilatancy plot (η vs D_{min}), it is possible to obtain D_{min}.

As the critical state line is known, as well as the initial void ratio of the samples, the state parameter ψ is easy to find using $\psi = e - e_c$.

The plastic hardening parameter, H, is obtained by fitting the results obtained by the drained triaxial tests and iterating to have the best match. H is fabric dependent and hence, not an intrinsic parameter. Based on previous calibrations H is found to be either a constant value or linearly related to the state parameter, ψ, under the form $H = a - b\psi$.

χ_{tc} is a constant for each sand and is defined as the slope of the plot plastic dilation $\left(\dot{\varepsilon}_v^p / \dot{\varepsilon}_q^p\right)$ at peak strength and the initial state parameter from drained tests on dense samples, ie $D_{min}^P = \chi_{tc}\psi_i$.

The elastic property Ir is calculated by obtaining the shear modulus from bender elements during the triaxial tests. If bender elements are not included unload-reload cycles can be performed. The Poisson's ratio is assumed to be between 0.15 to 0.2.

Finally, Table 2.8 shows a summary of the CSSM constitutive models.

Table 2.8: Summary of CSSM constitutive models

CSSM model	Yield surface	Hardening rule	Stress-dilatancy rule
Original Cam Clay	$\frac{\eta}{M} = 1 - \ln\left(\frac{p'}{p_c'}\right)$	$\frac{\dot{p_c}'}{p_c'} = \frac{(1+e)\dot{\varepsilon}_v^p}{\lambda - \kappa}$	$D^P = M - \eta$
Modified Cam Clay	$\frac{p'}{p_c'} = \frac{M^2}{M^2 + \eta^2}$	$\frac{\dot{p_c}'}{p_c'} = \frac{(1+e)\dot{\varepsilon}_v^p}{\lambda - \kappa}$	$D^P = \frac{M^2 - \eta^2}{2\eta}$
NorSand (1993)	$\frac{\eta}{M} = 1 - \ln\left(\frac{p'}{p_i'}\right)$	$\frac{\dot{p_i}'}{p_i'} = H\exp(1-\eta/M)\left(\left(\frac{p_i'}{p'}\right)_{\max} - \left(\frac{p_i'}{p'}\right)\right)\dot{\varepsilon}_q^p$	$D^P = \frac{M - \eta}{1 - N}$
NorSand (2002)	$\frac{\eta}{M_i} = 1 - \ln\left(\frac{p'}{p_i'}\right)$	$\frac{\dot{p_i}'}{p_i'} = H\exp(1-\eta/M)\left(\left(\frac{p_i'}{p'}\right)_{\max} - \left(\frac{p_i'}{p'}\right)\right)\dot{\varepsilon}_q^p$	$D = M_i - \eta$

CHAPTER III: MATERIAL PROPERTIES

In order to characterize the sand and establish parameters needed for the NorSand constitutive model, a series of tests were performed in the Graduate Geotechnical Laboratory at UBC. First, a description of the sand is given with reference to attributes of the grains and grain size distribution curve. Second, the strength of the sand is reported with reference to triaxial tests on reconstituted specimens.

3.1. Description of the soil

The soil used for this study is a silica sand that was used by Raju (1995) for geosynthetic pullout tests, and produced by the Badger Mining Corporation. For convenience, this sand is subsequently referred to as "Badger Sand".

Figure 3.1 shows the grain size distribution of Badger sand. The sand is a uniformly graded coarse sand with no fines, a coefficient of uniformity of 1.3 and a coefficient of curvature of 1.1. After the Unified Soil Classification System (USCS), Badger sand classifies as SP- a poorly graded sand. Particle sizes are between 0.6 mm and 2 mm, with a D_{50} of 0.87 mm. The particles shape is well-rounded (Figure 3.2). The specific gravity is G_s = 2.65 and the color varies from light brown to dark brown. Table 3.1 summarizes the properties of the grain size distribution of Badger sand.

Table 3.1: Properties of the grain size distribution curve

Soil Description	D_{85} (mm)	D_{60} (mm)	D_{50} (mm)	D_{30} (mm)	D_{15} (mm)	D_{10} (mm)	C_u (D_{60}/D_{10})	C_c $(D_{30}^2/D_{10} \times D_{60})$
Uniformly graded with little or no fines	0.95	0.91	0.87	0.83	0.76	0.72	1.3	1.1

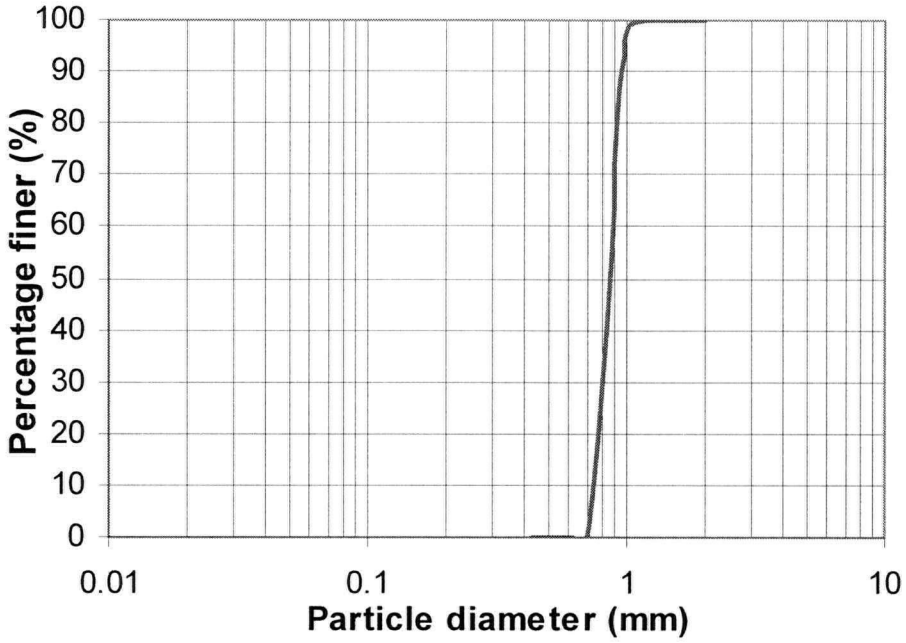

Figure 3.1: Grain size distribution curve of Badger sand

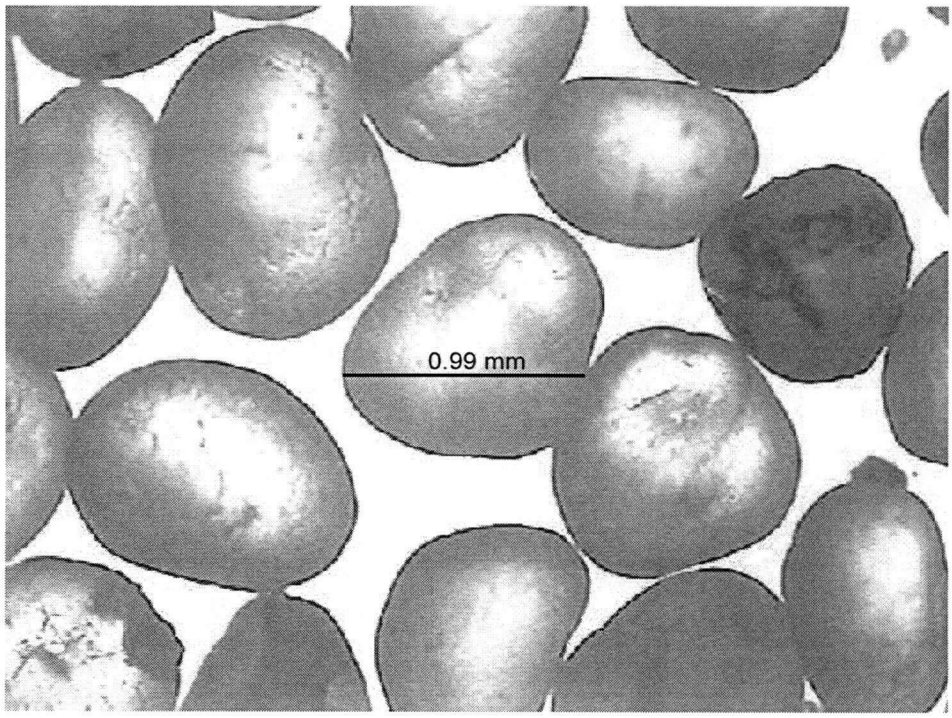

Figure 3.2: Microscope photograph: well-rounded particles

3.3.1. Extreme void ratios

The minimum and maximum void ratios were determined according to ASTM D 4253-93 and ASTM D 4254-91, respectively, as shown in Figure 3.3. In each case, knowing the volume, the weight and the specific gravity of the sand, it is possible to calculate the void ratio.

The maximum void ratio was obtained using Test Method B of ASTM D4254. This method is applicable to soils for which 100%, by dry mass, of the particles pass a 19 mm (3/4-inch) sieve. A thin-walled tube of inside diameter of about 0.7 times the inside diameter of the mold is placed inside the mold and the dry sand is poured inside the tube. The tube is then quickly removed allowing the particles to slide inside the mold and not to drop. Upon leveling the surface, the mass of the mold plus soil is recorded. This procedure was repeated 6 times, yielding an average e_{max} = 0.69 (see Table 3.2).

Table 3.2: e_{max} calculations for Badger sand

Test	Mass of mold + soil (g)	Mass of soil (g)	ρ_{min} (g/cm^3)	e_{max}
1	8046.0	4431.0	1.56	0.70
2	8060.9	4445.9	1.57	0.69
3	8049.9	4434.9	1.56	0.70
4	8045.0	4430.0	1.56	0.70
5	8051.3	4436.3	1.56	0.69
6	8049.2	4434.2	1.56	0.70
average			1.58	0.69

The minimum void ratio was obtained by placing the dry sand inside the mold. It was leveled and a surcharge plate was placed on top, making sure the surface of the plate is in full contact with the sand. The mold was then attached to a vibrating table, with a guide sleeve on the mold in order to apply the surcharge, and vibrated at 60 Hz for 8 min. Finally the surcharge and guide sleeve were removed and 10 height measurements were taken of the surcharge plate. Knowing the volume and mass of the sand inside the mold it is possible to determine e_{min}. The procedure was repeated 4 times yielding an average value of 0.49 (see Table 3.3).

Table 3.3: e_{min} calculations for Badger sand

Test	Mass of mold + soil + cap (g)	Mass of soil (g)	H (cm)	H_f (cm)	V (cm^3)	ρ_{max} (g/cm^3)	e_{min}
1	9319	3959	2.078	12.10	2224.06	1.78	0.49
2	9146	3786	2.700	11.47	2109.61	1.79	0.48
3	9350	3990	1.934	12.24	2250.52	1.77	0.49
4	9368	4008	1.944	12.23	2248.62	1.78	0.49
average						1.78	0.49

Values obtained for the maximum and minimum void ratio were very repeatable. It is important to note that the range of $I_e=e_{max}-e_{min}$ is only 0.2, which is a somewhat narrow and unusual value for sands. For example, Ottawa sand is also a rounded sand with a C_u = 1.1 but e_{min} = 0.5 and e_{max} = 0.8, hence I_e = 0.3. It appears that the minimum void ratio obtained for Badger sand is within the expected values, although the maximum void ratio is perhaps slightly lower than expected.

Cubrinovski and Ishihara (2002) measured the minimum and maximum void ratios of about 300 soils including clean sands, sands with fines and silty soils. They found a correlation between e_{min} and e_{max} for clean sands (as Badger sand) given by:

$$e_{max} = 0.072 + 1.53e_{min} \qquad 3.1$$

Similarly, from tests on 17 crushed sands from Georgia, 16 natural sands, and materials such as glass beads, granite powder and Syncrude tailings, Cho et al (2005) found a correlation between e_{max} and e_{min} taking into consideration the coefficient of uniformity C_u, given by:

$$e_{max} = 1.35e_{min} + 0.15(C_u - 1) \qquad 3.2$$

Also, Shimobe and Moroto (1995), established a relation, based on 182 data points on uniform samples ($C_u \leq 2$), where

$$I_e = 0.574e_{max} - 0.198 \qquad 3.3$$

and I_e is the difference between the maximum and the minimum void ratios ($I_e = e_{max} - e_{min}$).

Each of these three relations is reproduced in Figure 3.4, together with the data for Badger sand. The generally good agreement with Cho et al (2005) and Shimobe and Moroto (1995) is attributed to their consideration of grain size, as it is known that the minimum and maximum void ratios increase as the particle size decreases.

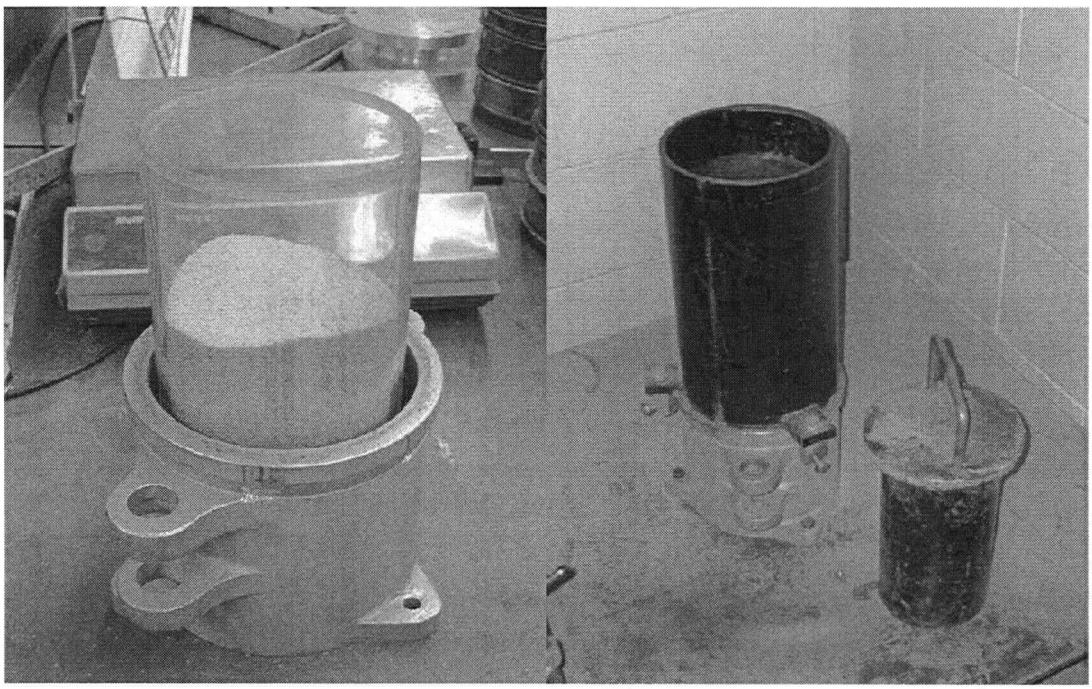

Figure 3.3: e_{max} and e_{min} determinations

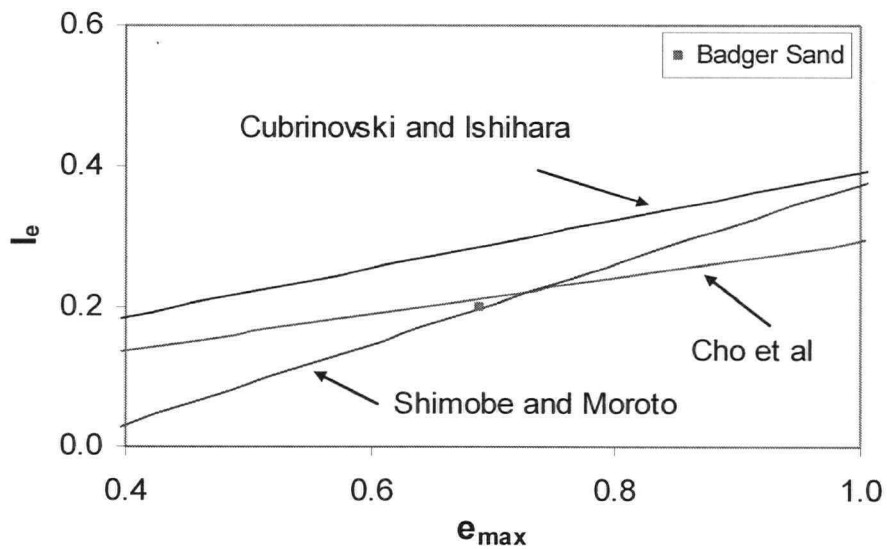

Figure 3.4: Correlations between minimum and maximum void ratio

3.3.2. Angle of repose

The angle of repose was determined according to ASTM C1444-00. As defined in Chapter II, the angle of repose is the angle of a heap formed by dry sand deposited as loose as possible before the heap starts flowing.

A funnel with an internal diameter of discharge spout of 9.54 mm was used to pour the sand onto a metal plate, using a constant drop height of 38.1 mm. A stopper was initially placed in the tip of the funnel nozzle, and the funnel filled with sand. The stopper was then removed, allowing the sand to drop. When the tip of the sand cone formed on the base plate entered the funnel nozzle, the test was stopped. The diameter of the resulting cone was measured at 4 different locations and the angle of repose calculated using Equation 3.4 (see Figure 3.5).

$$\phi_{rep} = \tan^{-1}\left[\frac{2H}{D_A - d}\right] \qquad 3.4$$

where: H is the height of the cone (38.1 mm);
D_A is the average diameter of the test determinations; and,
d is the internal diameter of the funnel nozzle (9.54 mm).

The procedure was repeated 10 times obtaining an average value of the diameter of the cone of 136.9 mm. The angle of repose obtained was $\phi_{rep} = 30.9^{o}$.

3.3.3. Roundness and sphericity

The roundness of Badger sand grains was obtained using the definition given in Equation 2.29 proposed by Youd (1973), Shimobe and Moroto (1995), and Santamarina and Cho (2004). The method described by Santamarina and Cho (2004) was used to calculate the sphericity of Badger sand. It involves analysis of a two-dimensional image, from microscopic enlarged pictures of the individual grains, and was considered entirely suitable for these small rounded particles.

After the law of large numbers, if a sample is selected with simple random sampling, the mean of the sample will approach the mean of the population as the sample size grows. When calculating the mean value of a sample, it is important to know the confidence interval and the sampling error to indicate the accuracy of the sample mean as an estimate of the true population mean (Lemay, 2005).

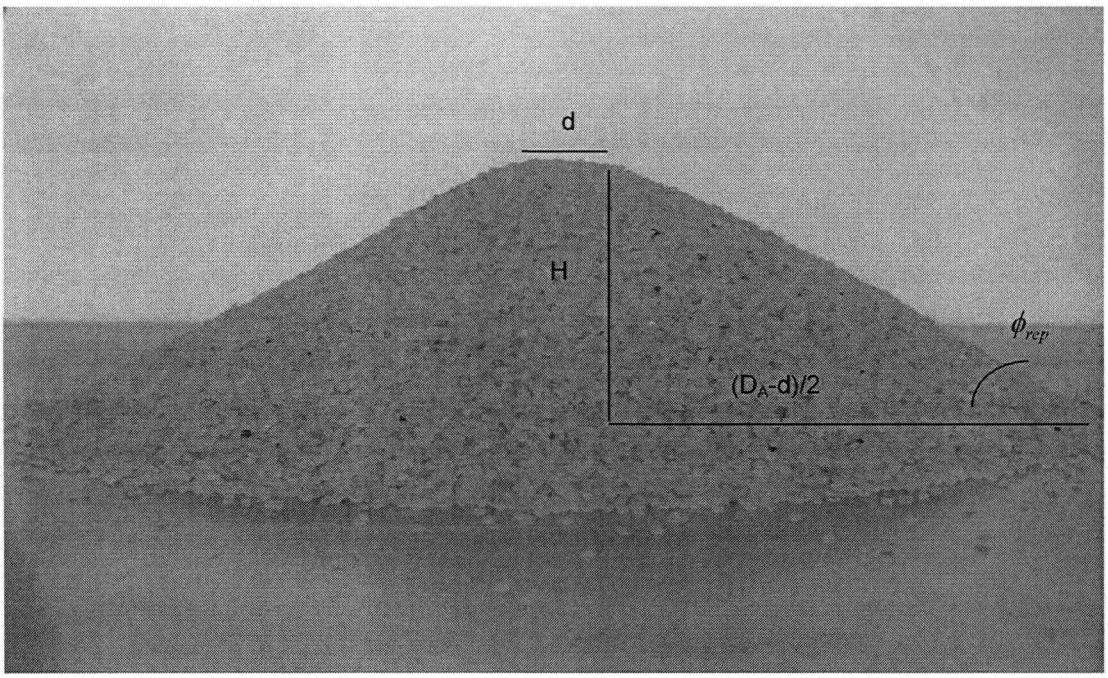

Figure 3.5: Angle of repose of Badger Sand

As a rule of thumb, before taking a sample, it is commonly accepted that the strong law of large numbers applies with a number of elements equal to 30 or more (Moore and McCabe, 2003). Hence, as the sand grains are not expected to vary much, 30 particles of Badger sand were taken randomly and the sphericity and roundness calculated using Equations 2.28 and 2.29 (see Figure 3.6).

$$S = \frac{r_{max}}{R_{min}} \quad \text{and} \quad R = \frac{\sum \frac{r_j}{N}}{r_{max}} \qquad \text{(Eqs. 2.28 and 2.29)}$$

Values of 0.77 and 0.81 respectively (see Tables 3.5 and 3.6), classify the Badger sand as a well-rounded sand (after Powers (1953) and Table 2.2)

The variance of a sample is calculated as:

$$\sigma^2 = \frac{\sum\left(x - \bar{x}\right)^2}{n-1} \qquad 3.5$$

were $\bar{x}$ is the mean value of the sample. $n-1$ is taken to calculate the variance given that this is the variance of a sample of size "n" and it is not the variance of the entire population. Hence, the variance obtained for the 30 particles of Badger sand was 0.006 and 0.011 for roundness and sphericity respectively.

The standard deviation (σ) is obtained by taking the square root of the variance. For Badger sand, the values are 0.078 and 0.1 for roundness and sphericity respectively.

The confidence interval is the maximum difference between the observed sample mean $\bar{x}$ and the true value of the population, and it is given by:

$$\bar{x} \pm t \frac{\sigma}{\sqrt{n-1}} \qquad 3.6$$

where t is taken from Table 3.4:

Table 3.4: Relation between t for a 95% confidence and size "n" of a sample

n	10	20	30
t	2.228	2.086	2.042

Replacing the values obtained for Badger Sand in Equations 3.5 and 3.6, the sampling error obtained for a 95% confidence interval for 30 particles of Badger sand is ± 0.028 and ± 0.039 for roundness and sphericity, respectively. Hence, it is possible to report, with 95% confidence that the mean values of roundness (R=0.81) and sphericity (S=0.77) obtained from the 30 particles are between (0.782, 0.838) and (0.731, 0.809). The Badger Mining Corporation reported values of R=0.8 and S=0.75 following the method of Krumbein/Sloss, which is in very good agreement with the values obtained with the Santamarina and Cho approach.

Table 3.5: Sphericity of Badger sand

Number of Particles	Mean Value	Variance	Standard Deviation	Confidence interval
10	0.75	0.007	0.084	0.059
20	0.77	0.011	0.105	0.050
30	0.77	0.011	0.105	0.039

Table 3.6: Roundness of Badger sand

Number of Particles	Mean Value	Variance	Standard Deviation	Confidence interval
10	0.80	0.005	0.071	0.053
20	0.81	0.007	0.084	0.040
30	0.81	0.006	0.075	0.028

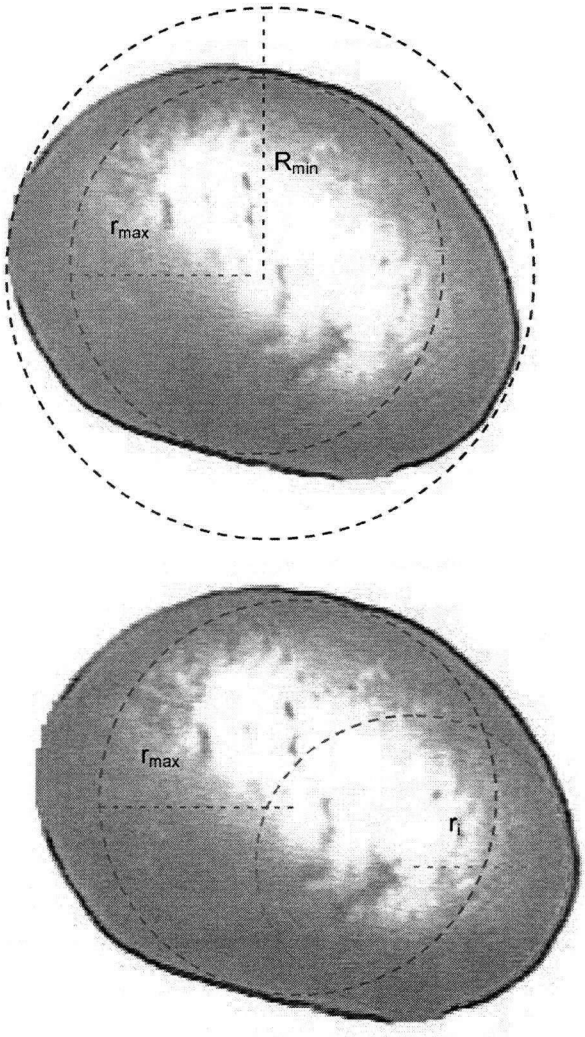

Figure 3.6: Sphericity and roundness after Santamarina and Cho, 2004

3.2. Triaxial testing program

3.2.1. Description of the triaxial equipment

The triaxial apparatus used at UBC is shown in Figure 3.7. A schematic diagram is shown in Figure 3.8. The cell pressure (P1) and back pressure (P2) are applied to the specimen through air hoses from the pressure regulator. The cell pressure and pore water pressure acting on the specimen are measured with pressure transducers (T1 and T2 respectively). An LVDT (Linear Variable Differential Transformer) measures axial deformation of the test specimen. Change in volume is deduced from the change in water level in a pipette using a differential pressure transducer (D). An external load cell and a frictionless (continually air leaking) seal on the loading ram ensure an accurate measurement of the deviator stress.

3.2.2. Data acquisition system

The triaxial apparatus uses a "National Instrument AT-MIO16x" 16-bit high speed data acquisition card for signal input. Five A/D channels are used; one for each transducer, one for axial load, one for volume change and one for axial displacement. One D/A channel is used for stress controlled tests to control the electro-pneumatic system.

The channels in this card are connected to a computer and software is used to monitor axial displacement (from the LVDT), volume change (from DPT), effective confining pressure (from pressure transducer), deviator stress (from load cell) and pore water pressure (from pressure transducer).

3.2.3. Calibration of the system and measurement resolutions

All readings on the computer are in mV. Hence it is necessary to apply a known pressure, force or displacement, in order to obtain the appropriate calibration factors, and thereby transform the mV/V excitation signal into engineering units. The calibration of the pressure transducers was done through a DPI (Differential Pressure Indicator) which reads the pressure applied in kPa, connected to the transducer. The LVDT was calibrated through a micrometer, reading the displacement in mm and reading the associated voltage on the computer. The calibration of the cell pressure was calculated by reading the load applied to the load cell through a proving ring (in

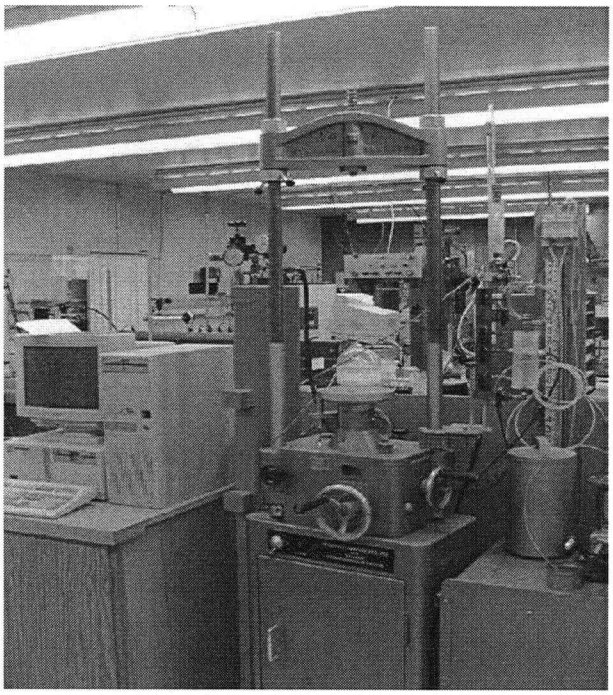

Figure 3.7: Triaxial apparatus

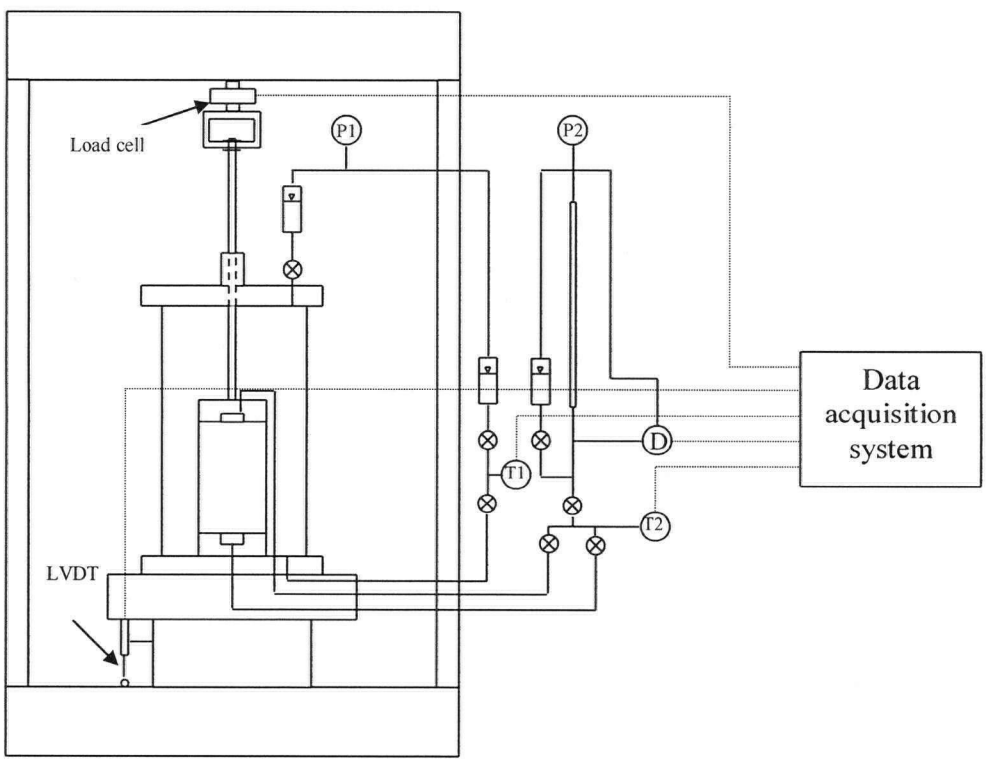

Figure 3.8: Schematic diagram of UBC triaxial apparatus

kgf) and on the computer (on mV). Finally the calibration of the volumetric deformation pipette and differential pressure transducer was done by letting water drain from the pipette and recording the volume of water in mL, reading the mV in the computer and the head of water in the pipette.

3.2.4. Preparation and testing of the specimen

Specimens were reconstituted using a water pluviation technique; a known dry mass of sand is boiled with de-aired water and then deposited in the membrane lined cavity of a split mold filled with de-aired water. This technique ensures complete saturation of the sand as the grains are not in contact with air. Prior to the preparation of the sample, it is important to saturate all the lines in the triaxial apparatus. For that, a pressure of around 120 kPa was applied for 24 hours from the pressure regulator to the reservoirs of the triaxial frame (P1 and P2).

A step by step preparation of the sample is explained below:

- Boil a known dry mass of sand and water. Let it cool, and apply vacuum in order to dissolve the air bubbles trapped in the sand.
- Boil the porous stones for 10 minutes and let them cool to room temperature.
- Grease the O-rings.
- Build up a dummy specimen with the aluminum sample and the loading cap used in the test. Take reference height to determine later the height of the specimen.
- Saturate drainage line from the sample and place bottom porous stone.
- Put the membrane and an O-ring around the pedestal. Place split mold steel jacket around the pedestal and stretch the membrane over its top.
- Apply a small vacuum to the jacket (-20 kPa) and fill it with de-aired water.
- Prepare the picnometer, fill it with de-aired water then put the stopper with glass stem and fill it with water. Invert the flask and fill the jacket with the sand. When the jacket is filled with sand to the desired height and touches the exit tip, the flow of sand will stop. The nominal dimensions of the samples are about 125 mm in height and 63 mm in diameter.
- Carefully remove all the excess sand. This must be dried and weighed to compute the relative density of the sample from subtraction.
- Carefully place the top cap with the top porous stone into the jacket in contact with the sand surface. Measure height. Snap the membrane and fit the O-ring, being careful to not

have air bubbles between the membrane and the top cap. Make sure that the top cap is leveled. Take height measurement again.

- Apply vacuum of -20 kPa through the drainage line (the sample now stands because of the vacuum and not the jacket). Take measurement of height. Remove the steel jacket and measure the diameter (top, middle, and bottom) and height of the specimen. Figure 3.9 shows the shape of the sample before placing in the triaxial chamber.
- Carefully assemble triaxial chamber and fill the chamber with de-aired water.
- Close the vacuum valve and take the final height measurement and place the specimen in the triaxial apparatus.
- On the computer, take offset values, being sure that the cell pressure and pore pressure transducers are opened to air.
- Connect a line from the specimen to the cell pressure transducer and connect the air hose to the specimen through the reservoir at its top.
- Apply a small pressure to the sample (30 kPa); this action will allow water to flow through the lines to get rid of the air bubbles and connect the drainage line to the pore pressure transducer.
- Check the Skempton B value by opening the drainage valve from the sample and increasing the cell pressure step by step until a target pressure is reached checking the B value at each time.

When a B value greater than 98% is obtained, apply the back pressure in order to impose the effective stress desired for the test, carry out the consolidation phase and then finally perform the triaxial test. A rate of displacement of 0.02 inch/min (about 0.5 %/minute) was used for every test allowing drainage of the specimen at the base only. A picture of the final shape of one test specimen is shown in Figure 3.10.

3.3. Triaxial test results

The objective of the triaxial test program is to obtain properties and thereby establish parameters of Badger sand for the critical state soil model, NorSand. As explained in Chapter II, the parameters needed are critical state parameters (Γ and λ), elastic parameters (G and ν) and plastic parameters (M, H and χ).

3.3.1. Test description

Five triaxial compression tests were performed at UBC: two consolidated undrained (CU) tests at confining pressures of 100 kPa and 150 kPa, and three consolidated drained (CD) tests at confining pressures of 50 kPa, 100 kPa and 150 kPa. Test codes and characteristics are summarized in Table 3.7.

Table 3.7: Codes and characteristics of tests

Code	Cell Pressure (kPa)	Void Ratio After Consolidation e_0 (DR%)	Drainage
CUP100	100	0.624 (33%)	Undrained
CUP150	150	0.620 (35%)	Undrained
CDP50	50	0.623 (34%)	Drained
CDP100	100	0.624 (33%)	Drained
CDP150	150	0.620 (35%)	Drained

The initial void ratio of all five tests is very similar, which shows the reconstitution method was very repeatable. It was not possible to obtain specimens looser than 33% relative density after consolidation, considered indicative of a loose state, yet one that is close to that of a medium dense state (DR ≥ 35%), which is attributed to the shape of the sand particles. As they are well-rounded particles, any minor disturbance yielded a rearrangement of the grains and densification of the sample. Therefore, although it was intended to test loose specimens, all the specimens showed an initial dilative behaviour of the sand. Hence, the steady state or critical state line was very difficult to achieve. Studies have shown that even after 25% to 30% strain, dilative specimens have not reached the steady state (Sivathayalan, 2000).

3.3.2. Void ratio determination

The determination of void ratio for each test was made by measuring the height and cross-sectional area of the specimen. The height was obtained by comparison to a dummy sample of known height. The cross-sectional area was obtained by filling the steel jacket (which had the membrane snapped and vacuumed), with de-aired water. By calculating the mass of water inside

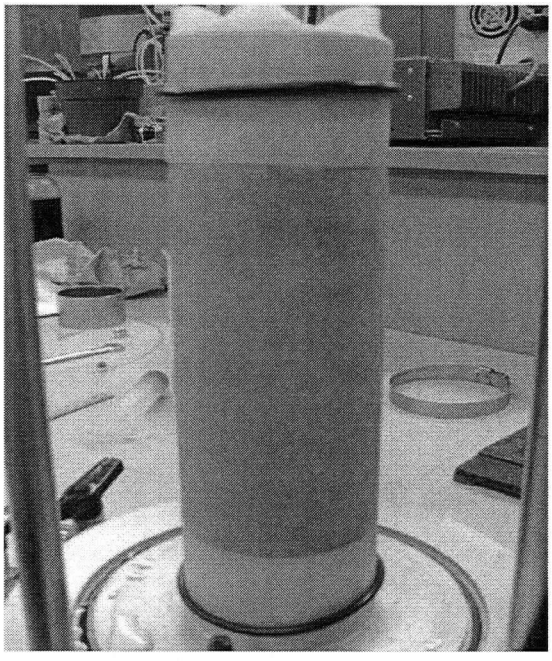

Figure 3.9: Sand sample before testing (dummy sample)

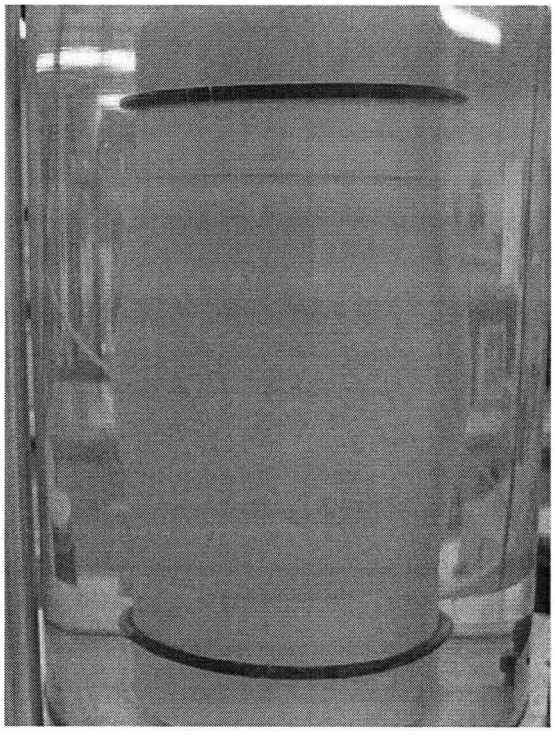

Figure 3.10: Shape of the specimen after testing (CDP100)

the jacket, corrected for temperature, and the height of water, the average diameter of the specimen obtained was 63.38 mm and was taken as a constant for every test.

3.3.3. Triaxial test results

The variation of deviator stress and volumetric strain, with axial strain, for the three drained tests is shown in Figure 3.11. The specimens are very stiff at strains less than 0.5%, and the maximum strength is reached at about 10% axial strain. With reference to the volumetric strain, the sand contracts until the maximum volumetric strain is reached (or maximum contraction), at about 1% axial strain, and then dilates until the test was terminated prior to reaching the critical state. Note the final rate of dilation in all tests is very similar, which is attributed to the very similar initial void ratio of the specimens. Interestingly, CDP100 contracts more than CDP150. As CDP100 is slightly looser than CDP150, it is possible that the void ratio-confining pressure combination made CDP100 more susceptible to contraction.

Figure 3.13 shows the void ratio observed in all five tests. The open circle indicates the void ratio at the end of the test. The drained tests clearly show a little contraction before the sample starts dilating through to the end of the test. Given the density of the specimens and the low confining pressures, all the samples dilated, hence obtaining the critical state line (CSL) was not straightforward.

Figure 3.12 shows the deviator stress and the pore water pressure for the two undrained tests. Again, the specimens are very stiff at strains less than 0.5%, then the slope reduces after 1% axial strain, and the higher the confining pressure, the higher the strength of the specimen. The tests initially tend to contract, generating a positive value of excess pore water pressure, until they reach the maximum pore pressure (or phase transformation) at about 1% axial strain, which is consistent with the maximum contraction points found for the drained tests. The sand then tends to dilate. Hence the excess pore water pressure decreases until the tests are stopped. A steady state condition was not reached as the sand continued to dilate until the end of the test.

Figure 3.14 shows the stress path for the five triaxial tests in q-p' space. Both undrained tests show an initial contraction, where the pore pressure increases, until they reach the phase transformation point (defined by Ishihara et al (1975) as the maximum excess pore water pressure), and then dilate until the end of the test. The drained tests follow the expected 1:3 slope, reaching the peak angle of friction and then softening for the rest of the test.

a)

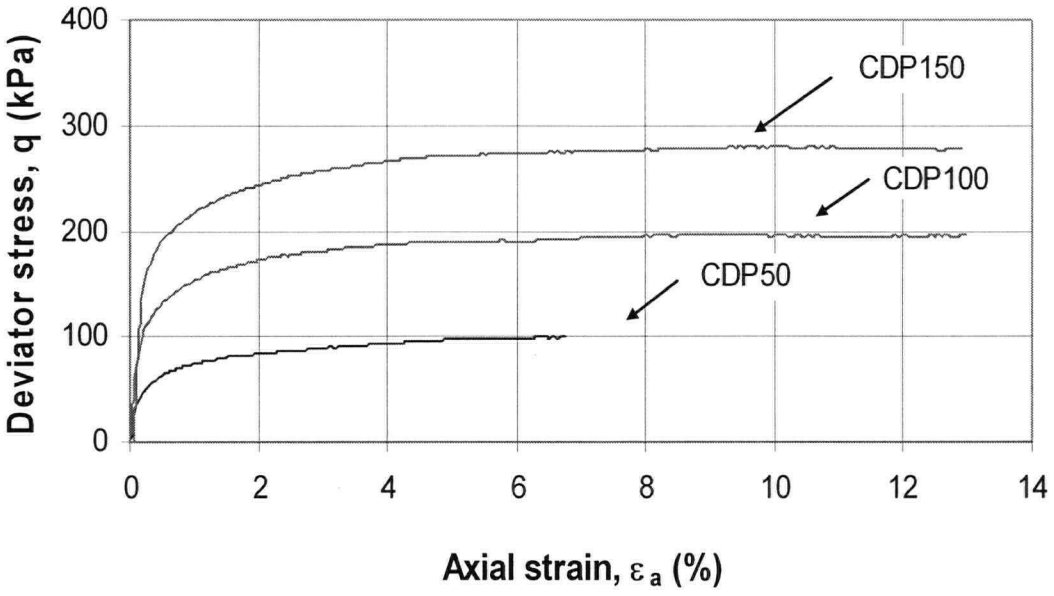

b)

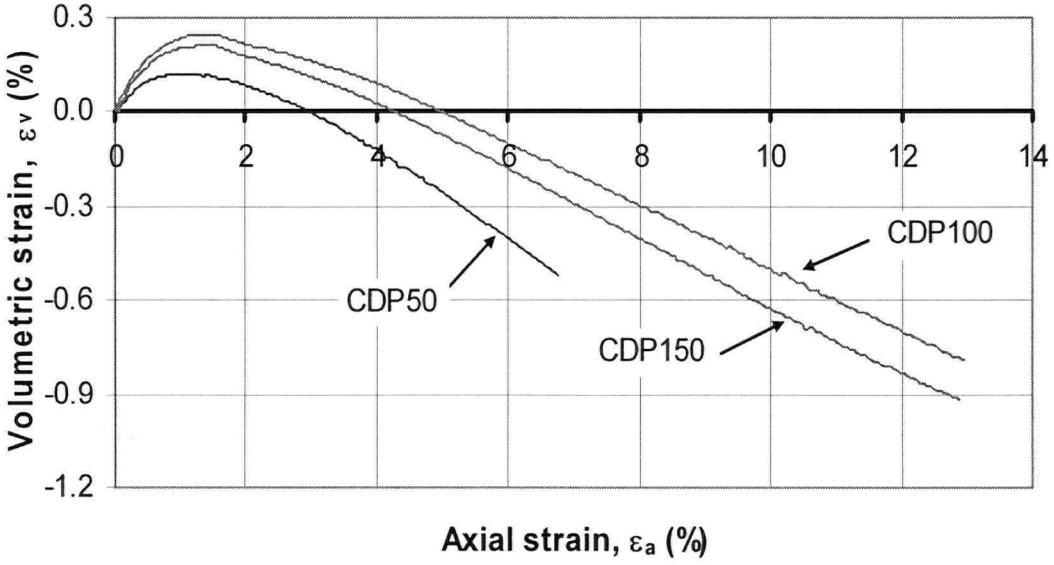

Figure 3.11: Triaxial (CD) test results: a) deviator stress and b) volumetric strain

a)

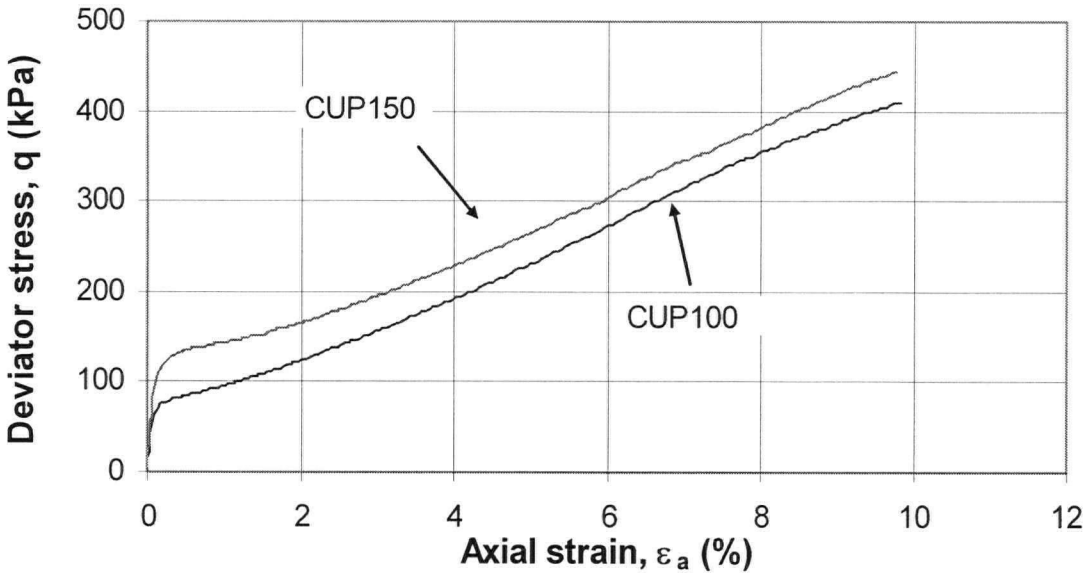

b)

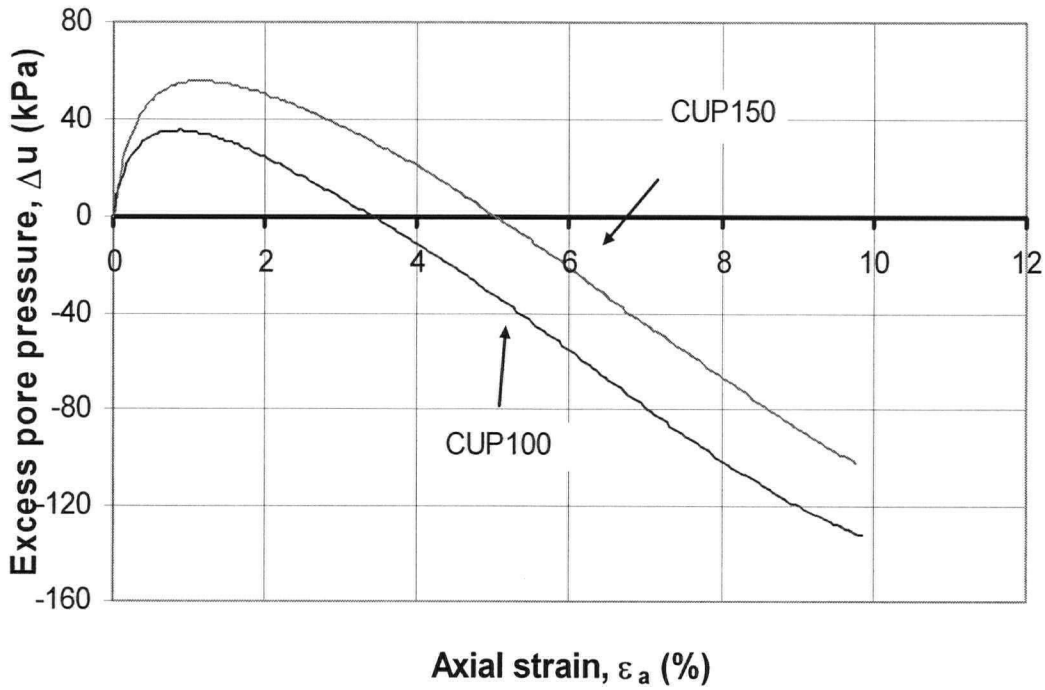

Figure 3.12: Triaxial (CU) test results: a) deviator stress and b) excess pore pressure

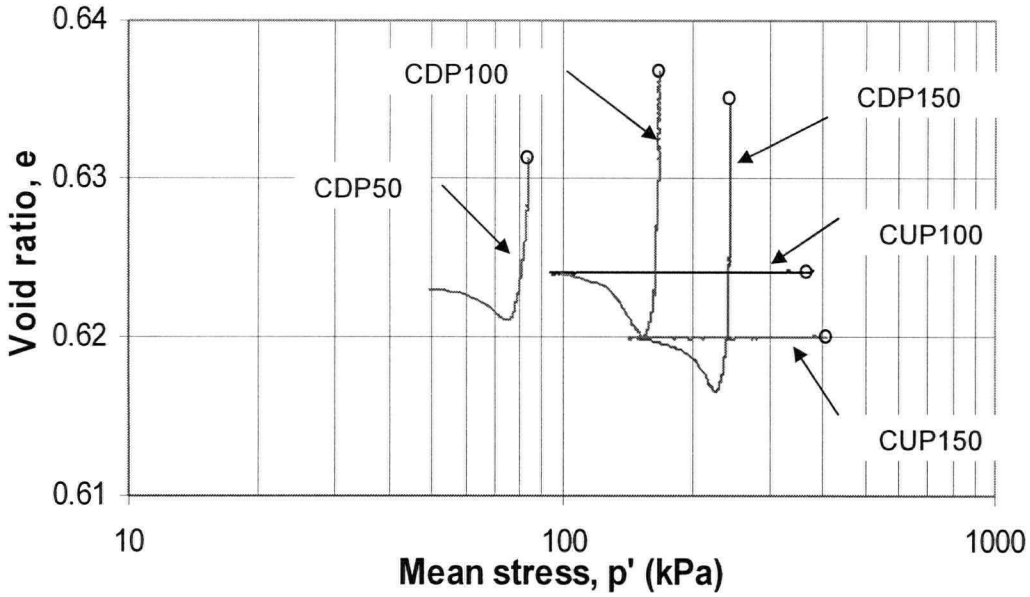

Figure 3.13: Triaxial test results: void ratio

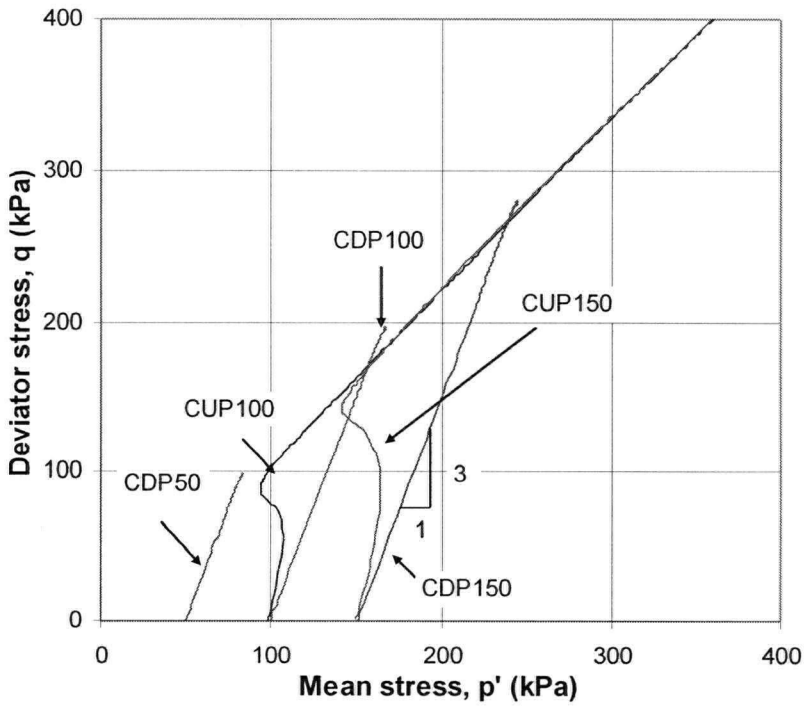

Figure 3.14: Triaxial test results: stress path

3.3.4. Shear modulus

Additional triaxial tests on specimens of Badger sand, that were reconstituted by moist tamping, were reported by Golder Associates (2004). By attaching bender elements to the specimen and recording the shear wave velocities as the specimen was tested, it was possible to obtain the value of the shear modulus as a function of the confining pressure (see Figure 3.15). The relation obtained between shear modulus and mean stress is:

$$G_{max} = 9.35\ (p')^{0.47} \times 1000\ (MPa) \qquad 3.7$$

It is well recognised that the specimen reconstitution method determines the fabric of a sand specimen, hence the value of G_{max} from a water pluviated specimen will be different to the G_{max} obtained from moist tamped specimens. However, as elasticity parameters are needed later in this study (see Chapter V), this finding is reported, in order to establish a value for the same well-rounded sand rather than assuming a value believed appropriate to Badger sand.

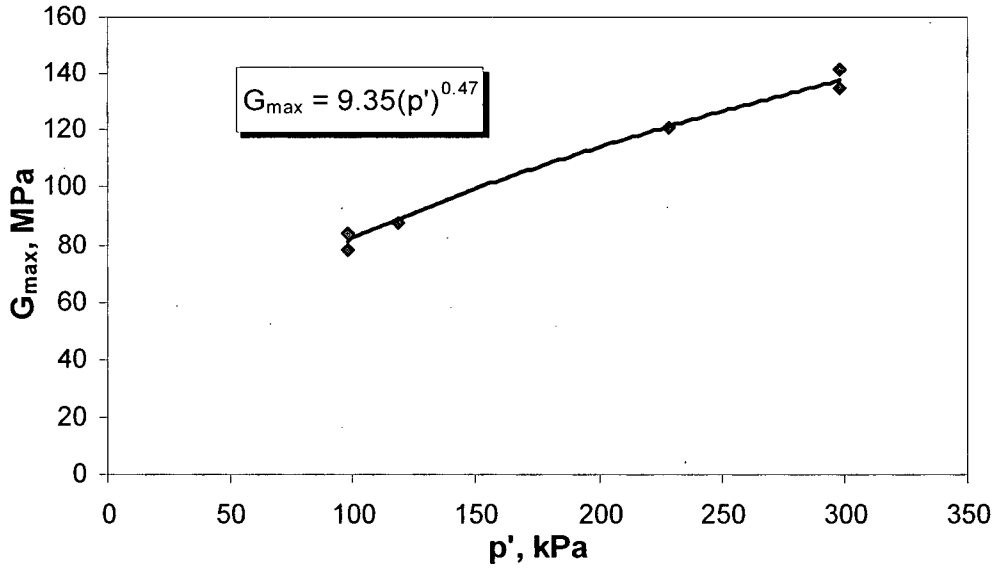

Figure 3.15: G_{max} in function of mean stress for Badger sand (Golder Associates, 2004)

CHAPTER IV: ANALYSIS OF RESULTS

The parameters derived from the UBC triaxial testing program described in Chapter III, are somewhat unusual for a silica sand, given the relatively low friction angles and a difference between extreme void ratios equal to 0.2. Also, in contrast to many sands, the grains are very rounded. In order to determine if the approaches used to describe typical sands are able to capture the behaviour of rounded sands such as Badger sand, results obtained from the triaxial tests are analyzed and discussed. Properties for Badger sand are determined: some of the properties are measured, and others are curve fitted with the help of the NorSand model.

4.1. Friction angles results from triaxial test program

The angles were obtained following the definitions given in Chapter II. In summary, the angle of repose, (ϕ_{rep}), is calculated by measuring the angle of the heap formed when sand is deposited as loose as possible. The peak friction angle, (ϕ_p), is obtained from drained tests on dense sand samples. The maximum contraction friction angle, (ϕ_{MC}), is obtained from drained tests and corresponds to the point where the incremental volumetric strain changes from contractive to dilative. The phase transformation friction angle, (ϕ_{PT}), is measured in undrained tests and corresponds to the maximum pore water pressure. Finally, the maximum obliquity, (ϕ_{MO}), is the state of maximum effective stress ratio, ie, (σ_1'/σ_3') in undrained tests.

4.1.1. Constant volume friction angle (ϕ_{CV})

In order to obtain the critical state friction angle, loose specimens must reach the critical state within the strain limitations of the test. As explained in Chapter III, although loose tests were planned, it was not possible to obtain specimens looser than the critical state line by the water pluviation method: the relative densities were 34%, 33% and 35%, for tests CDP50, CDP100 and CDP150, respectively (see Table 3.7). The same phenomenon was found by Vaid and Chern (1985) with Ottawa sand (which is also a rounded sand). The minimum relative density they obtained by the water pluviation method was DR=30%. In addition, Golder Associates used the moist tamped specimen reconstitution method, which is supposed to give the loosest possible state with no success; the sand specimens were always denser than the critical state. Dense

samples dilate and the critical state is reached at very large strains. Studies have shown that even after 25% to 30% strain, dilative specimens have not reached the critical state (Sivathayalan, 2000). The tests on Badger sand were carried to a maximum strain of 15%, so, the critical state was not reached by the end of the tests. Hence, another approach is needed to determine the critical state friction angle for Badger sand.

It is possible to establish the critical stress ratio, M, from the D_{min} versus η_{max} plot from several drained triaxial tests. As D=0 at the critical state, taking the best fit through the points as a basis for extrapolation, and taking η_{max} at D_{min}=0, M_{tc} can be obtained (Bishop, 1966). The advantage of the method is that it does not require triaxial test data at large strain. Values for CDP50, CDP100 and CDP150 are plotted in Figure 4.1. It may be seen that the best fit through these three drained tests gives a straight line. Projecting this line to D_{min}=0 the value of M_{crit} was found to be equal to 1.13, which corresponds to a constant volume friction angle of 28.4°

Figure 4.2 shows the plot η versus D^P, for CDP100. M_{crit} can also be estimated by plotting the stress ratio versus the dilatancy for the drained tests and projecting the post peak η line to the critical state D^P=0. This procedure is most accurate if the tests approach the critical state. The values obtained from the three drained tests on Badger sand, were about 1.125, 1.13 and 1.133 for CDP50, CDP100 and CDP150, respectively.

Hence from the two methods described above a good estimate of the critical state friction angle for Badger Sand is $\phi_{cv} = 28.4^\circ$.

Following the ASTM method described in Chapter III, the angle of repose obtained for Badger sand was 30.9°. This value agrees with Fannin et al (2005), who reported an angle of repose for Badger sand of 31° following the method described by Bolton (1986). This method consists in excavating the toe of a heap formed by loose dry sand.

It is generally assumed that the angle of repose corresponds to the internal friction angle of a material. Cornforth (1973) suggests that ϕ_{CV} can be predicted by performing a static angle of repose test on dry sand. However, for Badger sand the angle of repose is 2.5° higher than the critical state friction angle (see Table 4.5). Many factors such as amount of material, rate of pouring of the material and surface roughness influence the value of the angle of repose (Miura et al, 1997). As well, properties such as grain size and angularity influence the value of ϕ_{rep}.

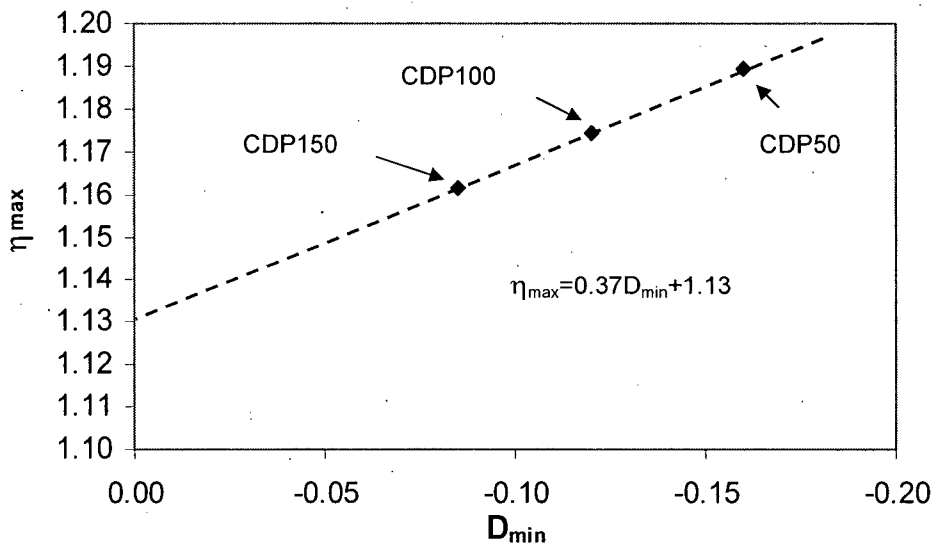

Figure 4.1: D_{min} versus η_{max} for CDP50, CDP100 and CDP150

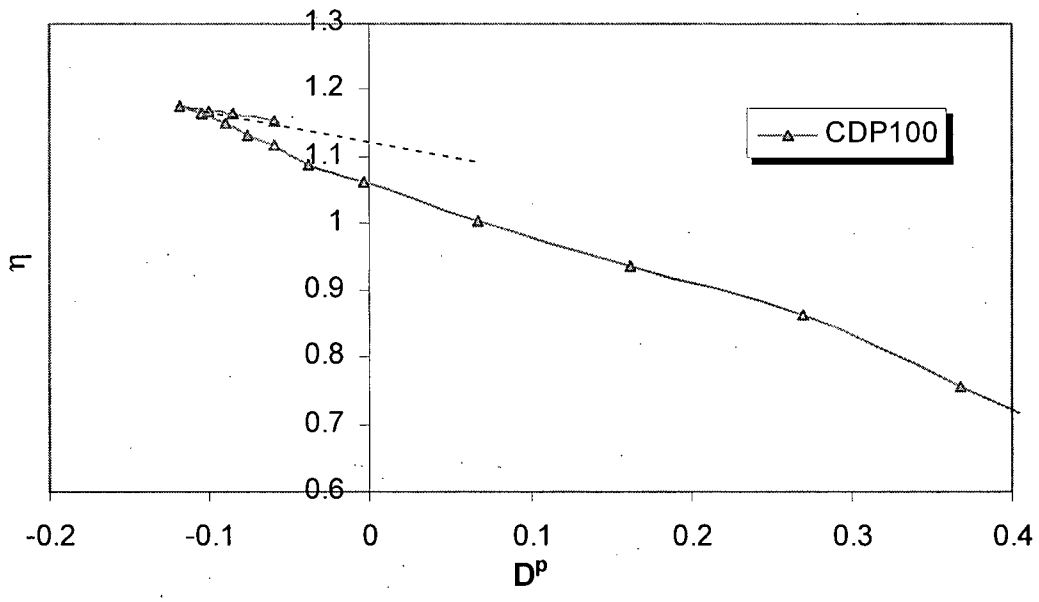

Figure 4.2: Stress dilatancy plot for CDP100

4.1.2. Peak friction angle (ϕ_p)

The peak friction angles for the three drained tests are reported in Table 4.1; the peak friction angles for Badger sand are very similar, with an average value of ϕ_p=29.4°. Bolton (1986) proposed a relative dilatancy index, I_R, given by Eq. 2.23.

$$I_R = DR(Q - \ln p') - R \qquad \text{(Eq. 2.23)}$$

This relative dilatancy index was obtained considering 17 different sands for confining pressures between 150 kPa and 600 kPa. Table 4.1 shows the values obtained for Badger sand using Q=10 and R=1.

Table 4.1: Relative dilatancy index for Badger sand

Test	DR	p' (kPa)	I_R	$3I_R$	ϕ_{peak}	ϕ_{cv}	ϕ_{peak}-ϕ_{cv}
CDP50	0.34	50	1.07	3.21	29.7	28.4	1.3
CDP100	0.33	100	0.78	2.34	29.4	28.4	1.0
CDP150	0.35	150	0.75	2.25	29.1	28.4	0.7

As well, Bolton (1986) suggested a relation between the peak friction angle, the constant volume friction angle and the relative dilatancy index, given by (Eq. 2.24).

$$\phi_p - \phi_{cv} \approx 3I_R \qquad \text{(Eq. 2.24)}$$

From Table 4.1 the difference between Bolton's prediction and the values of Badger sand is approximately 1.5°, which suggests that the peak friction angle might be lower than expected.

Similarly, Bolton (1986) suggested a relation between I_R and the rate of dilatancy given by:

$$\left(-\frac{d\varepsilon_v}{d\varepsilon_1}\right)_{max} = 0.3I_R \qquad 4.1$$

Table 4.2 shows the predicted values with Equation 4.1 and the values obtained for Badger sand. Again, the predicted values are larger than the ones obtained with the triaxial tests.

Table 4.2: Rate of dilatancy for Badger sand

Test	DR	p' (kPa)	$\left(-\frac{d\varepsilon_v}{d\varepsilon_1}\right)_{max}$	$0.3I_R$
CDP50	0.34	50	0.19	0.32
CDP100	0.33	100	0.17	0.23
CDP150	0.35	150	0.19	0.23

It is known that maximum strength is related to maximum dilatancy and that maximum dilatancy is affected by initial density and effective stress. From Table 4.2 the rate of dilatancy obtained for the three triaxial tests on Badger sand is very similar, which is consistent with the very similar values of peak friction angle. It will be shown later in this Chapter that the dilatancy of Badger sand is unusual, which may contribute to the low values of peak friction angle obtained with the triaxial tests.

4.1.3. Maximum contraction friction angle (ϕ_{MC})

Table 4.3 shows the values obtained for the maximum contraction friction angle for Badger sand found with the triaxial tests, which are very similar. Miura et al (1998) found that the angle of maximum contraction and the friction angle at failure depend on the void ratio extent ($I_e = e_{max} - e_{min}$) and the angularity of the grains; as I_e and angularity increase (or roundness decreases), ϕ_{MC} and ϕ_{cv} increase.

Table 4.3: Maximum contraction friction angle for Badger sand

Test	DR (%)	$(\varepsilon_v)_{max}$	$(\sigma_1'/\sigma_3')_{(\varepsilon_v)_{max}}$	ϕ_{MC}
CDP50	34%	0.12	2.51	25.4
CDP100	33%	0.25	2.63	26.7
CDP150	35%	0.21	2.50	25.4
(average)				25.8

They reported the values of ϕ_{MC} and ϕ_{rep} as shown in Figure 4.3. The values for Badger sand are added to that database. The maximum contraction angle plots between the proposed boundaries and links sands with glass beads.

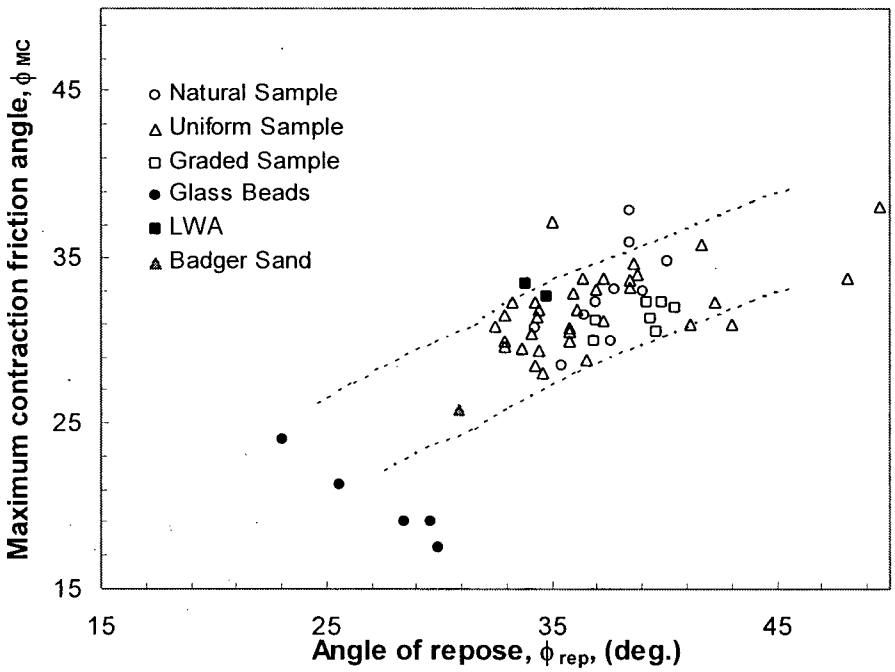

Figure 4.3: Relation between angle of repose and maximum contraction friction angle (after Miura et al, 1998) [3]

4.1.4. Phase transformation friction angle (ϕ_{PT})

Table 4.4 shows the values of the phase transformation friction angles obtained at the point where the pore water pressure is maximum for CUP100 and CUP150.

[3] After Miura et al (1998), Natural samples are selected from natural sand, Uniform samples and Graded samples are reconstituted sand samples, and L.W.A. (Light Weight Aggregates) and Glass beads are artificial granular materials.

Table 4.4: Phase transformation friction angle for Badger sand

Test	DR (%)	$(\Delta U)_{max}$ (kPa)	$\phi_{(\Delta U)_{max}}$
CUP100	33%	35.3	25.5
CUP150	35%	55.7	25.6
(average)			25.6

There has been considerable discussion of the uniqueness of ϕ_{CV}, ϕ_{PT} and ϕ_{MC} in the literature. Further debate has addressed whether or not the critical state friction angle, steady state friction angle, maximum contraction friction angle and phase transformation friction angle are the same. The following is a summary, by authors, in chronologic order:

- Kirkpatrick (1961) suggested that ϕ_{MC} is a unique parameter for each sand. He also suggested that ϕ_{MC} and ϕ_{CV} are the same, and independent of the specimen behaviour (contractive or dilative).

- Luong (1980) performed triaxial compression and extension tests on various cohesionless materials. He found that the maximum contraction friction angle is independent of stress path, initial porosity, grain size and anisotropy. He also found that, for contractive specimens, ϕ_{CV} and ϕ_{MC} are the same.

- Vaid and Chern (1985) performed monotonic and cyclic triaxial tests on Ottawa sand and a mine tailings sand. They found that the phase transformation and the steady state line are the same for contractive specimens, and that ϕ_{PT} is a unique property.

- Negussey et al (1988) performed ring shear tests on medium Ottawa sand and fine and coarse copper particles. They found that ϕ_{CV} is independent of normal stress, density, and grain size, and hence a unique parameter. They suggested that for loose samples, ϕ_{CV} and ϕ_{MC} are the same and that ϕ_{MC} decreases with initial relative density and increases with increasing confining pressure. As well, they found that ϕ_{PT} and ϕ_{CV} are the same and that ϕ_{PT} is a unique property of sands, independent of density and effective stress.

- Oyenuga and Tisot (1989) performed triaxial tests and direct shear box tests to measure ϕ_{PT} and ϕ_{MC}, and ring torsion tests to measure ϕ_{CV} with Fountainebleau sand and three Moselle sands. They found that ϕ_{CV} is independent of grain size distribution, effective stress and density. As well they suggest that ϕ_{CV} and ϕ_{MC} are the same.

- Vaid et al (1990) performed triaxial tests Ottawa sand. They found that the phase transformation friction angle and the steady state friction angle are the same and a unique property for contractive sand specimens but are different for dilative sand specimens. They found that ϕ_{PT} is a unique property of a sand for contractive specimens, independent of initial void ratio, consolidated state and mode of loading.

- Chu (1995) performed a different triaxial test in order to reach the critical state with dense sand specimens of Sydney sand. The procedure is to isotropically consolidate a dense sand sample and shear it to failure at constant confining pressure. When failure is reached, a constant volume condition is imposed. A full description of the procedure is found in Chu and Lo (1993). With this procedure they ensured homogeneous deformations and that the critical state was reached in the homogeneous zones. They observed that the critical state friction angle is stress level dependent, the higher the confining pressure, the smaller the friction angle, but independent of the initial density. The same conclusion was found for the phase transformation and maximum contraction friction angle but these angles are also dependent on the initial density of the specimen. As well, Chu (1995) found that for contractive soils, ϕ_{CV}, ϕ_{PT} and ϕ_{MC} are the same. However for dilative specimens ϕ_{PT} and ϕ_{MC} are the same but different from ϕ_{CV}.

Table 4.5 provides a summary of the different friction angles obtained during the triaxial testing program for Badger Sand. The values of M_{tc} and their corresponding angle of friction are reported for different states; repose, failure envelope, maximum contraction, phase transformation and constant volume. From Table 4.5 the two numbers for Badger sand are very close and indistinguishable within the experimental resolution of the triaxial tests.

Table 4.5: Different friction angles for Badger sand

State	M_{tc}	ϕ (°)
Repose	1.24	30.9
Maximum obliquity (MO)	1.13	28.4
Maximum contraction (MC)	1.02	25.8
Phase transformation (PT)	1.01	25.6
Critical state (CV)	1.13	28.4

From Table 4.5 the maximum contraction friction angle is practically the same than the phase transformation friction angle. However, the constant volume friction angle is higher than the phase transformation friction angle (or maximum contraction friction angle) and is equal in magnitude to the maximum obliquity friction angle. These results are consistent with the findings of Chu (1995). Additionally, the maximum obliquity friction angle is equal to the phase transformation friction angle plus 2.8°. This finding agrees with Sivathalayan (2000). As Badger sand always had a dilative behaviour for the void ratio – mean stress combination presented in the triaxial testing (see Figs 3.11 and 3.12), it seems reasonable to have a different value for the angle of friction for the phase transformation state and the constant volume state.

Typical values of critical state friction angles for sands stated in chapter II range between 30° and 39° (see Table 2.1). Hence, the values found for Badger sand are lower than commonly found. Also, the angle of repose and the constant volume friction angle measured for Badger sand are different. Similarly, the values of the peak friction angle were found to be lower than expected. Additionally, as explained in Chapter III, the values of the minimum and maximum void ratio were somewhat unusual. In order to be confident that the values found for Badger sand in the triaxial tests are correct, these atypical results are now compared with values of other sands found in the literature.

4.2. Comparison of Badger sand properties with literature

As reported in Chapter III, the minimum and maximum void ratios found for Badger sand are unusual: e_{min} = 0.49 and e_{max} = 0.69, yielding $I_e = e_{max} - e_{min}$ = 0.2, which is a very low value for sands. Table 4.6 summarizes values of roundness, minimum and maximum void ratio and I_e for different materials, with roundness ranging from 0.2 to 0.6. As suggested by Shimobe and Moroto (1995) and Cubrinovski and Ishihara (2002), the values of e_{min} and e_{max} increase with decreasing the roundness of the particles, and $I_e = e_{max} - e_{min}$ increases with decreasing roundness.

Table 4.6: Values of roundness and void ratio for various sands (from Youd, 1973)

Material	R	e_{max}	e_{min}	I_c
Ottawa sand	0.60	0.704	0.408	0.296
Lapis Lustre sand	0.44	0.754	0.460	0.294
Monterey sand	0.39	0.772	0.469	0.303
Del Monte sand	0.27	0.971	0.503	0.468
Crushed basalt	0.20	1.190	0.700	0.490

In order to determine if the values of the maximum and minimum void ratios found for Badger sand are reasonable, 30 particles were taken randomly, and following the procedure explained in Chapter III and Eqs. 2.28 and 2.29 of Santamarina and Cho (2004), the sphericity and roundness were determined. Average values of S = 0.77 and R = 0.81 were obtained, as shown in Table 3.5 and Table 3.6. This value of roundness classifies Badger sand as a well rounded sand (Powers, 1953, Table 2.2).

Figure 4.4 shows the relations for the minimum and maximum void ratios defined by Santamarina and Cho (2004), Shimobe and Moroto (1995), and Youd (1973). A clear tendency of decreasing void ratios with increasing roundness is appreciable, converging to a null slope as roundness approaches a value of 1. As well, the difference between e_{max}-e_{min} decreases with increasing roundness. Youd (1973) reported materials with roundness between 0.17 and 0.60. Shimobe and Moroto (1995) correlated e_{max} and the roundness from 76 different materials; they reported values of roundness between 0.1 and 0.7 for sands and a roundness of 1 for glass beads. As well, Santamarina and Cho (2004) reported values of roundness between 0.2 and 1 from natural and crushed sands. The values of R, e_{min} and e_{max} obtained for Badger sand are included, and lend confidence to the general trend in the data.

Santamarina and Cho (2004) found that the constant volume friction angle of granular materials depends on the shape of the particles. Based on observations of 54 specimens they measured ϕ_{CV} as the angle of repose for materials with roundness between 0.1 and 1 and proposed:

$$\phi_{CV} = 42 - 17R \qquad 4.2$$

The values of ϕ_{CV} and ϕ_{repose} are added to the database, showing an excellent agreement with the proposed relation (Figure 4.5).

Generally, the values of mobilized friction angles given in Table 4.5 indicate the range of friction angles for Badger sand is very narrow: the difference between the maximum obliquity and the phase transformation friction angle is $\phi_{MO} - \phi_{PT} = 2.8^{o}$. Table 4.7 shows the values of ϕ_{MO} and ϕ_{PT} for Fraser River sand (Vaid and Eliadorani, 1998), which is an angular sand, and Ottawa sand which is a rounded sand (Vaid and Chern, 1985). Data for the rounded Badger sand appear in excellent agreement with the findings for Ottawa sand.

Table 4.7: Friction angles for Ottawa sand and Fraser River sand

Material	ϕ_{MO}	ϕ_{PT}	$\phi_{MO} - \phi_{PT}$
Ottawa sand	31.5°	29.4°	2.1°
Fraser River sand	37°	32°	5.0°

This interpretation of the data for Badger sand and comparison with the literature, confirms the shape of the grain plays an important role in governing intrinsic parameters of granular materials. As the roundness of the particles increases, the maximum and minimum void ratios decrease, as does the difference $I_e=e_{max}-e_{min}$. Also, the constant volume friction angle decreases as the roundness of the particle increases. In addition, it seems that for rounded sands the difference between the mobilized friction angles is smaller than for angular sands.

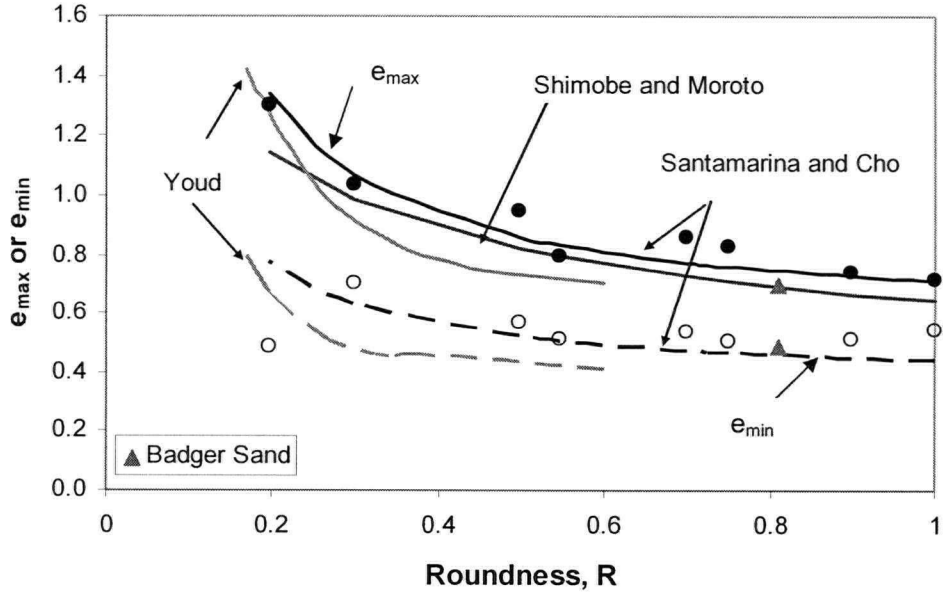

Figure 4.4: Relation between roundness and extreme void ratios

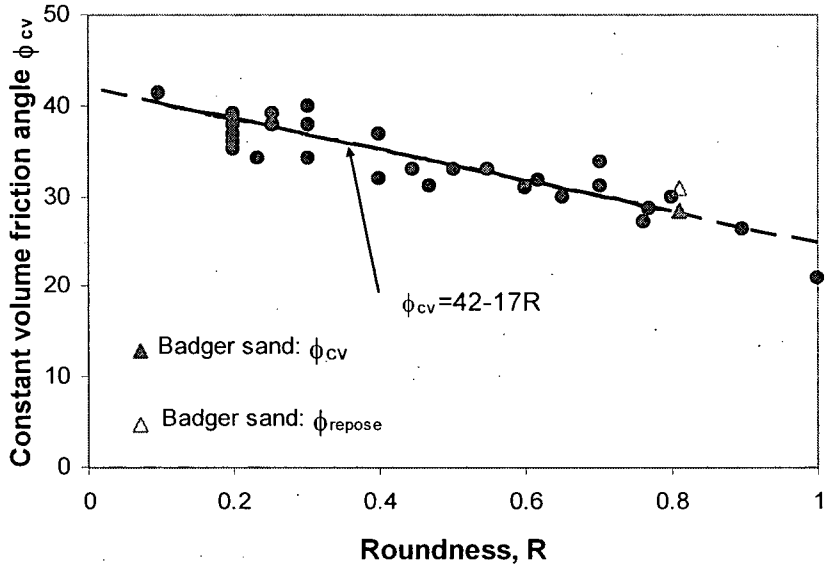

Figure 4.5: Relation between roundness and constant volume friction angle (from Santamarina and Cho, 2004)

4.3. Analysis of NorSand results

As explained in chapter II, the NorSand constitutive model has seven input parameters; two critical state parameters (Γ and λ), three plastic parameters (M_{tc}, H and χ_{tc}) and two elastic parameters (Ir and ν).

The critical state parameters, Γ and λ, are ideally obtained from drained and undrained tests on very loose reconstituted sand samples at different confining pressures. M_{tc} is obtained from the end of test condition of very loose triaxial drained tests or Bishop's η-D plot for dense specimens.

The plastic hardening parameter, H, is a fabric dependent parameter and is obtained by fitting the curves and iterating to have the best match. It is found that H is directly related to the state parameter, ψ.

χ_{tc} is found by plotting the state parameter at image condition, ψ_I, versus the minimum dilatancy D_{min}. It is believed that χ is also a fabric dependent parameter.

The elastic property Ir is obtained from bender elements during the triaxial tests. If bender elements are not included an unload-reload cycle can be performed.

Poisson's ratio, ν, is measured in laboratory tests and is about 0.2 and is typically assumed between 0.1 and 0.2. Generally a value of ν close to 0.1 is used for modelling purposes.

4.3.1. Comparison between triaxial data and NorSand model for Badger sand

Figure 4.6, Figure 4.7 and Figure 4.8 show the comparison between the three drained triaxial tests (CDP50, CDP100 and CDP150, respectively) and the predictions with NorSand. The parameters used for the fittings are described later and a summary table is presented at the end of this chapter.

The peak deviator stresses predicted by NorSand are larger than the ones obtained with the tests (for CDP50 and CDP150), and they are very similar for the CDP100 test. Nevertheless the initial stiffness and final trends show on average a good fit, capturing the drained behaviour of the Badger sand. The main purpose of the comparison between the triaxial data and the model is to obtain the parameters needed to describe the behaviour of Badger sand by having a reasonable fit to all the tests and not one really good fit and the others poor.

Similarly, for the volumetric strain, the model predicts more contraction than the real data, but the rate of dilation of the sand is captured until the 10% axial strain.

A better fit for the initial stiffness and the contraction of the sand can be found by increasing the hardening parameter, H, as shown in Figure 4.9. However, the rate of dilation is not captured, the model showing a lower rate than the triaxial data.

Also, Figure 4.10 and Figure 4.11 show the fitting for the undrained tests with the same parameters used to fit the drained tests. In this case, the deviatoric stress predicted by NorSand is smaller than the one obtained by the triaxial tests. Also, the test data show less pore water pressure than the prediction with NorSand, hence the difference in strength. However, for both, deviatoric stress and pore water pressure NorSand is able to capture the behaviour of Badger sand for the strains up to 10%.

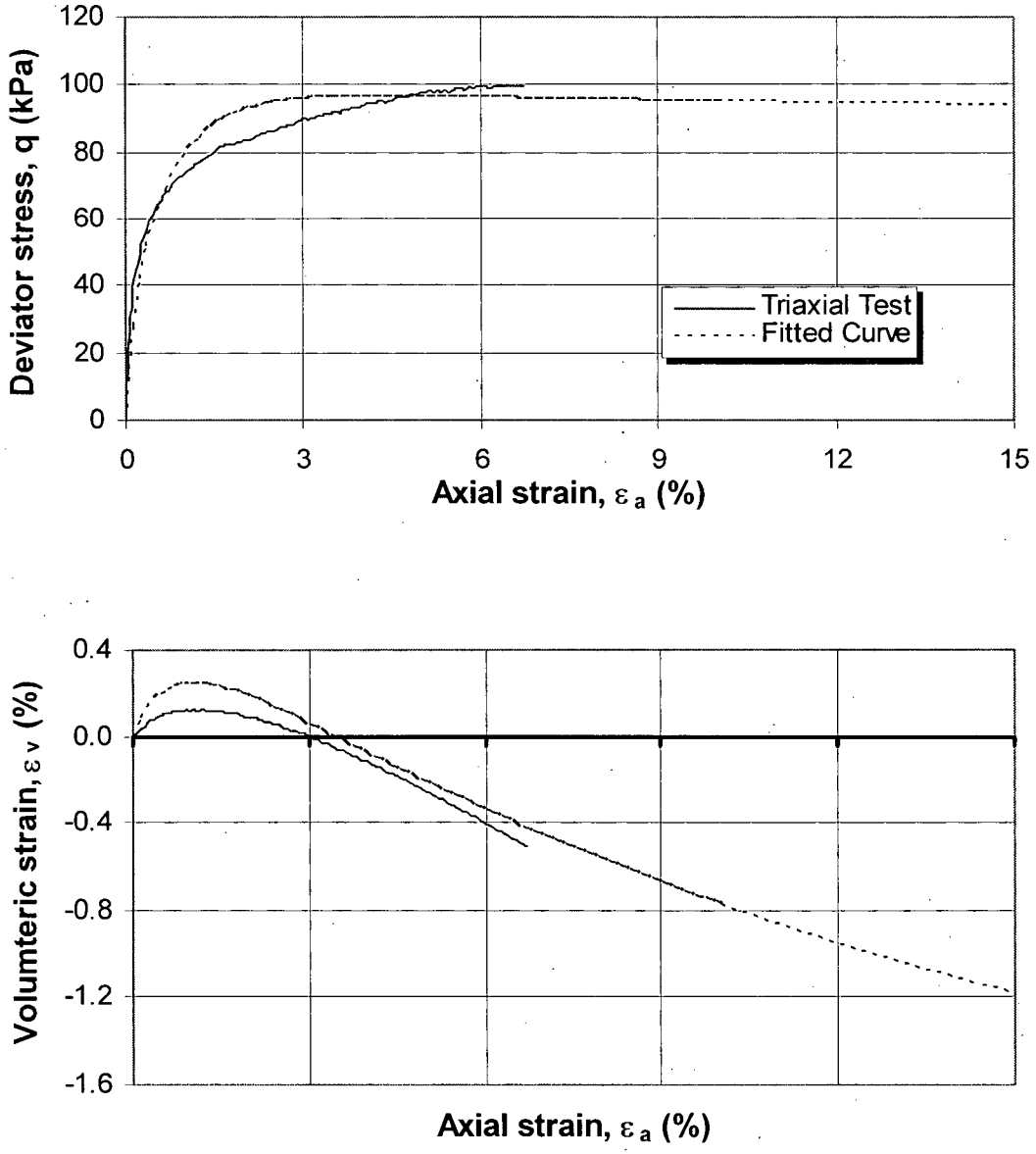

Figure 4.6: Comparison of deviator stress and volumetric strain between triaxial data and NorSand model for CDP50

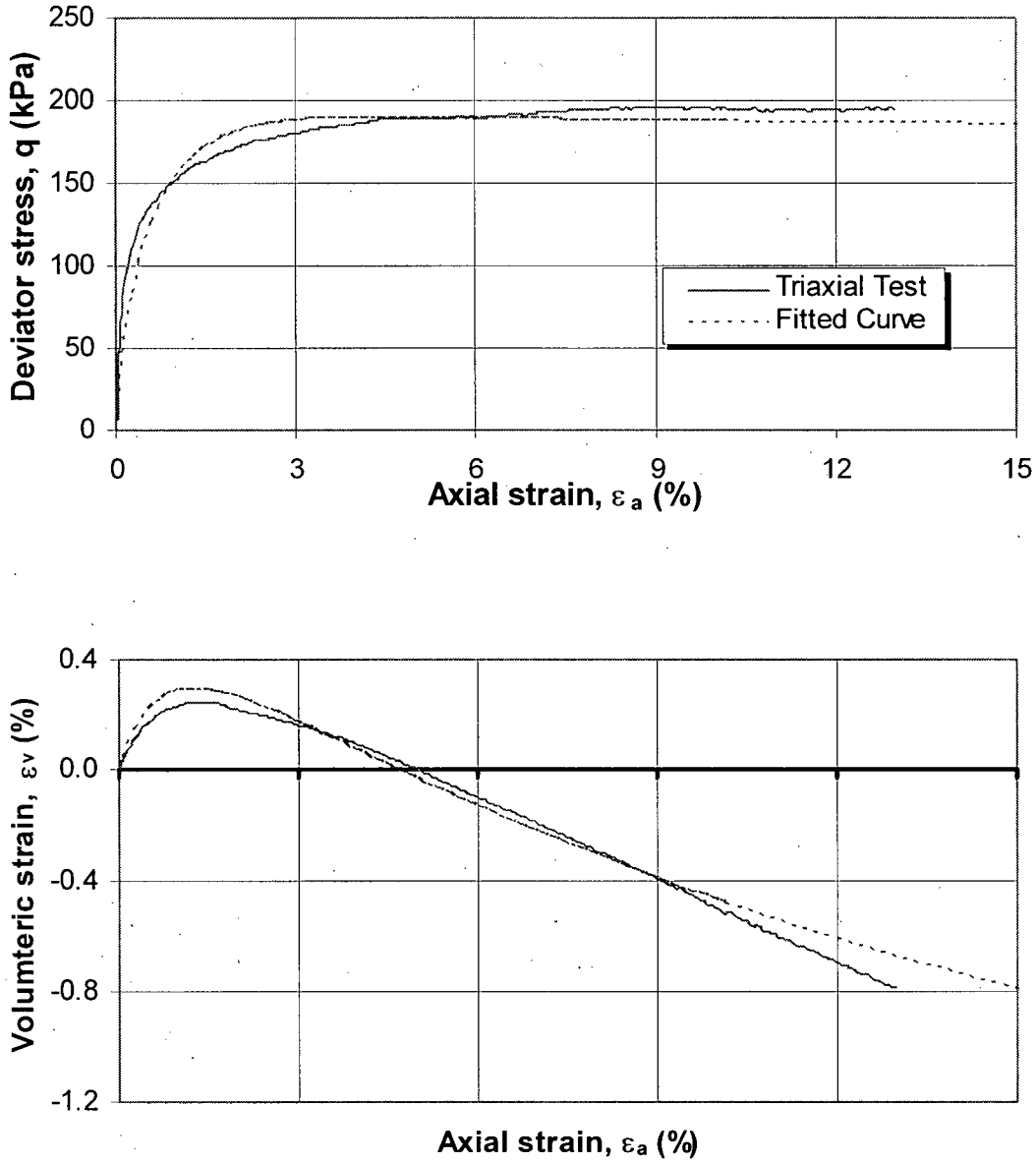

Figure 4.7: Comparison of deviator stress and volumetric strain between triaxial data and NorSand model for CDP100

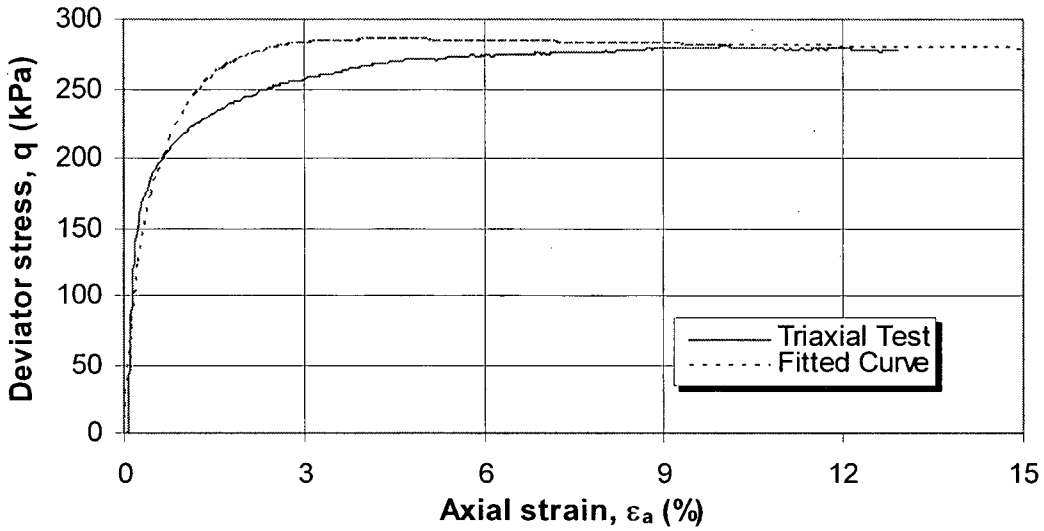

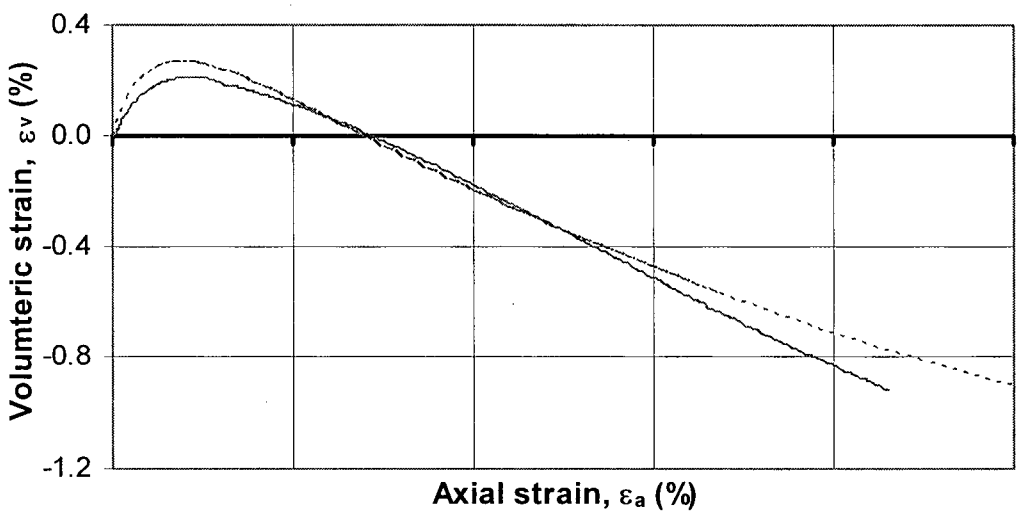

Figure 4.8: Comparison of deviator stress and volumetric strain between triaxial data and NorSand model for CDP150

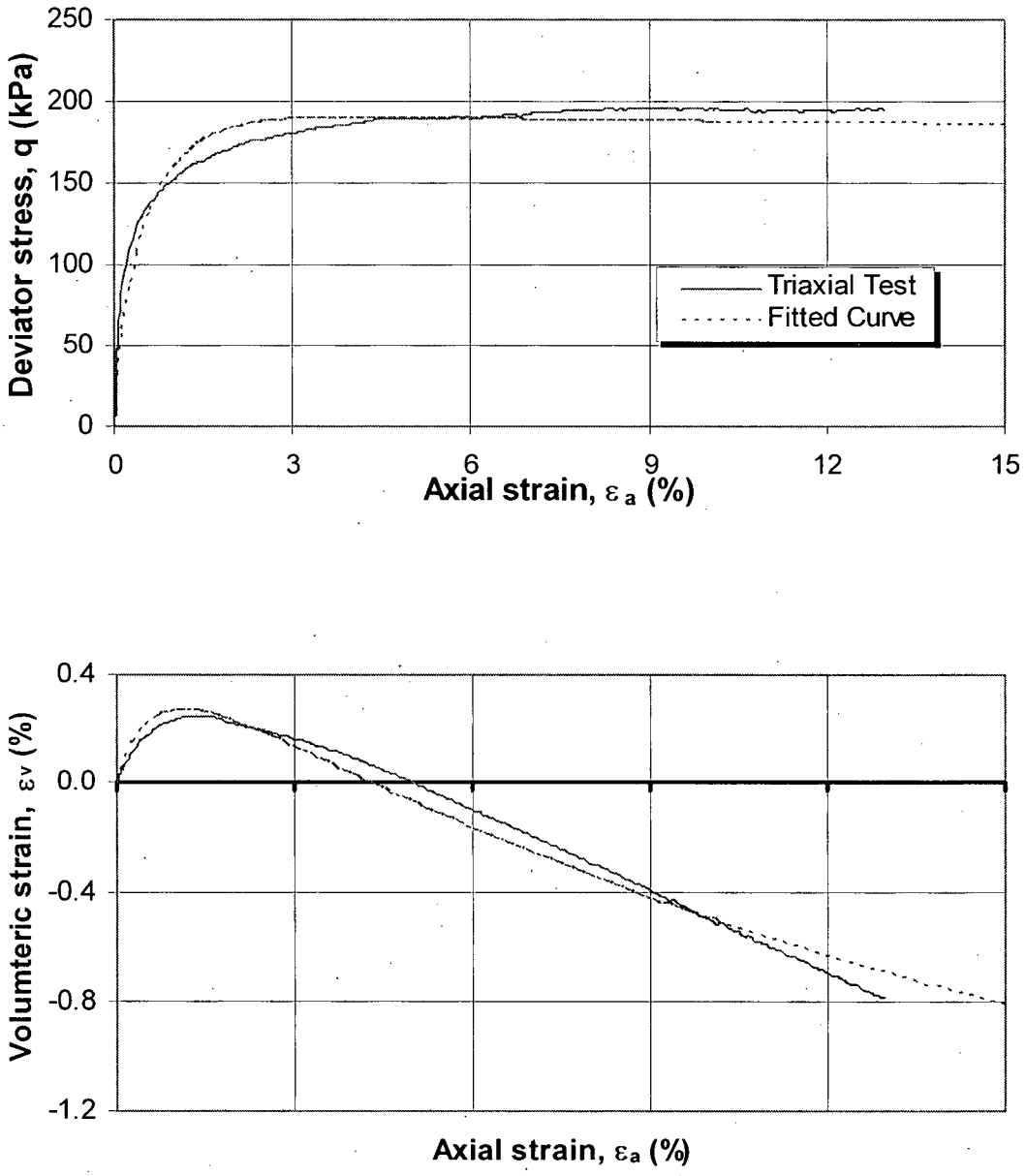

Figure 4.9: Comparison between CDP100 and NorSand model for a greater hardening

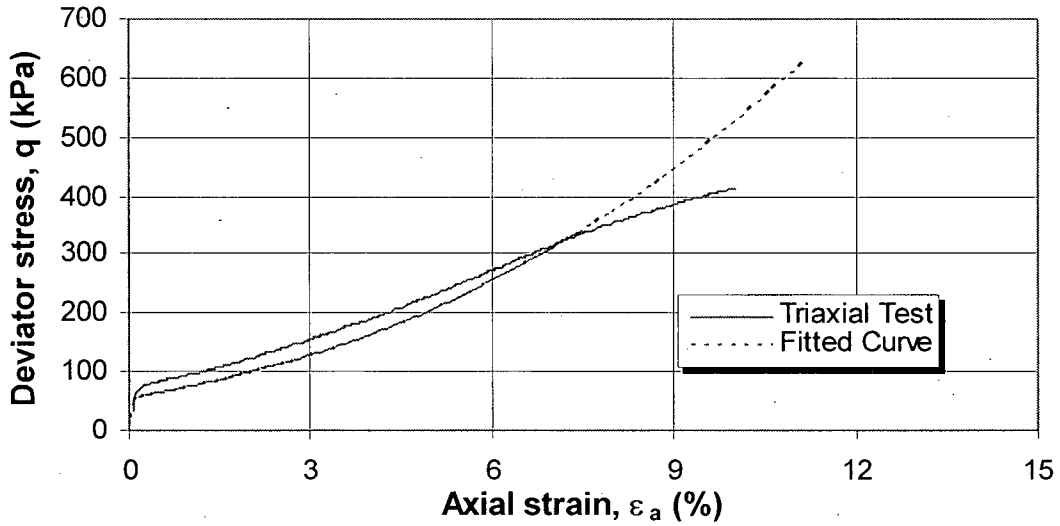

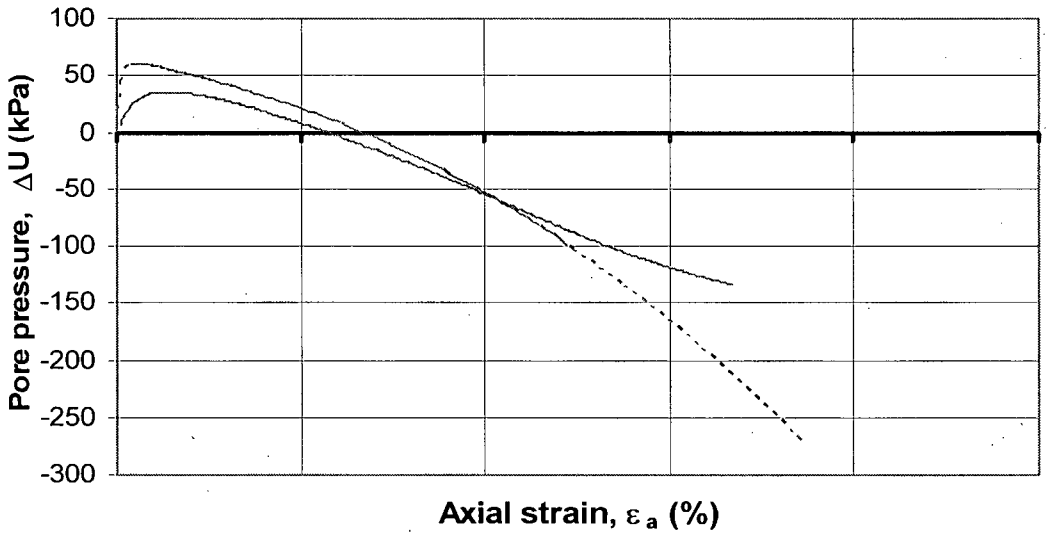

Figure 4.10: Comparison of deviator stress pore water pressure between triaxial data and NorSand model for CUP100

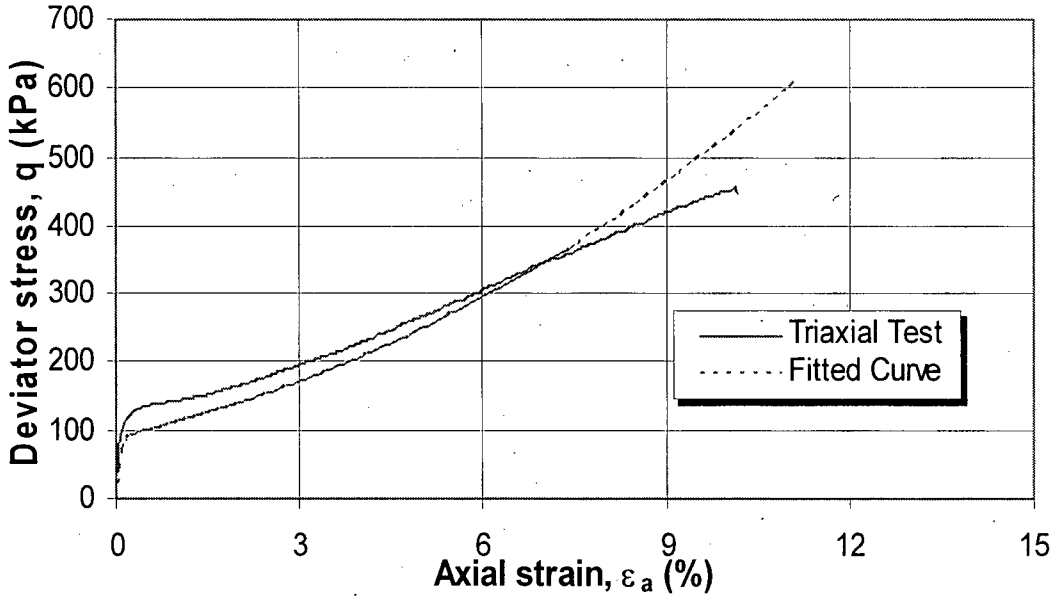

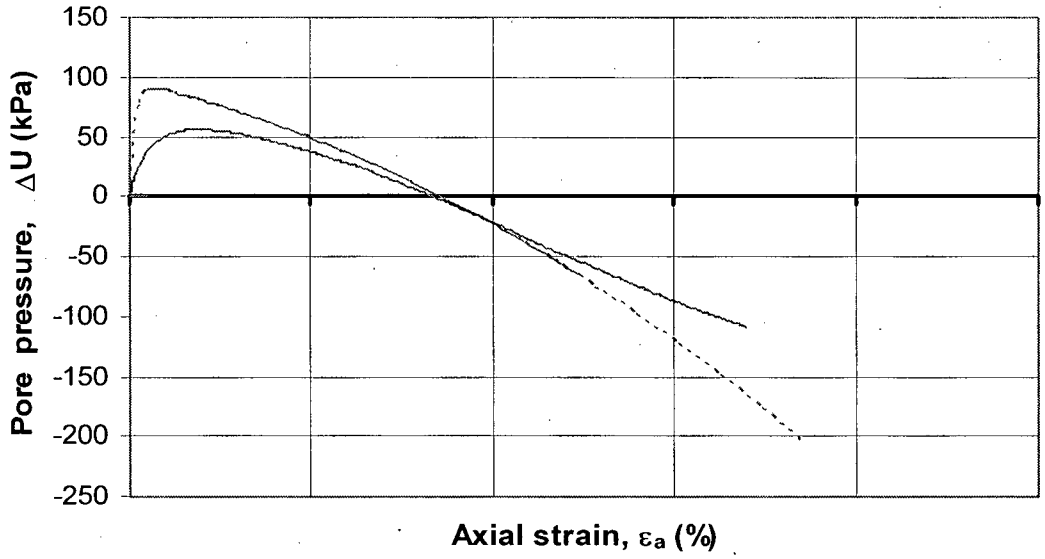

Figure 4.11: Comparison of deviator stress pore water pressure between triaxial data and NorSand model for CUP150

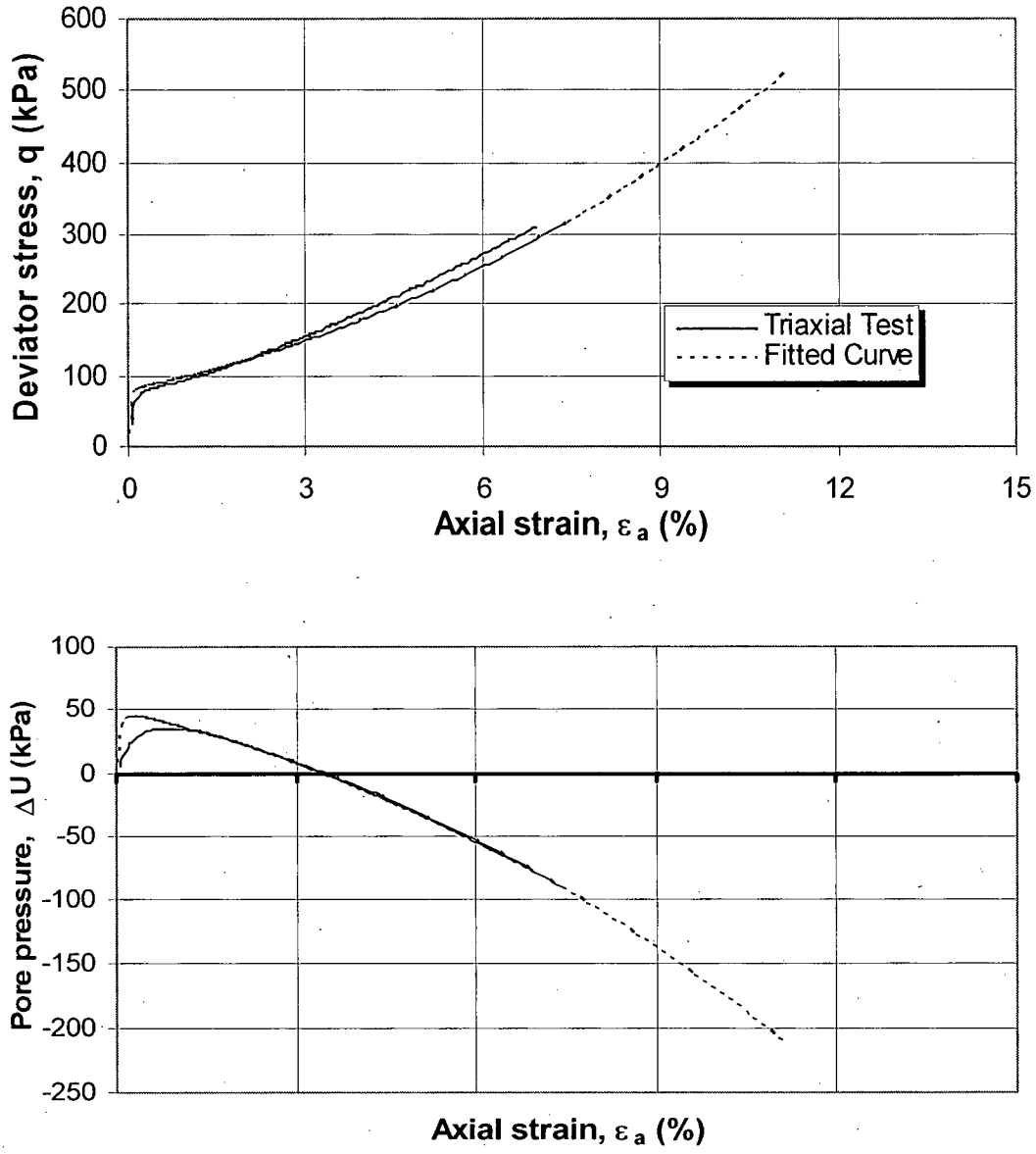

Figure 4.12: Comparison of deviator stress pore water pressure between triaxial data and NorSand model for CUP100, for R =2

The preceding figures show a good fit to dilation rate but a poor fit for the initial contraction. A better fit for the undrained tests can be obtained by raising the overconsolidation ratio to 2. The comparison between the predicted values and the triaxial test for CUP100 is shown in Figure 4.12. This change makes the predicted deviatoric stress increase and fit the triaxial data almost perfectly. In the case of the excess pore water pressure, the prediction with NorSand shows more contraction (less than the case where R=1), but the final trend shows a perfect fit.

4.3.2. Determination of NorSand parameters

Critical state parameters

The average value of M_{tc} equal to 1.13 obtained using the method described by Bishop (1966) was used to fit the three drained and the two undrained tests the best.

Badger sand only dilated for the void ratios – confining pressure used in these tests, the critical state line in the e-lnp' space has been estimated with the help of NorSand. Γ and λ were found to be equal to 0.697 and 0.0105 respectively, giving the equation for the Critical State Line in the e-lnp' space equal to $e = 0.697 - 0.0105 \times \ln(p')$. This equation ensures that the tests start and end at the left of the CSL. Even if the critical state friction angle associated to M_{tc}=1.13 is smaller than typical values for quartz sands, it is consistent with the values proposed by Santamarina and Cho, as explained before.

Figure 4.13 shows the place of the Critical State Line (CSL) estimated with the help of NorSand, in relation to the void ratios obtained during the lab tests. As said before, the critical state line remains above the tests which confirms that the samples were not loose, hence, after a short contraction they started dilating. Tests CDP100 and CDP150 are very close to the estimated CSL at the end of the tests. However, CDP50 is far away from the CSL as the two undrained tests are.

Plastic parameters

The value of the hardening parameter, H, used to fit the triaxial tests on Badger sand was taken constant and equal to 200. As the state parameter varies very little for the tests performed on Badger sand it is difficult to determine whether H should vary with ψ. Higher values of H could have matched better the triaxial results but in that case the rate of dilation would have been off as shown in Figure 4.9.

From the drained tests, a relation between the plastic dilation $\left(\dot{\varepsilon}_v^p \Big/ \dot{\varepsilon}_q^p\right)$ at peak strength and the initial state parameter was determined and is equal to:

$$D_{min} = 3.6\psi \qquad 4.3$$

Theoretically, $D_{min} = 0$ at $\psi = 0$. The best fit line in Figure 4.14 has a ($9e^{-5}$) intercept which is practically 0, which reconfirms the approach.

From Figure 4.14 the value of χ_{tc} can be determined as the slope of the line, hence:

$$\chi_{tc} = 3.6 \qquad 4.4$$

On the other hand, as explained in Chapter II, the slope of the line of Figure 4.1 (η_{max} vs $-D_{min}$) is $(1-N)$, hence for Badger sand the value of N is found to be equal to 0.63. Typical values of N and χ for sands are about 0.3 and 3.5, respectively. Given those values, the later version of NorSand described in Chapter II assumes that $N \times \chi = 1.0$. Hence, the flow rule described in Equation 2.91. However, given the values obtained for Badger Sand (N=0.63 and χ_{tc} = 3.6), the product between N and χ is equal to 2.3.

In order to capture the behaviour of Badger sand, and given the unusual values found for N the flow rule has been modified to fit these tests. Instead of the conventional flow rule described in Chapter II, the flow rule used is $M_i = M(1-\psi/M_{tc})$ for ψ positive (or loose state) and $M_i = M(1+2.3\psi/M_{tc})$ for ψ negative (or dense state). The fits in Figure 4.6 to Figure 4.11 show that this modified flow rule is able to capture the stress-strain behaviour of Badger sand.

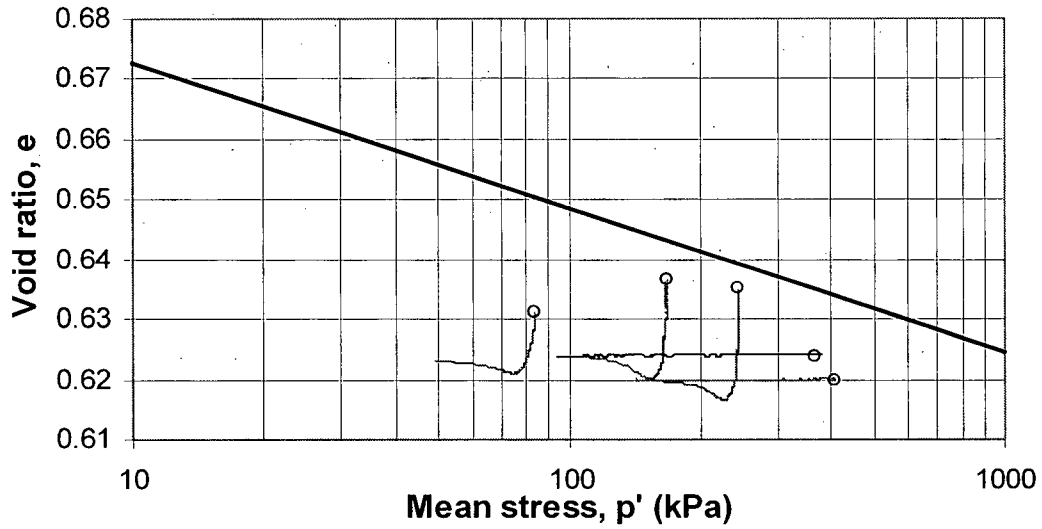

Figure 4.13: Critical State Line and void ratios

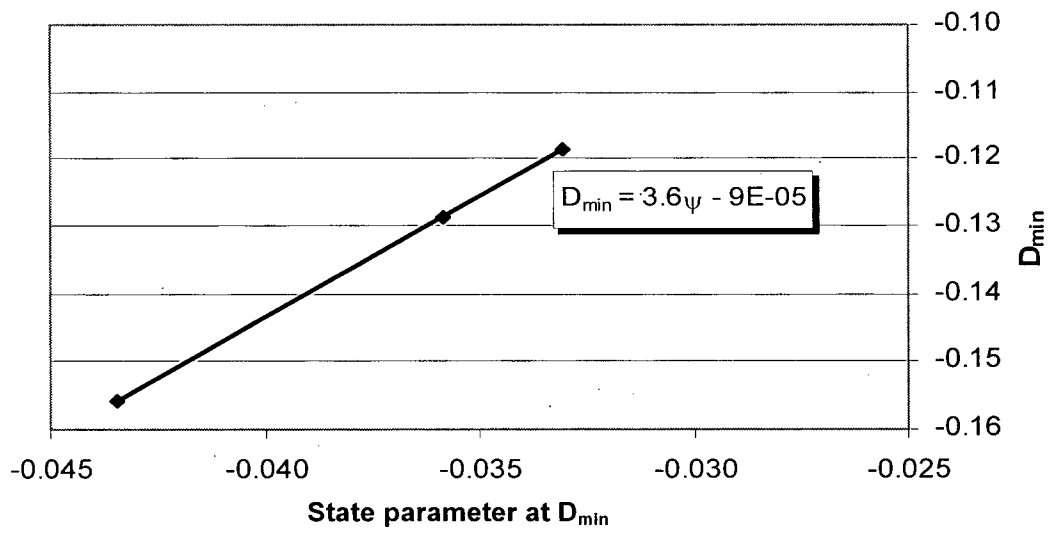

Figure 4.14: Dilation at peak strength, D_{min}, as a function of the state parameter

Figure 4.15 shows the stress-dilatancy behaviour for CDP100 compared with the stress-dilatancy predicted using the modified flow-rule for NorSand. The figure shows a very good agreement between the predicted and the values measured for this test. As found by Been and Jefferies (2004) for Erksak sand, the graph is approximately linear, showing a natural reverse as the stress ratio reaches the maximum, as expected for dense sand samples. Again, this plot confirms that the value of ϕ_{CV} obtained by Bishop's method is reasonable. If we assume that ϕ_{PT} in undrained tests is actually the constant volume friction angle, the rebound line of Figure 4.15 should end up at η= 1.06, which seems extremely unlikely.

Finally the properties determined for the Badger Sand are summarized in Table 4.8. As stated previously, the critical state parameters, Γ and λ, were deduced from the fits with the NorSand model and the lab test data. M_{tc} was obtained with the methods of Bishop and stress-dilatancy. The elastic parameters were obtained from a test with bender elements and assuming a Poisson's ratio of 0.15. Finally the plastic parameters were deduced by iterating and finding the best fit in order to be consistent with all the other parameters. With this parameter combination, the average error between the initial void ratio obtained from the triaxial tests (e_{0r}) and the one obtained by fitting (e_{0i}) is 0.01, which is with the accuracy expected from the lab testing.

Most of the parameters obtained to fit Badger sand fall all between the expected values (Table 2.7). M is lower than expected and the parameter N is higher than normal values, hence the change in flow rule described above. As well, the dilatancy of Badger sand is unusual (Figure 4.6 to Figure 4.11) which explains the low values of peak friction angles obtained in the drained tests.

As a general conclusion it is possible to say that Badger sand is a very unusual sand; the values of e_{min}, e_{max}, ϕ_{CV} , ϕ_{PT}, ϕ_{MC} and peak friction angles are lower than expected values for sands. However, these values were confirmed and explained by the shape of the sand grains, which, after Powers (1953) classifies Badger sand as a well-rounded sand with a roundness of R=0.81. As R increases, e_{min}, e_{max}, ϕ_{CV} , ϕ_{PT} and ϕ_{MC} decrease. Peak strength is related to maximum dilatancy. The dilatancy for Badger sand is also unusual which explains the low peak friction angles obtained in the drained tests. Finally, the NorSand constitutive model is able to capture the behaviour of Badger sand and confirm that the value of ϕ_{CV} obtained by Bishop's method is correct and it is different from the phase transformation friction angle.

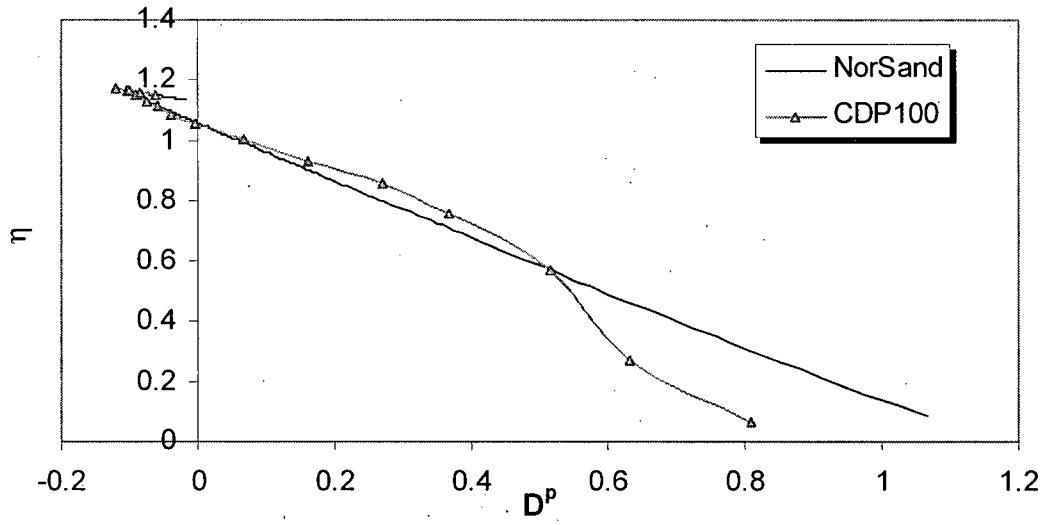

Figure 4.15: Stress-Dilatancy comparison between NorSand and CDP100

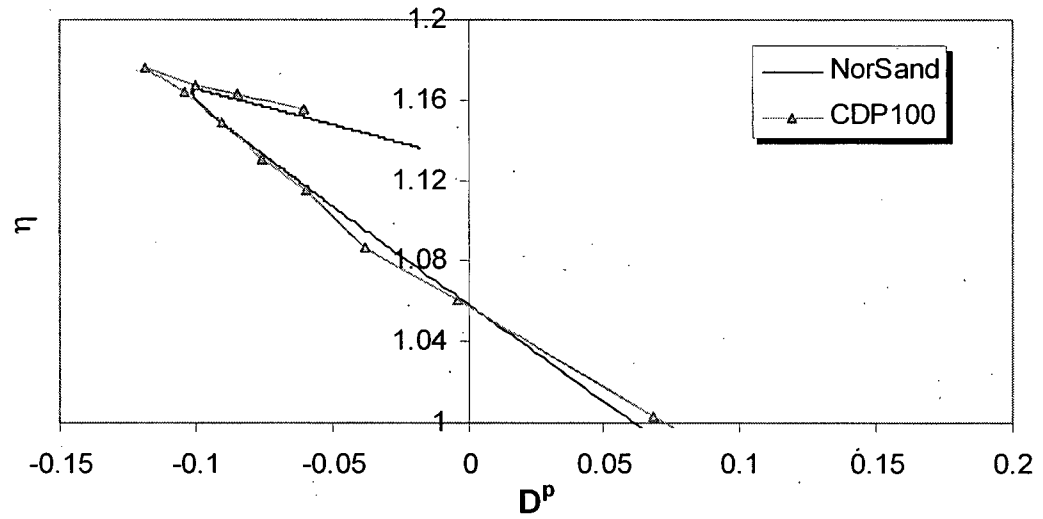

Figure 4.16: Zoom of stress-dilatancy for CDP100

Table 4.8: Parameters summary of NorSand[4] for Badger sand

	CDP50	CDP100	CDP150	CUP100	CUP150	Comments
Γ	0.697	0.697	0.697	0.697	0.697	at 1 kPa
λ	0.0105	0.0105	0.0105	0.0105	0.0105	base e
M_{tc}	1.13	1.13	1.13	1.13	1.13	
H	200	200	200	200	200	
χ	3.6	3.6	3.6	3.6	3.6	
I_r	1184.6	822.0	1200.0	831.8	664.7	$I_r = G/p'$
G (MPa)	59	82	99	81	99	$G = 9.35(p')^{0.47}$
ν	0.15	0.15	0.15	0.15	0.15	
E (MPa)	136	189	228	187	228	
R	1	1	1	1	1	
ψ	-0.043	-0.033	-0.036	-0.037	-0.034	
e_{0r}-e_{0t}	0.011	0.008	0.012	0.012	0.010	

[4] Details of the implementation of NorSand in FLAC are shown in Appendix A.

CHAPTER V: SUMMARY AND CONCLUSIONS

This research examines the properties of a well-rounded sand, in order to characterize it for purposes of numerical modelling. The silica sand is produced by the Badger Mining Corporation. The Badger sand is a uniformly graded coarse sand, for which C_u = 1.3 and C_c = 1.1 and D_{50}=0.87 mm. The general intent is to contrast properties of Badger sand with those of other sands, and determine if the different available tools are able to capture the behaviour of well-rounded grains such as Badger sand. For this, the main objectives of this study were:

- Measure the physical properties of Badger sand grains, such as roundness, and the grain assembly, such as minimum and maximum void ratio.
- Determine the strength parameters of Badger sand, including the angle of repose, failure envelope friction angle, phase transformation friction angle, maximum contraction friction angle and constant volume friction angle.
- Correlate the roundness of Badger sand with its extreme void ratios, and constant volume friction angle, and contrast those findings with relations for sands published in the literature.
- Compare the relative magnitude of the different friction angles obtained for Badger sand, and examine the implications for characterization of well-rounded sands.
- Determine the elastic, plastic and critical state properties of Badger sand for modelling purposes.
- Capture the behaviour of Badger sand with the NorSand constitutive model.

A series of three drained and two undrained triaxial tests was performed at the graduate geotechnical laboratory of UBC, with complementary studies using the NorSand constitutive model and FLAC. A summary of the main results and findings is presented below.

Image analysis of the sand grains yielded a roundness R=0.81 and S=0.77. Values of the minimum and maximum void ratio obtained by following the ASTM method are e_{min} = 0.49 and e_{max}= 0.69. Friction angles established for Badger sand tests are as follow:

- Angle of repose: ϕ_{rep} = 30.9°
- Maximum obliquity: ϕ_{MO} = 28.4°
- Maximum contraction: ϕ_{MC} = 25.8°
- Phase transformation: ϕ_{PT} = 25.6°
- Constant volume : ϕ_{CV} = 28.4°

The angle of repose was obtained following the ASTM method for a loose heap of sand. Triaxial tests were performed on specimens reconstituted by water pluviation. All specimens had a relative density less than DR = 35%, indicative of a loose state, yet one close to that of a medium dense state (DR≥35%). All triaxial specimens exhibited considerable dilation. Accordingly, the constant volume friction angle was determined using the method proposed by Bishop (1966): it requires plotting the values of the maximum stress ratio, η_{max} , and the dilatancy, D_{min}, for drained tests, and taking the best fit through the points. It is possible to obtain the critical stress ratio, M, as the value of the maximum stress ratio, η_{max}, at D_{min}=0. A second method was used to confirm the value of the critical state friction angle: for each drained test, M was obtained by plotting the stress ratio versus the dilatancy, D^P, and projecting the post peak η line to D^P=0. The maximum contraction friction angle was obtained from the stresses related to the point where the behaviour of the sand passed from contractive to dilative in the three drained tests. The phase transformation friction angle was obtained from the stresses corresponding to the maximum pore water pressure in the undrained tests. The maximum obliquity friction angle was measured from the maximum effective stress ratio in the two undrained tests.

The NorSand constitutive model was used to fit the triaxial tests on Badger sand. A summary of the parameters used is presented in Table 5.1.

Table 5.1: Summary of Badger sand parameters

Parameter	Badger sand	Remark
Γ	0.697	At 1 kPa
λ	0.0105	Defined in base e
M	1.13	In triaxialcompression
H	200	
χ	3.6	
G	$9.35(p')^{0.47}\times1000$	MPa
ν	0.15	Assumed
R	1	Assumed

As all the reconstituted test specimens were dilatant, the critical state parameters in the e-ln(p') space, Γ and λ were obtained with the help of NorSand and ensuring that the CSL stays to the right of the end of test condition. H was found by iteration. χ was found as the slope of the line in the ψ-D_{min} plot of the three drained tests. The relation of G with the mean effective stress was found using bender elements attached to the specimen and provided by Golder Associates.

From the results presented above, the following conclusions can be stated:

1. For Badger sand it was not possible to reconstitute specimens looser than 33% relative density, with the method of water pluviation, which is consistent with the experience of Vaid and Chern (1958) for Ottawa sand.

2. For Badger sand the maximum contraction friction angle (25.8°) appears equal to the phase transformation friction angle (25.6°), and occurs at the same axial strain of about 1% to 1.5%.

3. For Badger sand the maximum contraction friction angle (25.8°) appears equal to the phase transformation friction angle (25.6°), and they are both different from the constant volume friction angle (28.4°). This finding is in agreement with that of Chu (1995).

4. For Badger sand the maximum obliquity friction angle (28.4°) is greater than the phase transformation friction angle (25.6°), by approximately 3°. This finding is consistent with the observation of Sivathayalan (2000).

5. The constant volume friction angle (28.4°) was found to be lower than the angle of repose (30.9°).

6. For Badger sand the maximum obliquity friction angle (28.4°) was found equal in magnitude to the constant volume friction angle (28.4°).

7. Notwithstanding the limited number of triaxial tests, an excellent agreement was found between the roundness (0.81) and constant volume friction angle (28.4°) of Badger sand, and a corresponding relation between R and ϕ_{CV} proposed by Santamarina and Cho (2004). The latter relation is based on the assumption that the critical state friction angle is equal to the angle of repose.

8. For Badger sand, e_{max}=0.69 and e_{min}=0.49, which is a very narrow range. A very good agreement was found between the roundness (0.81) and these extreme void ratios, and the relations proposed by Youd (1973), Shimobe and Moroto (1995), and Santamarina and Cho (2004).

9. Most sands exhibit a roundness of $0.2 < R < 0.7$. In contrast, glass beads are nearly perfect spheres ($R \cong 1.0$). There is little information on well-rounded sands $0.7 < R < 1.0$ in the literature, and the experimental data suggest these well-rounded sands exhibit somewhat unusual values for the angle of friction which can be attributed to grain shape. Accordingly, the Badger sand data provide a valuable link between data for commonly found sands and glass beads; they also serve to build confidence in empirical relations based on a quantification of grain shape.

10. The parameters used to fit Badger sand with NorSand fall between the expected values.

11. The volumetric coupling coefficient from Nova's flow rule, N, has an unusual value for Badger sand, equal to 0.63. As well χ has a value of 3.6. As the product N×χ is different from 1, a modification of the flow rule is proposed for Badger sand, given by:

$$M_i = M\left(1 + 2.3\psi / M_{tc}\right) \text{ for } \psi < 0$$

12. Peak strength is related to maximum dilatancy, and Badger sand was found to exhibit unusual dilatancy, which is believed to explain the unusually low friction angles found in the triaxial tests.

13. NorSand is able to capture reasonably well the behaviour of Badger sand, and therefore is believed to confirm the validity of the value of M deduced from the triaxial tests.

REFERENCES

Al Hattamleh, O., Muhunthan, B. and Zbib, H.M., 2005, "Stress distribution in granular heaps using multi-slip formulation", International journal for numerical and analytical methods in geomechanics", Vol. 29, pp. 713-727

Alarcon-Guzman, A., Leonards, G. and Chameau, J.L., 1988, "Undrained monotonic and cyclic strength of sands", Journal of geotechnical engineering, Vol. 114, No. 10, pp. 1089-1109

Allaby, A. and Allaby, M., 2003, "Dictionary of Earth Sciences", Second Edition, Oxford University Press

ASTM D 422-63, "Standard Test Method for Particle-Size Analysis of Soils", ASTM International

ASTM D 4254-91, "Standard Test Method for Minimum Index Density and Unit weight of soils and Calculation of Relative Density", ASTM International

ASTM D 4253-93, "Standard Test Methods for Maximum Index Density and Unit Weight of Soils Using a Vibratory Table", ASTM International

ASTM C 1444-00, "Standard Test Method for Measuring the Angle of Repose of Free-Flowing Mold Powders", ASTM International

Been, K., Jefferies, M.G. and Hachey, J., 1991, "The critical state of sands", Geotechnique, Vol. 41, No. 3, pp. 365-381

Been, K., 1999, "The critical state line and its application to soil liquefaction", Physics and mechanics of soil liquefaction, Lade and Yamamuro (eds), Balkema, Rotterdam, pp. 195-204

Been, K. and Jefferies, M., 2004, "Stress-dilatancy in very loose sand", Canadian Geotechnical Journal, Vol. 41, pp. 972-989

Bishop, A.W., 1966, "Strength of soils as engineering materials", 6th Rankine Lecture, Geotechnique, Vol. 16, pp. 89-130

Bolton, M., 1979, "A guide to soil mechanics", The Macmillan press ltd

Bolton, M.D., 1986, "The strength and dilatancy of sands", Geotechnique, Vol. 36, No. 1, pp. 65-78

Burland, J.B., 1965, "The yielding and dilation of clay", Correspondence, Geotechnique, Vol. 15, pp. 211-214

Casagrande, A., 1936, "Characteristics of cohesionless soils affecting the stability of earth fills, Journal of Boston Society of Civil Engineers, Vol. 23, pp. 257-276

Castro, G., 1975, "Liquefaction and cyclic mobility on saturated sands", Journal of Geotechnical Engineering Division, ASCE, Vol. 101, GT6, pp. 551-569

Chik, Z. and Vallejo, L.E, 2005, "Characterization of the angle of repose of binary granular materials", Canadian Geotechnical Journal, Vol. 42, No. 2, pp. 683-692

Cho, G., Dodds, J. and Santamarina C., 2005, "Particle Shape effects on Packing Density, Stiffness and Strength –Natural and Crushed Sands-", Internal Report, Georgia institute of technology (http://www.ce.gatech.edu/~carlos/laboratory/tool/Particleshape/ChoDoddsJCS.pdf)

Chu, J. and Lo, S-C.R., 1992, "The critical state of sands: discussion", Geotechnique, Vol. 42, No. 4, pp. 655-663

Chu, J. and Lo, S-C.R., 1993, "On the measurement of critical state parameter of dense granular soils", ASTM Geotechnical testing journal, Vol. 16, pp. 27-35

Chu, J. and Lo, S-C.R., 1993, Discussion on: "The critical state of sands", Geotechnique, Vol. 43, pp. 655-663

Chu, J., 1995, "An Experimental Examination of the Critical State and Other Similar Concepts for Granular Soils", Canadian Geotechnical Journal, 32, No. 6, pp. 1065-1075

Collins, I.F. and Muhunthan, B., 2003, "On the relationship between stress-dilatancy, anisotropy, and plastic dissipation for granular materials", Geotechnique, Vol. 53, No. 7, pp. 611-618.

Cornforth, D.H., 1973, "Prediction of drained strength of sands from relative density measurements", Evaluation of Relative Density and its Role in Geotechnical Projects Involving Cohesionless Soils, ASTM STP 523, American Society for Testing and Materials, pp. 281-303

Cornforth, D.H., 2005, "Landslides in Practice. Investigation, Analysis, and Remedial/Prevention Options in Soils", John Wiley & Sons, Inc

Cubrinovski, M. and Ishihara, K., 2002, "Maximum and Minimum Void Ratio Characteristics of Sands", Soils and Foundations, 42, No. 6, pp. 65-78

Das, B.M., 1979, "Soil mechanics", The Iowa State University Press/Ames

Fannin, R.J., Eliadorani, A. and Wilkinson J.M.T., 2005, "Shear strength of cohesionless soils at low stress", Geotechnique, Vol. 55, No. 6, pp. 467-478

Golder Associates, 2004, personal communication

Herle, I. and Gudehus, G, 1999, "Determination of parameters of a hypoplastic constitutive model from properties of grain assemblies", Mechanics of cohesive-frictional materials, Vol. 4, pp. 461-486

Horne, M.R., 1969, "The behaviour of an assembly of rotund, rigid, cohesionless particles.III", Proceedings Royal Society, A 310, pp. 21-34

Ishihara, K., Tatsuoka, F. and Yasuda, S., 1975, "Undrained deformation and liquefaction of sand under cyclic stresses", Soils and Foundations, 15, No. 1, pp. 29-44

Ishihara, K., 1993, Thirty-third Rankine Lecture: Liquefaction and flow failure during earthquakes", Geotechnique, Vol. 43, No. 3, pp. 349-416

Itasca Consulting Group, Inc. 2005, FLAC: Fast Lagrangian Analysis of Continua, User Manual, Version 5.0. Minneapolis

Jefferies, M.G., 1993, "Nor-Sand: a simple critical state model for sand", Geotechnique, Vol. 43, No. 1, pp. 91-103

Jefferies, M.G., 1999, "A critical view of liquefaction", Physics and mechanics of soil liquefaction, Lade and Yamamuro (eds), Balkema, Rotterdam, pp. 221-235

Jefferies, M.G. and Been, K., 2000, "Implications for critical state theory from isotropic compression sand", Geotechnique, Vol. 50, No. 4, pp. 419-429

Jefferies, M.G. and Shuttle, D.A., 2002, "Dilatancy in general Cambridge-Type models", Geotechnique, Vol. 52, No. 9, pp. 625-638

Jefferies, M.G. and Shuttle, D.A., 2005, "NorSand: features, calibration and use", Geotechnical special publication No.128, soil constitutive models: evaluation, selection and calibration, pp. 204-236, editors Jerry A. Yamamuro and Victor N. Kaliakin.

Jefferies, M. and Been, K., 2005, "Soil liquefaction, a critical state approach"

Jefferies, M., 2005, Personal communication

Kirkpatrick, W.M., 1961, "Discussion. Proceedings of the Fifth International Conference on Soil Mechanics and Foundations Engineering", 3, pp. 131-133

Krumbein, W.C., 1941, "Measurement and Geological Significance of Shape and Roundness of Sedimentary Particles", Journal of Sedimentary Petrology, Vol. 38, No. 2, pp. 64-72

Lade, P.V. and Abelev, A.V., 2003, "Effects of cross anisotropy on three dimensional behaviour of sand. II: volume change behavior and failure", Journal of engineering mechanics, Vol. 129, No. 2, pp. 167-174

Lade, P.V., 2005, "Overview of constitutive models for soils", GeoFrontiers 2005, Austin, Texas, GSP 139

Lambe, T.W. and Whitman, R.V., 1979, "Soils Mechanics SI Version"

Lemay, 2005, Personal communication

Li, X-S., Dafalias, Y.F. and Wang, Z-L., 1999, "State dependent dilatancy in critical state constitutive modeling of sand", Canadian geotechnical journal, Vol. 36, No. 4, pp. 599-611

Li, X-S. and Dafalias, Y.F., 2000, "Dilatancy for cohesionless soils", Geotechnique, Vol. 50, No. 4, pp. 449-460

Luong, M.P., 1980, "Stress-strain aspects of cohesionless soils under cyclic and transient loading", International Symposium on Soils Under Cyclic and Transient Loading, Swansea, pp. 315-324

Manzari, M.T. and Dafalias, Y.F., 1997, "A critical state two-surface plasticity model for sands". Geotechnique, Vol. 47, No. 2, pp. 255-272

Manzari, M.T. and Nour, M.A., 1997, "On implicit integration of bounding surface plasticity models", Computers and structures, Vol. 63, No. 3, pp. 385-395

Mitchell, J.K. and Soga, K., 2005, "Fundamentals of soil behavior", Third Edition, John Wiley and Sons, INC

Miura, K., Maeda, K and Toki, S., 1997, "Method of measurement for the angle of repose of sands", Soils and Foundations, Vol. 37, No. 2, pp. 89-96

Miura, K., Maeda, K., Furukawa, M. and Toki, S., 1998, "Mechanical characteristics of sands with the different primary properties", Soils and Foundations, Vol. 38, No. 4, pp. 159-172

Moore, D.S. and McCabe, G.P., 2003, "Introduction to the practice of statistics", Fourth Edition, W.H. Freeman and Company, New York

Negussey, D., Wijewickreme, W.K.D. and Vaid, Y.P., 1988, "Constant-volume friction angle of granular materials", Canadian Geotechnical Journal, 25, pp. 50-55

Negussey, D. and Islam, M.S., 1994, "Uniqueness of steady state and liquefaction potential", Canadian geotechnical journal, Vol. 31, No. 1, pp. 132-139

Nova, R., 1982, "A constitutive model under monotonic and cyclic loading", Soil mechanics-transient and cyclic loads (eds Pande and Zienkiewicz), pp. 343-373, Wiley

Oyenuga, D.A. and Tisot, J.P., 1989, "Looking for an intrinsic key for sands", Powders and grains, Edited by Biarez and Gourves, A.A. Balkema, Rotterdam, pp.171-175

Poorooshasb, H.B., Holubec, I. and Sherbourne, A.N., 1967, "Yielding and flow of sand in triaxial compression: parts II and III", Canadian geotechnical journal, Vol. 4, No. 4, pp. 376-397

Poorooshasb, H.B., Holubec, I. and Sherbourne, A.N., 1967, "Yielding and flow of sand in triaxial compression", Canadian geotechnical journal, Vol. 3, No. 4, pp.179-190

Poulos, S.J., 1981, "The steady state of deformation", ASCE Journal of the geotechnical engineering division, Vol. 107, GT5, pp. 553-562

Powers, M.C., 1953, "A New Roundness Scale for Sedimentary Particles", Journal of Sedimentary Petrology, Vol. 23, No. 2, pp.117-119

Raju, M., 1995, "Monotonic and Cyclic Pullout Resistance of Geosynthetics", The University of British Columbia, thesis submitted in partial fulfillment of the requirements for the Ph.D. degree.

Reynolds, O., 1885, "On the dilatancy of media composed of rigid particles in contact, with experimental illustrations", Philosophical magazine, Vol. 20, pp. 469-481

Reynolds, O., 1886, "Experiments showing dilatancy, a property of granular material, possibly connected with gravitation", Proceedings of the Royal Institution of Great Britain, pp. 217-227

Roscoe, K.H., Schofield, A.N. and Wroth, C.P., 1958, "On the yielding of soils", Geotechnique, Vol. 8, No. 1, pp. 22-53

Roscoe, K.H, Schofield, A.N. and Thurairajah, A., 1963, "Yielding of clays in states wetter than critical", Geotechnique, Vol. 13, No.3, pp. 211-240

Roscoe, K.H. and Burland, J.B., 1968, "On the generalized stress-strain behaviour of 'wet' clay". Engineering plasticity, Eds J. Heyman and F.A. Leckie, pp. 535-609, Cambridge University Press

Rowe, P.W., 1962, "The stress dilatancy relation for static equilibrium of an assembly of particles in contact", Proc. Royal Society of London, A 269, pp. 500-527

Santamarina, J., and Cho, G., 2004, "Soil behaviour: The Role of Particle Shape", Advances in Geotechnical Engineering: The Skempton Conference, Thomas Telford, London, pp. 604-617

Schanz, T. and Vermeer, P.A., 1996, "Angles of Friction and Dilatancy of Sands", Geotechnique 46, No. 1, pp. 145-151.

Schofield, A.N. and Wroth, C.P, 1968, "Critical state soil mechanics", London: McGraw-Hill

Shimobe, S. and Moroto, N., 1995, "A new Classification Chart for Sand Liquefaction", Proceedings 1st International Conference on Earthquake Geotechnical Engineering, Tokyo, Vol. 1, pp. 315-320

Shuttle, D. and Jefferies, M., 1998, "Dimensionless and unbiased CPT interpretation in sand", International journal for numerical and analytical methods in geomechanics, Vol. 22, pp. 351-391

Sivathayalan, S., 2000, "Fabric, Initial State and Stress Path Effects on Liquefaction Susceptibility of Sands, The University of British Columbia, thesis submitted in partial fulfillment of the requirements for the Ph.D. degree

Taylor, D.W., 1948, "Fundamentals of soil mechanics", John Wiley, New York

Vaid, Y.P. and Chern, J.C., 1985, "Cyclic and monotonic undrained response of saturated sands", Session No. 52, Advances in the art of testing soils under cyclic conditions, Annual convention and exposition, Detroit, MI

Vaid, Y.P., Chung, E.K.F. and Kuerbis, R.H., 1990, "Stress path and steady state", Canadian geotechnical journal, Vol. 27, No. 1, pp.1-7

Vaid, Y.P. and Eliadorani, A., 1998, "Instability and liquefaction of granular soils under undrained and partially drained states", Canadian geotechnical journal, Vol. 35, pp. 1053-1062

Verdugo, R., 1992, "The critical state of sands: discussion", Geotechnique, Vol. 42, No. 4, pp.655-663

Whitlow, R., 1995, "Basic soil mechanics", Third Edition, Longman Scientific and Technical

Wood, D.M., 1990, "Soil behaviour and critical state soil mechanics", Cambridge University Press

Wroth, C.P. and Basset, R.H., 1965, "A stress-strain relationship for the shearing behaviour of a sand", Geotechnique, Vol. 15, No. 1, pp. 32-56

Youd, T.L., 1973, "Factors Controlling Maximum and Minimum Densities of Sands", Evaluation of Relative Density and its Role in Geotechnical Projects Involving Cohesionless Soils, ASTM STP 523, American Society for Testing and Materials, pp. 98-112

Zhang, H. and Garga, V., (1997), "Quasi-steady state: a real behaviour?", Canadian Geotechnical Journal, Vol 34, pp 749-761.

APPENDIX A: NORSAND MODEL IMPLEMENTATION

In order to capture the behaviour of the Badger Sand and use it later for modelling purposes, a new constitutive model will be implemented within FLAC (Fast Lagrangian Analysis of Continua); NorSand. As explained in Chapter II, NorSand is able to realistically capture the dilatancy of sands through use of the state parameter. NorSand, unlike Original or Modified Cam Clay, is also able to simulate strain softening which is very important for dense sands.

As discussed in Chapter II, the Critical State Soil Models, Modified Cam Clay (MCC), Original Cam Clay (OCC) and NorSand are very similar in concept. Modified Cam Clay is already a built-in constitutive model in FLAC, written as a FISH function. Hence the approach used here is to take the MCC FISH function, adapt this function to OCC and verify the approach used. Then modify the function to NorSand. The only difference between MCC and OCC is the shape (equation) of the yield surface. Hence, the Modified Cam Clay yield surface is modified in order to obtain the Original Cam Clay model. Because of the different yield surface shape, different methodologies are used. Finally, as OCC and NorSand have the same yield surface but different hardening rules, the next step is direct.

This chapter explains the process followed to create the NorSand constitutive model function in FLAC, starting from Modified Cam Clay, continuing with Original Cam Clay and ending with NorSand (Figure A.1). The FLAC results are then compared with the results obtained with an Excel Visual Basic for Applications (VBA) (Jefferies and Shuttle, 2005) to verify that the FLAC function is working properly.

A.1. Fast Lagrangian Analysis of Continua (FLAC)

A.1.1. General description of FLAC

FLAC is a two-dimensional computational program that analyses the stress-strain response of solids subjected to static and dynamic states of load. FLAC's explicit finite difference formulation has been widely applied to model geotechnical and mining problems, and it is one of the most widely used programs world-wide for geotechnical stress-strain analysis. The FLAC program is able to simulate large deformations of continuous media, groundwater flow and pore water pressure dissipation. Interface elements are also available in FLAC, allowing simulation of the

separation of materials or slipping between them. FLAC also includes structural elements, such as cables, beams and reinforcing strips, among others, that behave in conjunction with the continuous media. Five optional features are also available to analyze specific problem types; dynamic analysis, thermal analysis, two-phase flow analysis, creep material behaviour and the ability to code user defined models (UDM) in C++ and compile them as dynamic link libraries (dll's). Well executed numerical models allow us to improve our understanding of the behaviour of soil and structures under the effect of different types of loading (static or dynamic).

FLAC (Version 5.0) has 11 built-in constitutive models for continuous elements. The constitutive models are: Null, Isotropic Elastic, Mohr-Coulomb, Modified Cam Clay, Transversely Isotropic Elastic, Drucker-Prager, Ubiquitous-joint, Strain Hardening/Softening, Bilinear Strain-Hardening/Softening Ubiquitous-joint, Double-yield, Hoek-Brown. However, none of these models are able to realistically capture the behaviour of sands under general paths; Mohr-Coulomb predicts the dilatancy wrong and the strain hardening/softening model only allows cohesion, dilation and friction angle to change with strain level.

A.1.2. FLAC nomenclature

Figure A.2 is an example of a FLAC model showing all the commonly used terms. The soil body is formed by a grid (or mesh) of quadrilateral elements (or zones) that behave depending on the constitutive model, forces and boundary conditions assigned to them.

A zone, or element, is the smallest quadrilateral domain where changes in stresses, fluid flow or heat transfer are calculated. Each zone is divided into four triangular subzones which are superimposed, as shown in Figure A.3. Each zone has four grid points (or nodes) associated with the four corners of the quadrilateral and each grid point is defined by a pair of x- and y-coordinates.

Each zone of the entire grid behaves depending on the constitutive model assigned to it. Constitutive model means a model which describes the deformation and strength behaviour of the simulated material. Some examples of constitutive models already included in FLAC are Elastic-Plastic, Mohr-Coulomb and Modified Cam Clay. Constitutive models and material properties can be assigned independently to every zone of the model.

The periphery of the grid is called the model boundary. Boundary conditions to the model can be applied as fixed boundaries (displacement restraint), stress boundaries or excavations. Excavations have the Null constitutive model assigned to them where no properties are assigned.

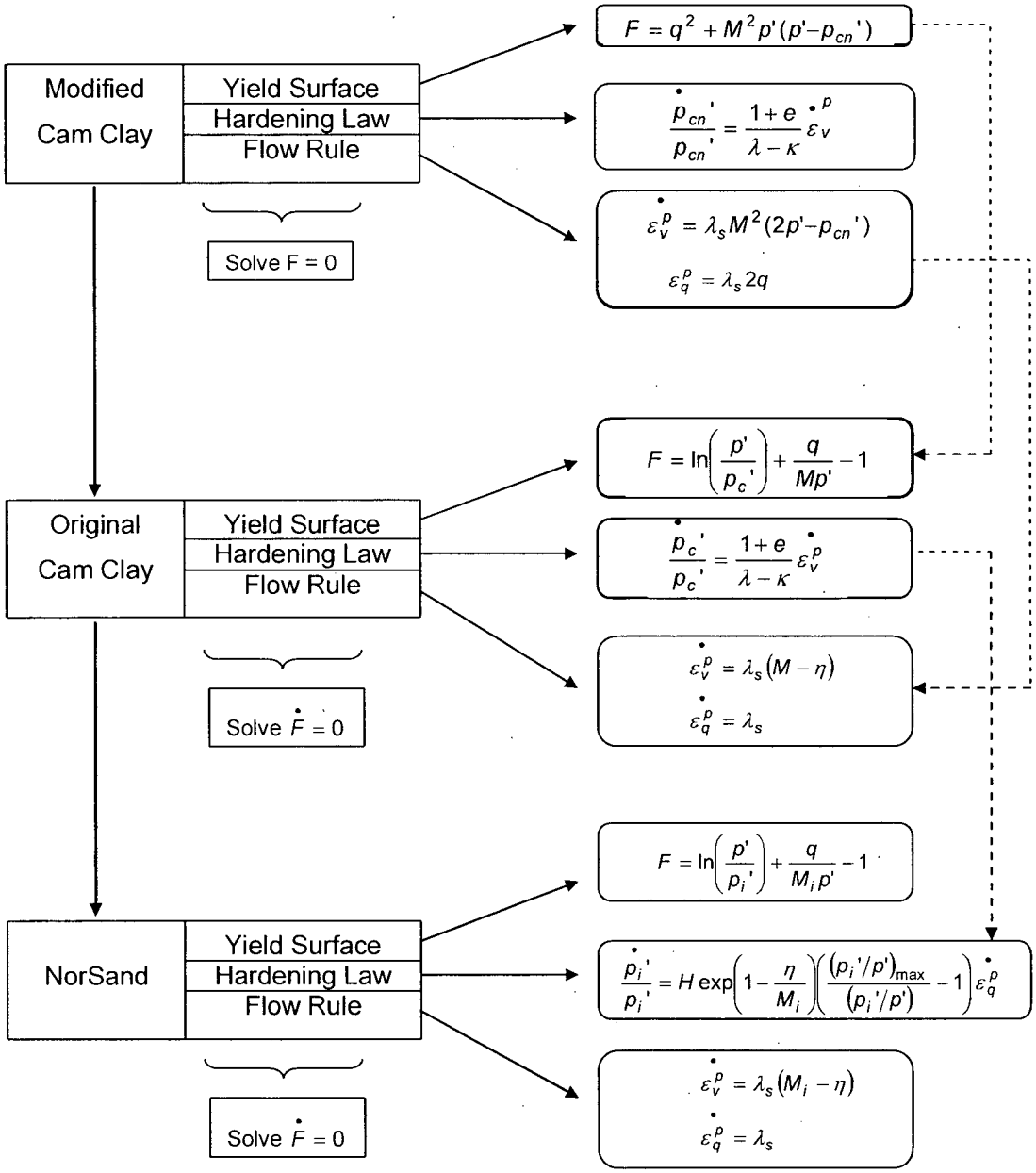

Figure A.1: General flow chart

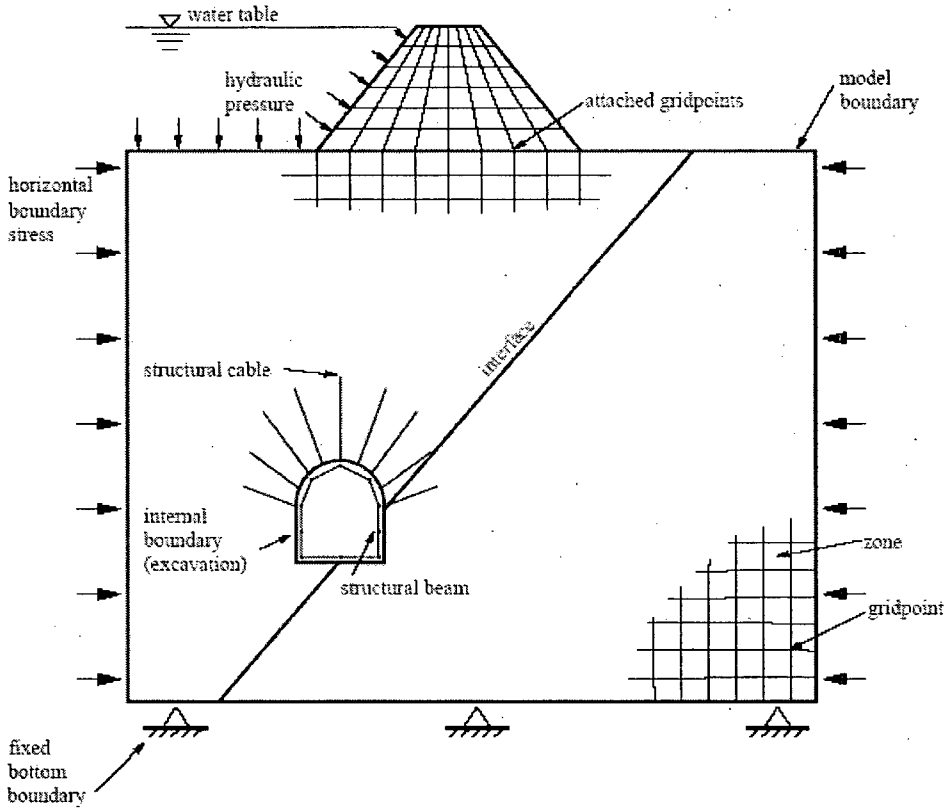

Figure A.2: Example of FLAC model (from FLAC Version 5.0 Manual)

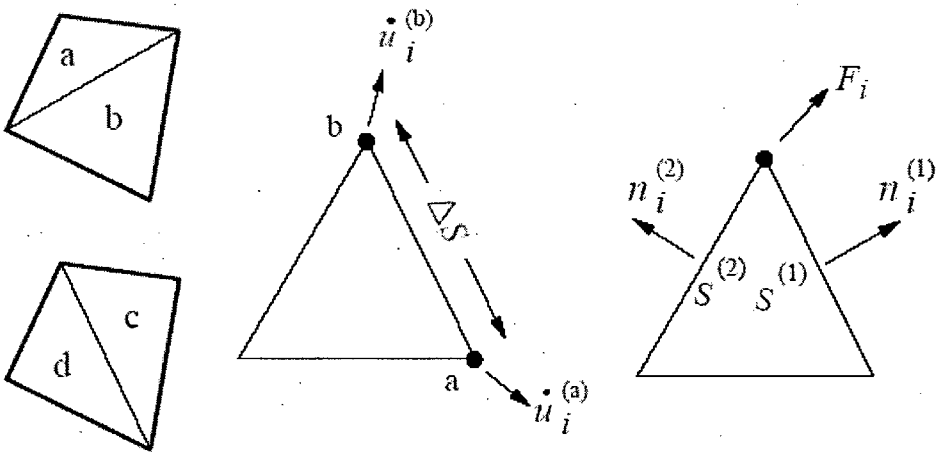

Figure A.3: FLAC zone divided in 4 triangles; triangular element with velocity vectors; nodal force vector (from FLAC Version 5.0 Manual)

Structural elements, such as cables, beams or interfaces are used to represent the interaction of structures. Interfaces are used to simulate separation or sliding between elements and beams and cables are used to represent, for example, reinforcement in a wall.

A.1.3. Sign convention and units in FLAC

In FLAC, positive normal stresses and strains indicate tension and extension respectively, and negative normal stresses and strains indicate compression. Conversely, the sign convention for pore pressure is: positive pore pressure indicates compression and negative pore pressure indicates tension. For gravitational force, positive gravity will make an element move downward and negative gravity makes an element move upward.

Figure A.4 shows the sign convention for positive shear stress components in FLAC and their associated shear strains. Positive shear stresses and strains are clockwise

The system of units for mechanical parameters used by FLAC is shown in Table A.1.

Table A.1: System of units used by FLAC

Length	m	m	m	cm	ft	in
Density	Kg/m^3	$10\ Kg/m^3$	$10^6\ Kg/m^3$	$10^6\ g/cm^3$	$slugs/ft^3$	$snails/in^3$
Force	N	KN	MN	Mdynes	lbf	lbf
Stress	Pa	kPa	MPa	bar	lbf/ft^2	psi
Gravity	m/sec^2	m/sec^2	m/sec^2	cm/sec^2	ft/sec^2	in/sec^2
Stiffness	Pa/m	kPa/m	MPa/m	bar/cm	lbf/ft^3	lb/in^3

where, $1slug = 1\frac{lb\sec 2}{ft}$ and $1snail = 1\frac{lb\sec 2}{in}$

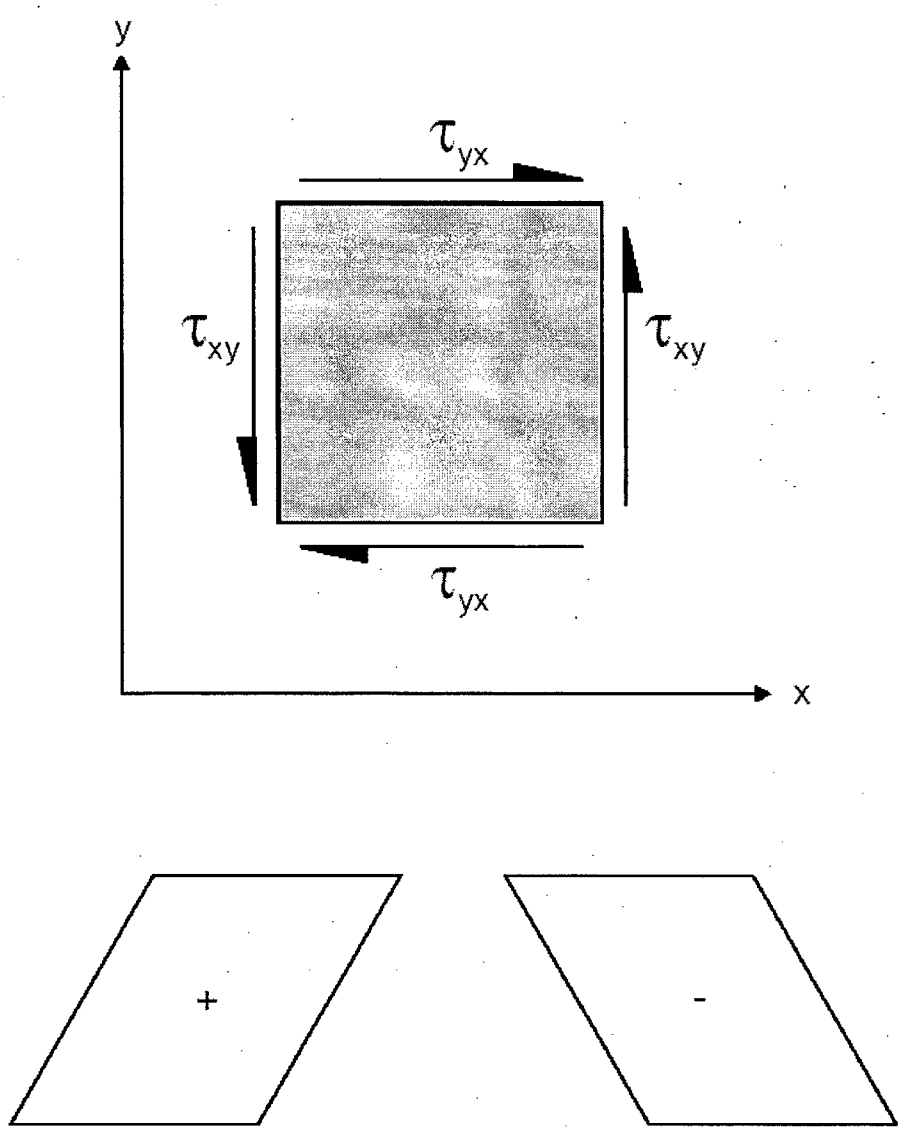

Figure A.4: Positive shear stress (or strain) convention and associated distortion (from FLAC Version 5.0 Manual)

4.1.4. FISH in FLAC

FISH is a programming language created by Itasca which allows FLAC users to code and define new functions and variables (the User Defined Model (UDM) option is not required to use FISH). An example of a FISH function which initializes the mean effective stress for the 'camclay' constitutive model is presented below.

```
def camclay_ini_p
  loop i (1,izones)
    loop j (1,jzones)
      if z_model(i,j)='camclay' then
      mean_p=-(sxx(i,j)+syy(i,j)+szz(i,j))/3.-pp(i,j)
      z_prop(i,j,'cam_cp')=mean_p
      end_if
    end_loop
  end_loop
end
```

FISH functions start with the command **DEFINE** and end with the command **END**. Within the FISH function other functions can be called and created. In the previous example, the FISH function loops through all the elements and initializes the mean effective stress to each zone. FISH functions can be embedded in a normal FLAC data file or entered directly from the keyboard.

The FISH language can also be used to implement new constitutive models within FLAC. A constitutive model is defined by the statement **CONSTITUTIVEMODEL <n>** where n is the number associated to the constitutive model. It will be executed as a built-in constitutive model, and will be called four times for each FLAC zone (1 time for each triangle shown in Figure A.3). Inside the constitutive model, new variables can be created and other FISH functions can be called.

However, one of the disadvantages of the constitutive models implemented with FISH is that it takes a long time to run. For larger problems, where simulation speed is important, the UDM in C++, which runs at the same speed as FLAC, is a better option.

A.2. FLAC finite difference formulation[5]

The basic FLAC formulation consists of three conditions; Newton's law of motion, a stress-strain equation and a general finite difference formula.Taking a simple mechanical example, where a force (F) is applied to a mass (m) , causing a displacement (u), velocity $\left(\frac{du}{dt}\right)$ and acceleration $\left(\frac{d^2u}{dt^2}\right)$, as shown in Figure A.5, from Newton's law of motion,

$$F = m \times a = m \times \frac{d\dot{u}}{dt} \qquad \text{A.1}$$

For a continuous body, Equation A.1 can be written as:

$$\rho \frac{d\dot{u}_i}{dt} = \frac{\partial \sigma_{ij}}{\partial x_j} + \rho g_i \qquad \text{A.2}$$

where, ρ is the mass density,

x_i is the coordinate vector (x,y)

σ_{ij} are the components of the stress tensor, and

g_i is gravitation.

In addition to the law of motion, a continuous solid must obey a stress-strain relation. For an elastic material this is:

$$\sigma_{ij} := \sigma_{ij} + \left\{ \delta_{ij} \left(K - \frac{2}{3} G \right) \dot{e}_{kk} + 2G \dot{e}_{ij} \right\} \Delta t \qquad \text{A.3}$$

where, δ_{ij} is the Kronecker delta,

$\dot{e}_{ij}$ is the strain rate component (Equation A.5),

K and G are the bulk and shear modulus,

---

[5] This is a summary of the FLAC User's Manual, for the full explanation, please refer to this manual.

Δt is the time step, and

:= means "replaced by".

Equation A.3 can be generally written as:

$$\sigma_{ij} := M\left(\sigma_{ij}, \dot{e}_{ij}, \kappa\right) \qquad \text{A.4}$$

where, M ( ) is the functional form of the constitutive law,

κ is a history parameter depending on the constitutive law, and

$$\dot{e}_{ij} = \frac{1}{2}\left[\frac{\partial \dot{u}_i}{\partial x_j} + \frac{\partial \dot{u}_j}{\partial x_i}\right] \qquad \text{A.5}$$

where, $\dot{u}_i$ are the velocity component.

In the finite difference method, each derivative in the equations of motion and strain are replaced by an algebraic expression relating variables at specific locations of the grid.

From the Gauss divergence theorem, the finite difference equation for all elements is given by (Figure A.3):

$$\int_S n_i f dS = \int_A \frac{\partial f}{\partial x_i} dA \qquad \text{A.6}$$

where: $\int_S$ is the integral around the surface, S;

n_i is a unit normal to the surface;

f is a scalar, vector or tensor;

dS is an incremental arc length;

A is the surface area of the element;

$\int_A$ is the integral over the surface area, A; and

∂x_i is a position vector.

Taking the average value of the gradient of f as:

$$\left\langle \frac{\partial f}{\partial x_i} \right\rangle = \frac{1}{A} \int_A \frac{\partial f}{\partial x_i} dA \qquad \text{A.7}$$

Substituting in Equation A.6 and approximating the integral through a sum over three sides of a triangular zone, the gradient can be written as:

$$\left\langle \frac{\partial f}{\partial x_i} \right\rangle = \frac{1}{A} \sum_S n_i \langle f \rangle \Delta S \qquad \text{A.8}$$

where ΔS is the length of the side of the triangle.

Substituting the average velocity vector in each side of Equation A.8, the strain rates can be written as nodal velocities for the triangular sub-zone as (Figure A.3):

$$\frac{\partial \dot{u}_i}{\partial x_j} \cong \frac{1}{2A} \sum_S \left(\dot{u}_i^{(a)} + \dot{u}_i^{(b)} \right) n_j \Delta S \qquad \text{A.9}$$

$$\dot{e}_{ij} = \frac{1}{2} \left[\frac{\partial \dot{u}_i}{\partial x_j} + \frac{\partial \dot{u}_j}{\partial x_i} \right] \qquad \text{A.10}$$

As for volumetric strains, they are averaged over each pair of triangle and the deviatoric stresses remain unchanged. Area weighting is used to obtain the new stress tensor from the strain-rate tensor.

$$\sigma_0^{(a)} = \sigma_0^{(b)} := \left[\frac{\sigma_0^{(a)} A^{(a)} + \sigma_0^{(b)} A^{(b)}}{A^{(a)} + A^{(b)}} \right] \qquad \text{A.11}$$

where: $\sigma_0^{(a)}$ is the isotropic stress in triangle (a); and

$A^{(a)}$ is the area of triangle (a).

Once all the stresses are calculated, the nodal forces are obtained from the traction acting on the sides of each triangle; each node receives two forces (one from each side of the triangle as shown in Figure A.3). Hence,

$$F_i = \frac{1}{2}\sigma_{ij}\left(n_j^{(1)}S^{(1)} + n_j^{(2)}S^{(2)}\right) \qquad \text{A.12}$$

At each node of the grid, the forces (from applied loads and gravity) of all the quadrilaterals are summed in order to obtain the net force vector $\sum F_i$. If the node is not in equilibrium, it will be accelerated according Newton's second law of motion:

$$\dot{u}_i^{(t+\Delta t/2)} = \dot{u}_i^{(t-\Delta t/2)} + \sum F_i^{(t)} \frac{\Delta t}{m} \qquad \text{A.13}$$

Finally, Equation A.13 is integrated to determine the new coordinate of the grid point, given by:

$$x_i^{(t+\Delta t)} = x_i^{(t)} + \dot{u}_i^{(t+\Delta t/2)} \Delta t \qquad \text{A.14}$$

In order to have a stable solution, the time-step chosen to solve the problem must be smaller than the critical time-step given by:

$$\Delta t < \frac{\Delta x}{C} \qquad \text{A.15}$$

where: Δx is the element size, and

C is the maximum speed at which information can propagate, and is given by:

$$C = \sqrt{\frac{K + 4G/3}{\rho}} \qquad \text{A.16}$$

For a triangular zone of area A, considering the shortest propagation distance as A/x_{max}, and taking $\Delta t = 1$, $C^2\rho = K + 4G/3$ and the zone mass as $m_z = \rho A$, the mass of a zone is given by:

$$m_z = \frac{(K + 4G/3)\Delta x_{max}^2}{A} \qquad \text{A.17}$$

Finally, as the grid point mass is one third of the zone mass, and the node mass is the sum of the masses of the grid points connected to the node, the mass of a node is given by:

$$m_n = \sum \frac{(K + 4G/3)\Delta x_{max}^2}{6A} \qquad \text{A.18}$$

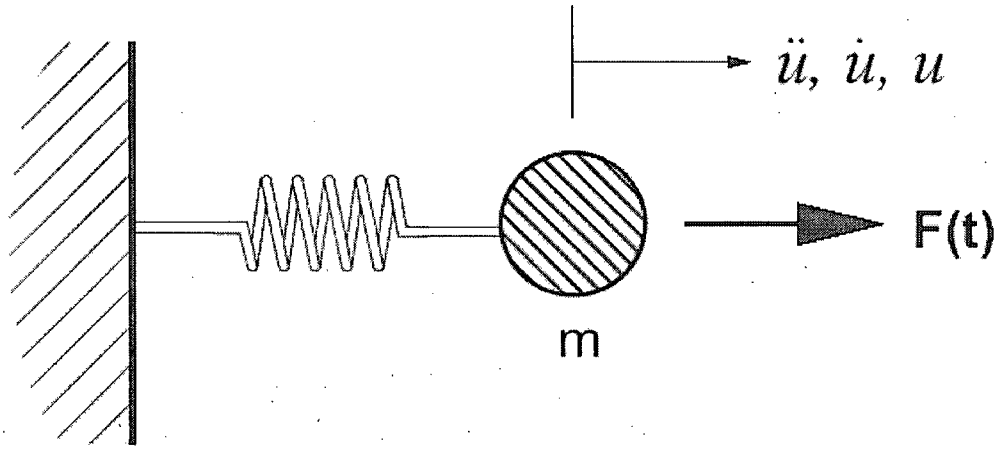

Figure A.5: Force acting on a mass

A.3. Summary of standard plasticity implementation

All elasto-plasticity models have four components, elasticity, a *yield function* which defines the stress combination for which plastic flow takes place, a *hardening/softening function* which controls the size of the yield surface and a *flow rule* which specifies the direction of the plastic strain increment vector.

Plasticity models considered in this thesis are formulated in terms of effective stresses. For the triaxial conditions used in the rest of this analysis all stresses and strains are principal values and

the shear component is not considered, the vertical direction is the direction of maximum principal stresses and strains. The two horizontal directions are both the direction of minimum stresses and strains. For triaxial conditions, the stress components used are the mean effective stress (p') and the deviator stress (q), defined as[6]:

$$p' = -\frac{1}{3}\left(\sigma_1' + 2\sigma_3'\right)$$
$$q = \left(\sigma_1' - \sigma_3'\right) \qquad \text{A.19}$$

The volumetric and shear strains are:

$$\varepsilon_v = \varepsilon_1 + 2\varepsilon_3$$
$$\varepsilon_q = \frac{2}{3}\left(\varepsilon_1 - \varepsilon_3\right) \qquad \text{A.20}$$

The volumetric and shear strain increments, $\dot{\varepsilon}_v$ and $\dot{\varepsilon}_q$ must be work-conjugate (Equation 2.10), and are defined as:

$$\dot{\varepsilon}_v = \left(\dot{\varepsilon}_1 + 2\dot{\varepsilon}_3\right)$$
$$\dot{\varepsilon}_q = \frac{2}{3}\left(\dot{\varepsilon}_1 - \dot{\varepsilon}_3\right) \qquad \text{A.21}$$

The specific volume (equal to 1 + void ratio) is defined as:

$$\upsilon = \frac{V}{V_s} \qquad \text{A.22}$$

where V is the total volume of the soil and V_s is the volume of solid particles. The incremental relation between volumetric strain and specific volume is:

$$\dot{\varepsilon}_v = \frac{\dot{\upsilon}}{\upsilon} \qquad \text{A.23}$$

---

[6] Using the FLAC sign convention explained in A.1.3.

From basic plasticity theory, the total strain increment can be decomposed into elastic and plastic components and that only the elastic part contributes to the stress increment. Hence,

$$\begin{aligned} \dot{\varepsilon}_v &= \dot{\varepsilon}_v^e + \dot{\varepsilon}_v^p \\ \dot{\varepsilon}_q &= \dot{\varepsilon}_q^e + \dot{\varepsilon}_q^p \end{aligned} \qquad \text{A.24}$$

Changes in stress are associated with the elastic strain only. Therefore from Hooke's law, the increment of mean effective stress and deviator stress is given by:

$$\begin{aligned} \dot{p}' &= K\dot{\varepsilon}_v^e \\ \dot{q} &= 3G\dot{\varepsilon}_q^e \end{aligned} \qquad \text{A.25}$$

where K is the bulk modulus and G is the shear modulus, which can be written in terms of the Young's modulus, E, and the Poisson's ratio, ν, as:

$$\begin{aligned} K &= \frac{E}{3(1-2\nu)} \\ G &= \frac{E}{2(1+\nu)} \end{aligned} \qquad \text{A.26}$$

Rearranging Equation A.24, and substituting in Equation A.25:

$$\begin{aligned} \dot{p}' &= K\dot{\varepsilon}_v - K\dot{\varepsilon}_v^p \\ \dot{q} &= 3G\dot{\varepsilon}_q - 3G\dot{\varepsilon}_q^p \end{aligned} \qquad \text{A.27}$$

The plastic flow is written as:

$$\begin{aligned} \dot{\varepsilon}_v^p &= \lambda_s \frac{\partial Q}{\partial p'} \\ \dot{\varepsilon}_q^p &= \lambda_s \frac{\partial Q}{\partial q} \end{aligned} \qquad \text{A.28}$$

where Q is the potential surface of the constitutive model and λ_s is the plastic volumetric multiplier.

For associated flow, the yield surface, F, and potential surface, Q, are identical and Equation A.28 may be written as:

$$\dot{\varepsilon}_v^p = \lambda_s \frac{\partial F}{\partial p'}$$

$$\dot{\varepsilon}_q^p = \lambda_s \frac{\partial F}{\partial q} \qquad \text{A.29}$$

A.4. Modified and Original Cam Clay in FLAC

Modified Cam Clay is a built-in constitutive model in FLAC. It is an incremental hardening/softening elastoplastic model including a particular form of non/linear elasticity and the behaviour is governed by volumetric plastic strain. Given that Modified Cam Clay already exists, the NorSand function development in FLAC will start from MCC. An intermediate step will be coding Original Cam Clay. Given that only the yield surface changes between both Cam Clays, OCC is a test that the proposed methodology works with FLAC.

A.4.1. Modified Cam Clay formulation

The Modified Cam Clay formulation is based on a combined shear and volumetric yield function (a closed yield surface) and an associated flow rule. In the FLAC version of Modified Cam Clay an elastic guess for the stress increment is first computed from the total strain increment. If the stresses violate the yield criteria, plastic deformation takes place and only the elastic part of the strain increment contributes to the stress increment. The stress increment is evaluated and corrected using the plastic flow rule to ensure that any stresses initially outside the yield function are end on the yield surface.

The shape of the yield surface of Modified Cam Clay is shown in Figure 2.16 and is defined by:

$$F = q^2 + M^2 p'(p' - p_{cn}') \qquad \text{A.30}$$

where M is the ratio q/p' at the critical state line and p_{cn}' is the consolidation pressure of the current yield surface. For Modified Cam Clay, the yield condition $F = 0$, is represented by an ellipse passing through the origin, with horizontal axis p_{cn}', and vertical axis $M\frac{p_{cn}'}{2}$.

Differentiating F with respect to p' and q:

$$\frac{\partial F}{\partial p'} = M^2(2p' - p_{cn}') = C_a$$

$$\frac{\partial F}{\partial q} = 2q = C_b \qquad \text{A.31}$$

Replacing Equation A.31 in Equation A.29, the flow rule for Modified Cam Clay is given by:

$$\dot{\varepsilon}_v^p = \lambda_s M^2 (2p' - p_{cn}')$$

$$\dot{\varepsilon}_q^p = \lambda_s 2q \qquad \text{A.32}$$

Replacing Equation A.32 into Equation A.27, the incremental mean pressure and deviator stress are:

$$\dot{p}' = K\left(\dot{\varepsilon}_v - \lambda_s C_a\right)$$

$$\dot{q} = 3G\left(\dot{\varepsilon}_q - \lambda_s C_b\right) \qquad \text{A.33}$$

For each step FLAC substitutes the new stresses into the yield surface by adding to the old stresses the stress increment, as shown in Equation A.34.

$$p'^N = p'^0 + \dot{p}'$$

$$q^N = q^0 + \dot{q} \qquad \text{A.34}$$

where the subscript N refers to the new converged stresses and O to the old ones. Substituting Equation A.33 into Equation A.34:

$$p'^N = p'^i - \lambda_s K C_a$$
$$q^N = q^i - \lambda_s 3GC_b \qquad \text{A.35}$$

where p'^i and q^i are the elastic guesses defined by:

$$p'^i = p'^0 + K\dot{\varepsilon}_v$$
$$q^i = q^0 + 3G\dot{\varepsilon}_q \qquad \text{A.36}$$

Substituting p'^N and q^N in $F\left(q^N, p'^N\right) = \left(q^N\right)^2 + M^2 p'^N \left(p'^N - p_{cn}{}'^N\right) = 0$, the equation to find λ_s is given by:

$$a\lambda_s^2 + b\lambda_s + c = 0 \qquad \text{A.37}$$

where:

$$a = \left(MKC_a\right)^2 + \left(3GC_b\right)^2$$
$$b = -\left(KC_a C_a^i + 3GC_b C_b^i\right) \qquad \text{A.38}$$
$$c = f\left(q^i, p'^i\right)$$

Equation A.37 is a polynomial of degree 2 which is easy to solve. From the two roots obtained the smaller must be retained.

At each step, the new specific volume is updated by:

$$\upsilon^N = \upsilon^o\left(1 - \dot{\varepsilon}_v\right) \qquad \text{A.39}$$

and preconsolidation pressure is updated by:

$$p_{cn}{}'^{N} = p_{cn}{}'\left(1+\dot{\varepsilon}_v^p \frac{\upsilon^N}{\lambda-\kappa}\right) \qquad \text{A.40}$$

where λ is the slope of the normal consolidation line in e-lnp' space, and κ is the slope of the elastic swelling line in the e-lnp' space.

The tangent bulk modulus is then updated using:

$$K = \frac{\upsilon p'}{\kappa} \qquad \text{A.41}$$

One of the idealizations of Cam Clay is that it is rigid in elastic shear. However Finite Element and Finite Difference programs do not allow such a condition. Hence, the shear modulus is calculated from K and Poisson's ratio, as:

$$G = \frac{3(1-2\nu)K}{2(1+\nu)} \qquad \text{A.42}$$

and the new elastic trials are calculated. Figure A.6 shows the flow chart for the model. Note that in Figure A.6 the yield surface is hardened after the new stresses are calculated. Hence, the yield surface is one step in arrears.

A.4.2. Original Cam Clay formulation

The shape of the yield surface for Original Cam Clay is shown in Figure 2.15 and is given by:

$$F = \ln\left(\frac{p'}{p_c{}'}\right) + \frac{q}{Mp'} - 1 \qquad \text{A.43}$$

where $p_c{}'$ is the critical mean effective pressure given by:

$$p_c{}' = \frac{p_{cn}{}'}{\exp(1.0)} \qquad \text{A.44}$$

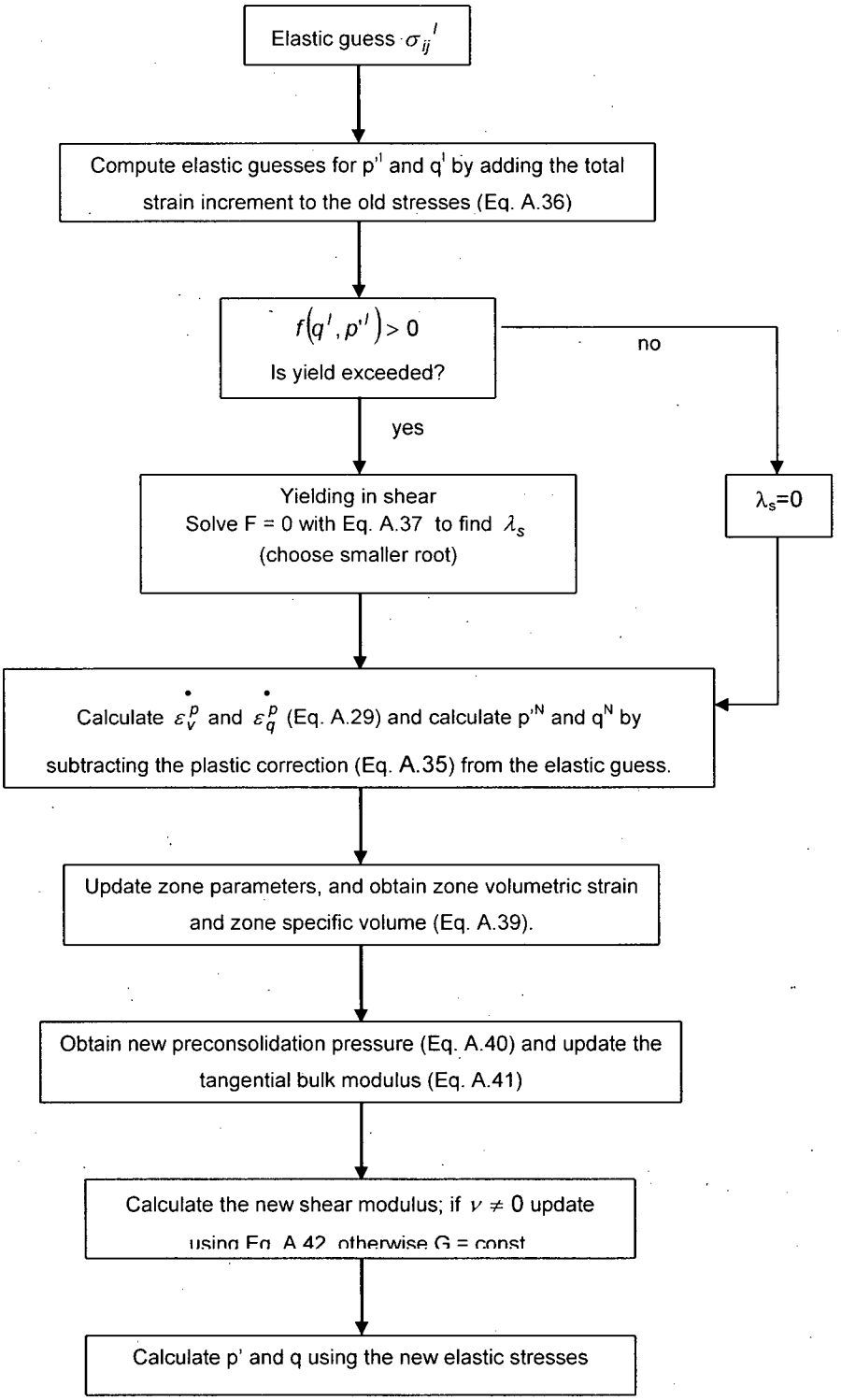

Figure A.6: Flow chart model Modified Cam Clay fish function

The yield surface for Original Cam Clay is non-linear, so a solution to Equation A.37 is not possible. Hence a different approach was used to derive parameter λ_s for OCC. In this case, instead of solving F = 0, the more usual plasticity approach of using the consistency condition is applied by solving $\dot{F} = 0$.

Differentiating Equation A.43:

$$\partial F = \frac{\partial F}{\partial p'}\dot{p}' + \frac{\partial F}{\partial q}\dot{q} + \frac{\partial F}{\partial p_c'}\dot{p}_c' \qquad \text{A.45}$$

$$\dot{F} = \frac{\dot{q}}{Mp'} - \frac{\eta \dot{p}'}{Mp'} + \frac{\dot{p}'}{p'} - \frac{\dot{p}_c'}{p_c'} \qquad \text{A.46}$$

Differentiating Equation A.46 with respect to p':

$$\frac{\partial F}{\partial p'} = \frac{1}{p'} - \frac{q}{Mp^2} \qquad \text{A.47}$$

Multiplying Equation A.47 by Mp':

$$\frac{\partial F}{\partial p'} = M - \eta = D^P \qquad \text{A.48}$$

As well, from Equation A.46:

$$\frac{\partial F}{\partial q} = 1 \qquad \text{A.49}$$

It is possible to swap between Equation A.47 and A.48 because $\dot{F} = 0$ (if $\dot{F} \neq 0$ this will not work).

Replacing in the plastic flow (Equation A.29), the volumetric and shear plastic strains for OCC are:

$$\dot{\varepsilon}_v^p = \lambda_s \frac{\partial F}{\partial p'} = \lambda_s D^P$$

$$\dot{\varepsilon}_q^p = \lambda_s \frac{\partial F}{\partial q} = \lambda_s \qquad \text{A.50}$$

Substituting A.50 in Equation A.27, the mean stress increment and deviator stress increment are:

$$\dot{p}' = K\left(\dot{\varepsilon}_v - \lambda_s D^P\right)$$

$$\dot{q} = 3G\left(\dot{\varepsilon}_q - \lambda_s\right) \qquad \text{A.51}$$

For Original Cam Clay, the consistency condition is applied by setting $\dot{F} = 0$ instead of using F = 0, and p_c' is allowed to harden during each load step and so convergence is obtained with the current yield surface.

The hardening rule is given by:

$$\dot{p_c}' = p_c' \frac{1+e}{\lambda - \kappa} \dot{\varepsilon}_v^p \qquad \text{A.52}$$

Hence, using Equation A.50,

$$\frac{\dot{p_c}'}{p_c'} = H\,\dot{\varepsilon}_v^p = H(M - \eta)\lambda_s \qquad \text{A.53}$$

where H is the hardening parameter given by $H = \frac{(1+e)}{\lambda - \kappa}$.

Substituting $\frac{\dot{p_c}'}{p_c'}$ from A.53, and $\dot{p}'$ and $\dot{q}$, from A.51, in Equation A.46 and applying the consistency condition the solution for λ_s is:

$$\lambda_s = \frac{3G\dot{\varepsilon}_q + K\dot{\varepsilon}_v D^P}{3G + HD^P p' M + K(M-\eta)^2} \qquad \text{A.54}$$

The flow chart for the Original Cam Clay fish function is presented in Figure A.7. In Figure A.7 the terms in bold font have changed from Figure A.6 (MCC).

Figure A.8 shows the comparison between the VBA Code and the fish function for Original Cam Clay, for the input parameters presented. It is possible to observe that the results show an excellent agreement. Hence, the formulation proposed is able to model Original Cam Clay correctly.

A.5. NorSand Formulation in FLAC

NorSand is similar to Original Cam Clay in that it has the same shape of yield surface. The original version of the NorSand constitutive model (Jefferies, 1993) is described in Chapter II. The changes to NorSand in this work are described below.

The yield surface for Norsand is shown in Figure 2.22 and is given by:

$$F = \ln\left(\frac{p'}{p_i'}\right) + \frac{q}{M_i p'} - 1 \qquad \text{A.55}$$

The size of the yield surface is controlled by p_i, which varies with hardening and M_i is related to the state parameter as:

$$M_i = M_{tc}\left(1 - \left|\frac{\psi}{M_{tc}}\right|\right) \qquad \text{A.56}$$

where M_{tc} is the critical stress ratio under triaxial compression condition.

In the case of NorSand used in this study, M_i is not constant so will become a variable, hence when differentiating Equation A.55 the term associated with M_i must be added as:

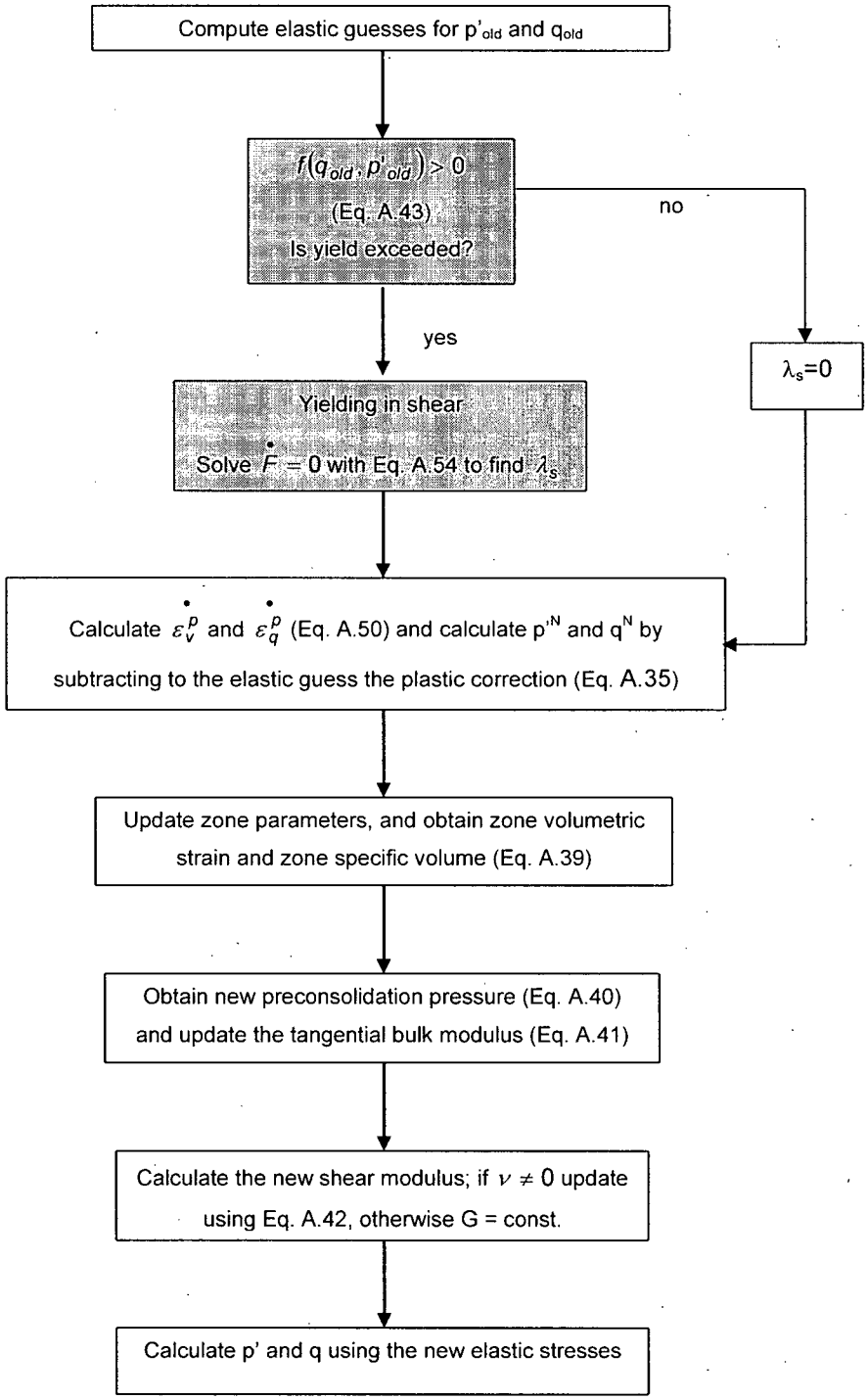

Figure A.7: Original Cam Clay fish function flow chart

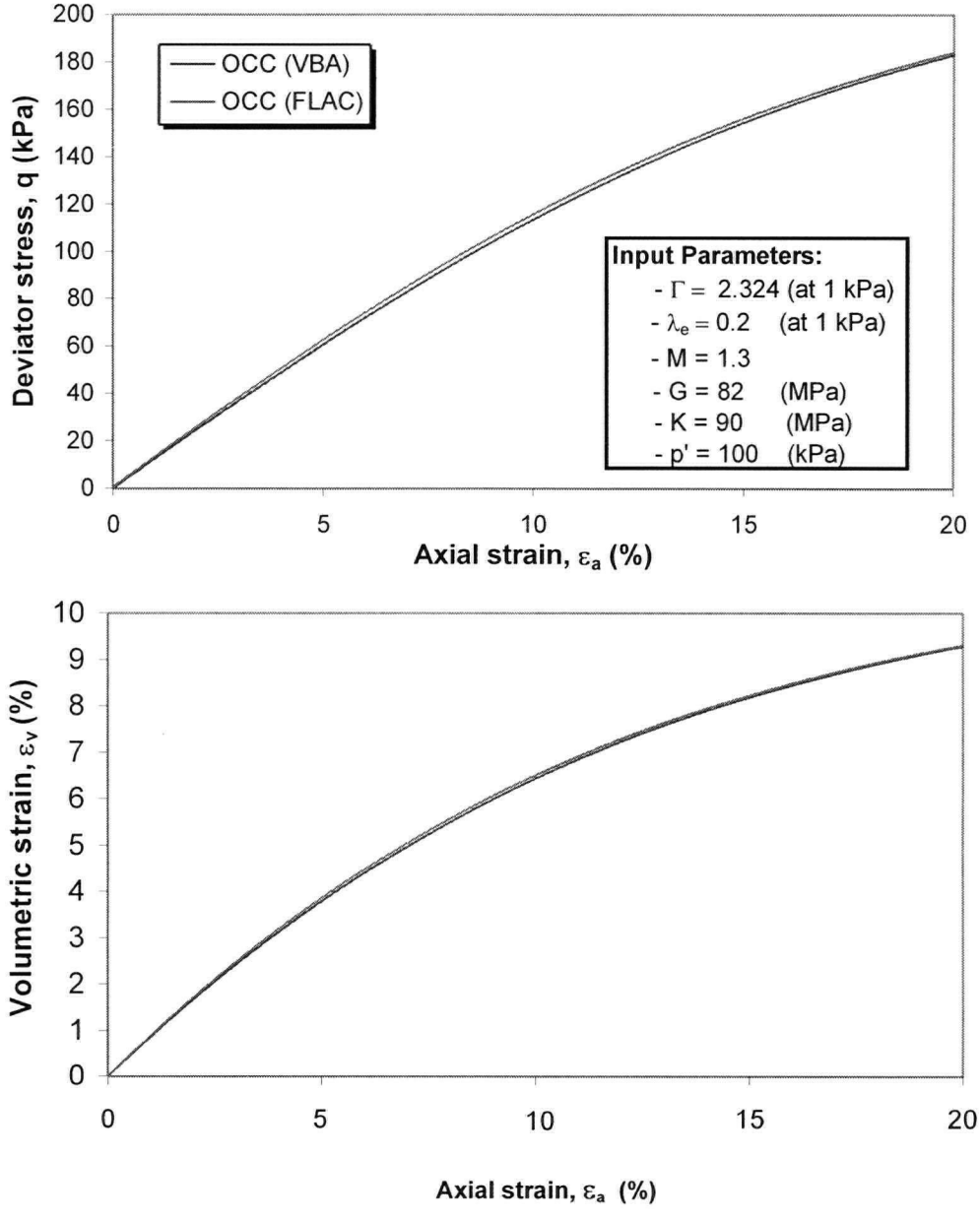

Figure A.8: Comparison of deviator stress and volumetric strain for Original Cam Clay, between VBA code and FLAC results

$$\dot{F} = \frac{\partial F}{\partial M_i}\dot{M}_i + \frac{\partial F}{\partial p'}\dot{p}' + \frac{\partial F}{\partial q}\dot{q} + \frac{\partial F}{\partial p_i'}\dot{p}_i' \qquad \text{A.57}$$

However, $\dot{M}_i$ is a second order term that can be eventually neglected to come back to:

$$\dot{F} = \frac{\partial F}{\partial p'}\dot{p}' + \frac{\partial F}{\partial q}\dot{q} + \frac{\partial F}{\partial p_i'}\dot{p}_i' \qquad \text{A.58}$$

Hence $\dot{F}$ can be written as:

$$\dot{F} = \frac{\dot{q}}{Mp'} - \frac{\eta\,\dot{p}'}{Mp'} + \frac{\dot{p}'}{p'} - \frac{\dot{p}_i'}{p_i'} \qquad \text{A.59}$$

Differentiating Equation A.59 with respect to p':

$$\frac{\partial F}{\partial p'} = \frac{1}{p'} - \frac{q}{M_i p'^2} \qquad \text{A.60}$$

Multiplying Equation A.60 by $M_i p'$:

$$\frac{\partial F}{\partial p'} = M_i - \eta \qquad \text{A.61}$$

Differentiating Equation A.59 with respect to q:

$$\frac{\partial F}{\partial q} = 1 \qquad \text{A.62}$$

Replacing in Equation A.29, the plastic volumetric strain increment and the plastic shear volumetric increment are:

$$\dot{\varepsilon}_v^p = \lambda_s\left(M_i - \eta\right)$$

$$\dot{\varepsilon}_q^p = \lambda_s \tag{A.63}$$

Re-writing the yield surface equation (Eq. A.55) as:

$$\exp\left(1-\frac{\eta}{M_i}\right)=\frac{p'}{p_i'} \tag{A.64}$$

the hardening rule is given by:

$$\frac{\dot{p_i}'}{p'} = H\exp\left(1-\frac{\eta}{M_i}\right)\left(\frac{(p_i'/p')_{\max}}{(p_i'/p')}-1\right)\dot{\varepsilon}_q^p \tag{A.65}$$

where:

$$\left(\frac{p_i'}{p'}\right)_{\max} = \exp\left(-\frac{\chi\psi_i}{M_i}\right) \tag{A.66}$$

and:

$$\psi_i = \psi - \lambda\left(1-\frac{\eta}{M_i}\right) \tag{A.67}$$

H is a constant for each sand and ψ is the state parameter.

Replacing in Equation A.59, λ_s is calculated as:

$$\lambda_s = \frac{3G\dot{\varepsilon}_q + K\dot{\varepsilon}_v D^P}{3G + H\exp\left(1-\frac{\eta}{M_i}\right)\left(\frac{(p_i'/p')_{\max}}{p_i'/p'}-1\right)p'M_i + K(M_i-\eta)^2} \tag{A.68}$$

A flow chart for NorSand is presented in Figure A.9.

Finally, the results obtained for Norsand with FLAC and the VBA Code are compared. The input parameters used are presented in the following table and are taken from the parameters found for

Ticino sand (Shuttle and Jefferies, 1998). Two extreme states are presented, an extremely loose state, where the state parameter is 0.15, and a dense state where the state parameter is -0.2. The results are presented in Figure A.10 and Figure A.11, respectively, showing an excellent agreement. The NorSand fish function is presented in Appendix B.

Table A.2: Parameter summary for NorSand model

Parameter	Dense	Loose	Remark
Γ	0.962	0.962	At 1 kPa
λ	0.0248	0.0248	Defined in base e
M	1.23	1.23	In compression
H	115-420ψ	115-420ψ	
χ	3.5	3.5	
G	50	50	MPa
ν	0.2	0.2	
ψ	-0.2	0.15	
σ_3'	100	100	kPa
K_0	1	1	

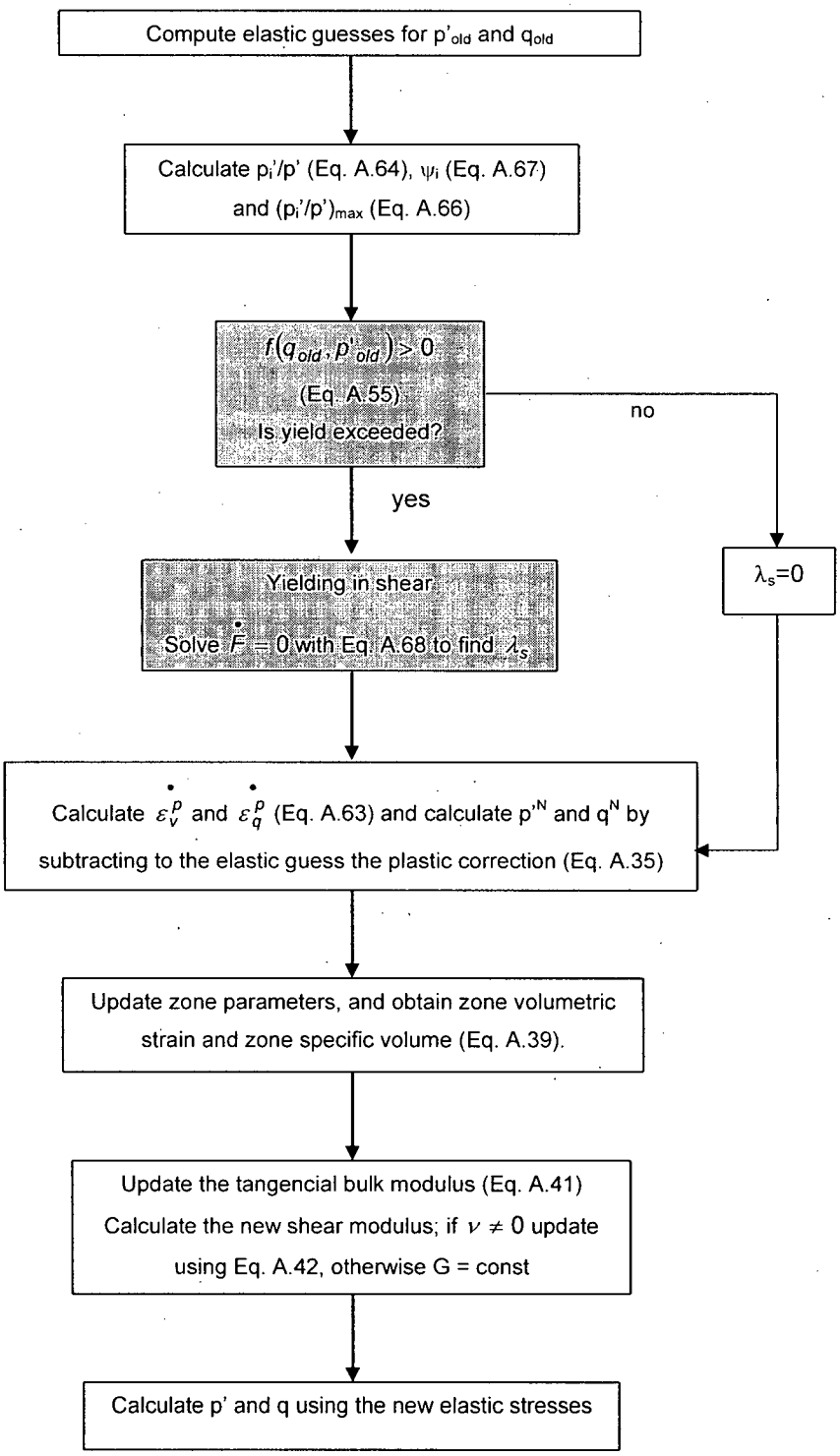

Figure A.9: NorSand fish function flow chart

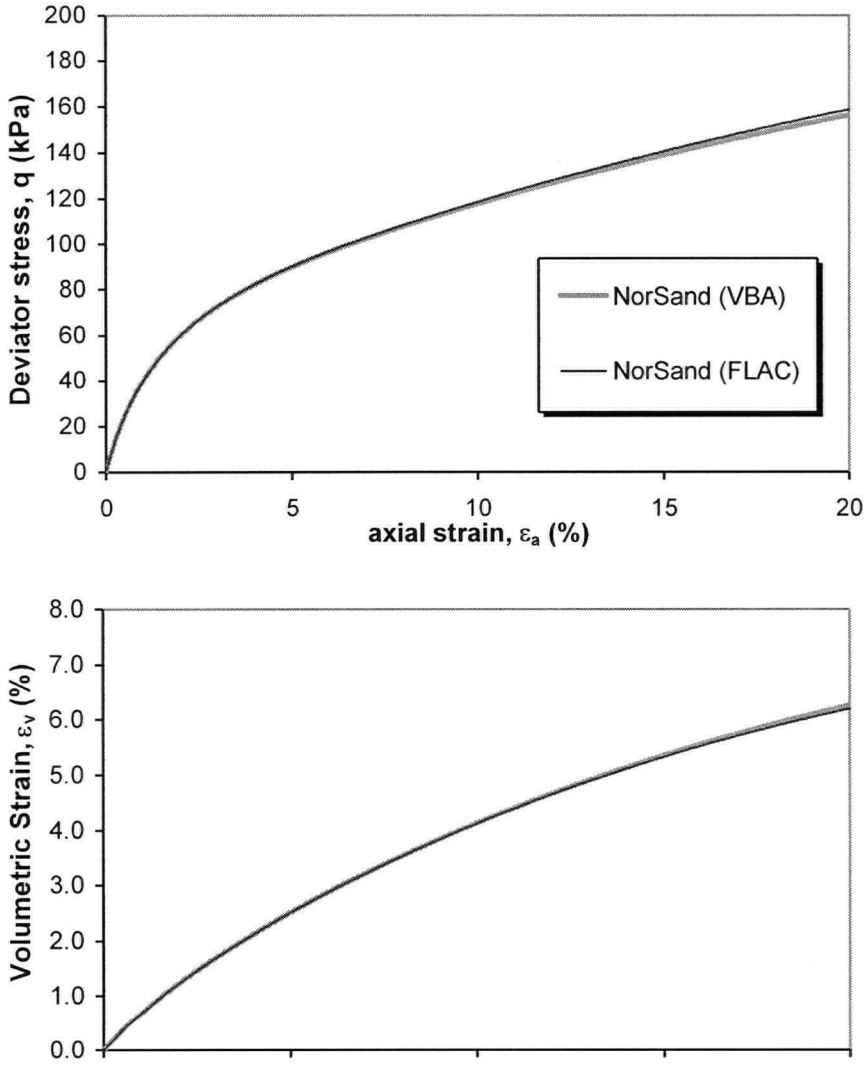

Figure A.10: Comparison of deviator stress and volumetric strain for NorSand, between VBA Code and FLAC results for a loose state

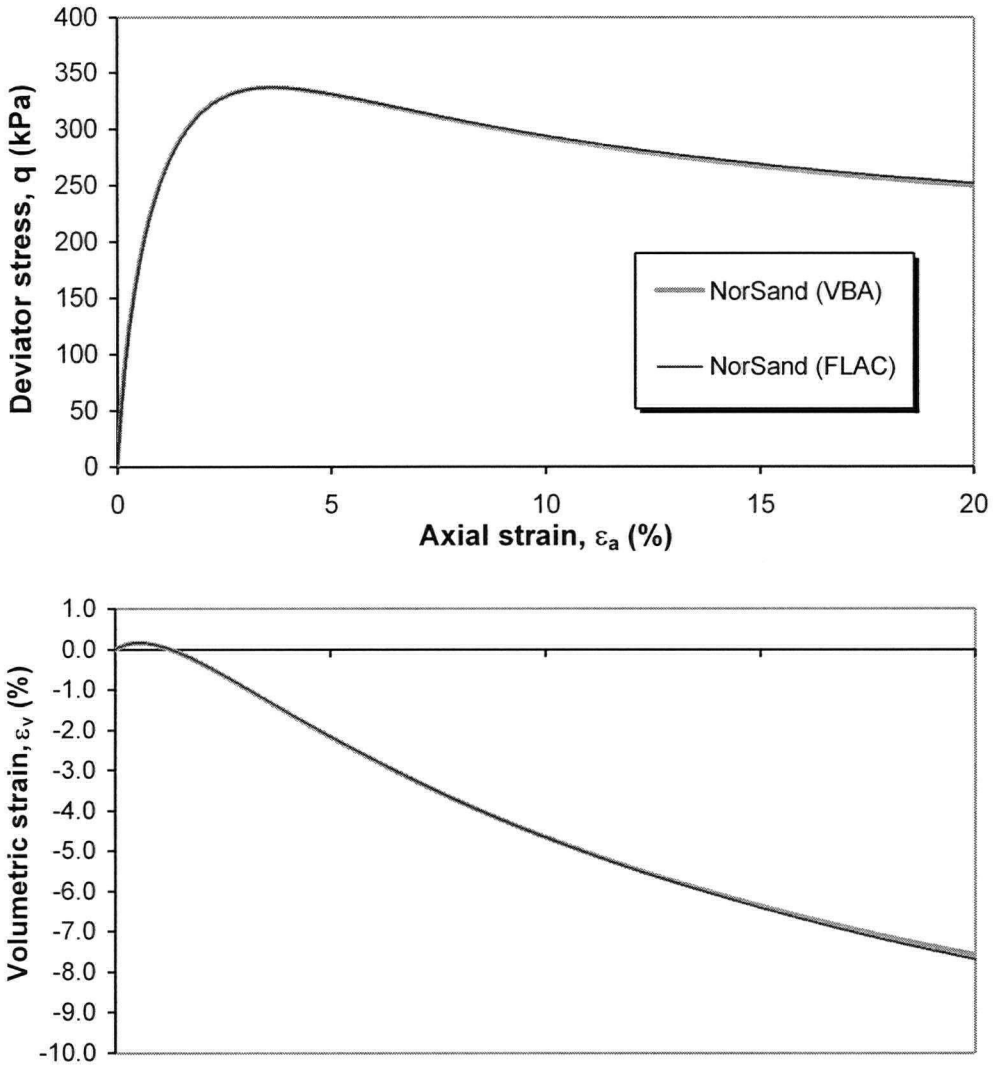

Figure A.11: Comparison of deviator stress and volumetric strain for NorSand, between VBA Code and FLAC results for a dense state

APPENDIX B: NORSAND FISH FUNCTION

```
; ------------------------------------------------------------
; FISH version of NorSand model
; September, 2005
; Pascale Rouse Master's Thesis
; ------------------------------------------------------------
set echo off
def nor_sand
  constitutive_model 110
  f_prop  m_g m_k m_m m_kappa m_lambda m_pi m_p1 m_v0 m_poiss
  f_prop  m_e m_ep m_v m_p m_q m_ind m_kc
  f_prop  m_psi m_hard m_chi m_gamma
  float   $sum_p $sum_q $sum_e $sum_ep $p $q $tk $tg $mm $pc $p1
  float   $e1 $e2 $sh2 $s11i $s22i $s33i $s12i $ds11 $ds22 $ds33 $ds12
  float   $fs $sa $sb $sc $ba $bb $bc $boa $sqr
  float   $alam $alam1 $qn $pn $add $v $vk $maxg $ming
  float   $hard $pold $qold $dP $dQ $eta $fs2 $pi2 $eta2 $pi3 $pidot
  float   $pt1 $pt2 $pt3 $pt4 $pt5 $pcrit
  float     $Mp $pi $pip $psi $psii $chi $ec $gamma $mvp
  int    $pind
  Case_of  mode
; ----------------------
; Initialisation section
; ----------------------
    Case 1
; --- data check ---
     if m_poiss < 0.0 then
       nerr = 126
       error = 1
     end_if
     if m_p1 = 0.0 then
       m_p1 = 1.0
     end_if
     if m_p1 < 0.0 then
       nerr = 126
       error = 1
     end_if
     if m_pi < 0.0 then
       nerr = 126
       error = 1
     end_if
     if m_kappa = m_lambda then
       nerr = 126
       error = 1
     end_if
     if m_kappa = 0.0 then
       nerr = 126
       error = 1
     end_if
; --- initialize current bulk modulus ---
     if m_kc = 0.0 then
```

```
      m_kc = m_k
    end_if
; --- initialize current shear modulus ---
    if m_g = 0.0 then
      if m_poiss # 0.0 then
        m_g = 3.0*m_kc*(1.0-2.0*m_poiss)/(2.0*(1.0+m_poiss))
      end_if
    end_if

  Case 2
; ---------------
; Running section
; ---------------
    zvisc = 1.0
    if m_ind # 0.0 then
      m_ind = 2.0
    end_if
    $pind = 0
; --- define constants locally ---
    $tk = m_kc
    $tg = m_g
    $mm = m_m
    $p1 = m_p1
    $e1 = $tk + 4.0 * $tg / 3.0
    $e2 = $tk - 2.0 * $tg / 3.0
    $sh2= 2.0 * $tg
    $hard=m_hard
    $chi=m_chi
;--- calculate old stress invariants, etc    ---
    $pold = -(zs11 + zs22 + zs33) / 3.0
; --- OLD deviatoric stresses ---
    $ds11 = zs11 + $pold
    $ds22 = zs22 + $pold
    $ds33 = zs33 + $pold
    $ds12 = zs12
; --- Qold  sqrt(3.0 * J2) ---
    $qold = sqrt(1.5*($ds11*$ds11+$ds22*$ds22+$ds33*$ds33)+3.0*$ds12*$ds12)
;--- get new trial stresses from old, assuming elastic increments ---
    $s11i = zs11 + (zde22 + zde33) * $e2 + zde11 * $e1
    $s22i = zs22 + (zde11 + zde33) * $e2 + zde22 * $e1
    $s33i = zs33 + (zde11 + zde22) * $e2 + zde33 * $e1
    $s12i = zs12 + zde12 * $sh2
;--- zone volumetric strain accumulation ------
    $sum_e = $sum_e + zde11 + zde22 + zde33
; --- mean pressure ---
    $p = - ($s11i + $s22i + $s33i) / 3.0
; --- deviatoric stresses ---
    $ds11 = $s11i + $p
    $ds22 = $s22i + $p
    $ds33 = $s33i + $p
    $ds12 = $s12i
; --- sqrt(3.0 * J2) ---
    $q = sqrt(1.5*($ds11*$ds11+$ds22*$ds22+$ds33*$ds33)+3.0*$ds12*$ds12)
    $eta=$qold/$pold
;--- Critical Void Ratio and State Parameter from old stresses ---
    $ec=m_gamma-m_lambda*ln($pold)
```

```
    $psi=($v-1.0-$ec)
;--- Definition of Mp ---
    if $psi>0.0 then
      $Mp=$mm*(1.0-$psi/$mm)
    else
      $Mp=$mm*(1.0+$psi/$mm)
    end_if
;--- Definition of NorSand parameters ---
    $pi=exp(($eta/$Mp)-1.0)
    $psii=$psi-m_lambda*(1.0-$eta/$Mp)
    $pip=exp(-m_chi*$psii/$Mp)
; --- check for yielding ---
    $fs =ln(1.0/$pi)+$eta/$Mp-1.0
    if $fs > 0.0 then
; --- yielding in shear ---
      $dP = $p - $pold
        $dQ = $q - $qold
        $pt1 = $dQ
        $pt2 = $dP * ($Mp-$eta)
        $pt3 = 3.0 * $tg
        $pt4 = $tk  * ($Mp-$eta)*($Mp-$eta)
        $pt5 = m_hard * $Mp*$pold*($pip/$pi-1.0)*exp(1.0-$eta/$Mp)
        $alam = ($pt1 + $pt2) / ($pt3 + $pt4 + $pt5)
      $sa = 3.0 * $tg
      $sc = $Mp -$eta
      $sb = $tk * $sc
      $pind  = 1
      if $alam < 0.0 then
        $alam = 0.0
      end_if
      $qn = $q - $sa * $alam
      $pn = $p - $sb * $alam
;---   new stresses ---
      if $q = 0.0 then
        $add = $pn - $p
        zs11 = $s11i - $add
        zs22 = $s22i - $add
        zs33 = $s33i - $add
        zs12 = $s12i
      else
        zs11 = ($ds11 / $q) * $qn - $pn
        zs22 = ($ds22 / $q) * $qn - $pn
        zs33 = ($ds33 / $q) * $qn - $pn
        zs12 = ($ds12 / $q) * $qn
      end_if
      $sum_p  = $sum_p  + $pn
      $sum_q  = $sum_q  + $qn
      $sum_ep = $sum_ep + $alam * $sc
      zvisc = 0.0
      m_ind = 1.0
    else
;---   no failure at all ---
      zs11 = $s11i
      zs22 = $s22i
      zs33 = $s33i
      zs12 = $s12i
```

```
      $sum_p = $sum_p + $p
      $sum_q = $sum_q + $q
    end_if
; --- update zone parameters ---
    if zsub > 0.0 then
      m_p   = $sum_p  / zsub
      m_q   = $sum_q  / zsub
      m_e   = m_e + $sum_e / zsub
      m_ep  = m_ep + $sum_ep / zsub
      $v    = m_v0  * (1.0+m_e)
; ---   data check ---
      if $v < 1. then
        nerr = 167
        error = 1
      end_if
      if m_p > 0.0 then
        error = 0
      else
        nerr = 168
        error = 1
      end_if
      if m_kc > m_k then
        nerr = 169
        error = 1
      end_if
; ---   update shear modulus ---
      if m_poiss # 0.0 then
; ---     constant Poisson's ratio ---
        m_g = 3.0*m_kc*(1.0-2.0*m_poiss)/(2.0*(1.0+m_poiss))
      else
; ---     constant G, check upper and lower bounds (nu=0 or 0.5) ---
        $maxg = 1.5*m_kc
        $ming = 0.0
        if m_g > $maxg then
          m_g = $maxg
        else
          if m_g < $ming then
            m_g = $ming
          end_if
        end_if
      end_if
; ---   reset for next zone ------
      $sum_p   = 0.0
      $sum_q   = 0.0
      $sum_ep  = 0.0
      $sum_e  = 0.0
    end_if
  Case 3
; ----------------------
; Return maximum modulus
; ----------------------
    cm_max = m_k + 4.0 * m_g / 3.0
    sm_max = m_g

  Case 4
; ----------------------
```

```
; Add thermal stresses
; ----------------------
    ztsa = ztea * m_kc
    ztsb = zteb * m_kc
    ztsc = ztec * m_kc
    ztsd = zted * m_kc
  End_case
end
opt nor_sand
; ------------------------------------------------------------
; FISH function to initialize initial specific volume
;     and tangent bulk modulus
; ------------------------------------------------------------
def set_v0
  loop i (1,izones)
    loop j (1,jzones)
      if model(i,j) = 110 then
        p0 = -(sxx(i,j)+syy(i,j)+szz(i,j))/3.-pp(i,j)
        if p0 > 0.0 then
                ec =  m_gamma(i,j) - m_lambda(i,j)*ln(p0)
                m_v0(i,j) = m_psi(i,j) + ec + 1.0
        else
          nerr  = 170
          error = 1
        end_if
      end_if
    end_loop
  end_loop
end
opt nor_sand
set echo on
```

The fish function for NorSand will be updated and available for download from the UBC Geotechnical web site [http://www.civil.ubc.ca/research/geotech/analytical.htm].